Summer 2010

Application of numerical models for improvement of flood preparedness

Daniel William Gilles
University of Iowa

APPLICATION OF NUMERICAL MODELS FOR IMPROVEMENT OF FLOOD PREPAREDNESS

by

Daniel William Gilles

A thesis submitted in partial fulfillment
of the requirements for the
Master of Science degree in
Civil and Environmental Engineering
in the Graduate College of
The University of Iowa

July 2010

Thesis Supervisors: Professor Larry J. Weber
Adjunct Associate Professor Nathan C. Young

Graduate College
The University of Iowa
Iowa City, Iowa

CERTIFICATE OF APPROVAL

_____

MASTER'S THESIS

_____

This is to certify that the Master's thesis of

Daniel William Gilles

has been approved by the Examining Committee
for the thesis requirement for the Master of Science
degree in Civil and Environmental Engineering at the July 2010 graduation.

Thesis Committee: _____
Larry J. Weber, Thesis Supervisor

_____
Nathan C. Young, Thesis Supervisor

_____
A. Allen Bradley Jr.

_____
Witold F. Krajewski

To my Grandma Dorothy

There are two big forces at work, external and internal. We have very little control over external forces such as tornadoes, earthquakes, floods, disasters, illness and pain. What really matters is the internal force. How do I respond to those disasters? Over that I have complete control.

Leo Buscaglia

ACKNOWLEDGMENTS

I would like to acknowledge the contributions of the faculty, staff, and students of IIHR-Hydroscience and Engineering during my graduate studies. The addition of their friendship has made my experience more enjoyable and fulfilling. I would especially like to thank Drs. Larry Weber and Nathan Young for providing guidance throughout my research efforts and the writing of this thesis. They have provided many opportunities to gain valuable experience through technical writing and presentation of my research. Jesse Piotrowski has also provided a great deal of technical support in the development of models and software. Brian Miller and Mark Wilson provided prompt computer and systems support. I would also like to thank my committee members, Drs. Witek Krajewski and A. Allen Bradley Jr. for their contributions and sharing of their expertise. Support of the Iowa Flood Center has made completion of this thesis possible.

I would like to acknowledge my parents for their support and sacrifices. They have given much so that I may have an education. I would like thank my wife, Amanda, for her support and understanding during my late nights at the lab.

ABSTRACT

Modeling the movement of flood waters can be accomplished using many different methods with varying degrees of physical detail. Numerical models utilizing simple routing methods or simplified versions of the Navier-Stokes equations can be used to improve the public's flood preparedness. Three numerical models are used in this thesis to investigate flood preparedness: (1) an existing HEC-ResSim model of Coralville Reservoir, (2) an existing one-dimensional HEC-RAS model of the Iowa River through Coralville and Iowa City, and (3) a coupled one/two-dimensional hydraulic MIKE Flood model of the Cedar River through Cedar Falls/Waterloo. The HEC-ResSim model of Coralville Reservoir, provided by the United States Army Corps of Engineers, requires reservoir elevation-storage curves, inflow hydrographs and user-defined operation rules. This model utilizes level pool routing to determine changes in reservoir water levels and attenuation of hydrographs. The Muskingum routing method is used to route controlled releases downstream and determine satisfaction of constraints. The model is used to determine the impact of operational changes and sedimentation effects on historic flood events. Simulations indicate sedimentation has no effect on peak discharges of extreme events, but more aggressive operations plans may provide additional storage prior to extreme events. The existing HEC-RAS of the Iowa River through Iowa City is used to develop a library of inundation maps to be hosted on the National Weather Service Advanced Hydrologic Prediction Service's river forecast website. The modeling method assumes steady gradually varied flow. Post-processing and visualization of simulation results are completed using a digital elevation map of the study area developed using topography, bathymetry, and structural elevations. A coupled one/two-dimensional MIKE Flood model is developed for the Cedar River through Cedar Falls/Waterloo using topography, bathymetry, land use, and structural data. The river channel is modeled using MIKE 11, a one-dimensional unsteady hydraulic model, while

the flood plain is modeled using MIKE 21, a two-dimensional hydraulic model utilizing depth-averaged Navier-Stokes equations. The model is used to develop a sequential levee closure plan for downtown Waterloo and will also be used to develop a library of inundation maps.

TABLE OF CONTENTS

LIST OF TABLES x

LIST OF FIGURES xi

CHAPTER I: INTRODUCTION 1

CHAPTER II: LITERATURE REVIEW 3

2.1 Reservoir routing 3
2.2 Hydrologic river routing 5
2.3 Steady gradually varied flow 7
2.4 Unsteady flow routing 9
2.4.1 One-dimensional numerical models 10
2.4.2 Two-dimensional numerical models 13
2.4.3 Coupling of 1D/2D numerical models 14
2.4.4 Numerical discretization 16
2.4.5 Sources of error 17
2.5 Summary 20

CHAPTER III: INVESTIGATION OF CORALVILLE RESERVOIR DURING HIGH FLOW PERIODS 27

3.1 Introduction 27
3.1.1 Study location 27
3.1.2 The 2008 Flood 28
3.1.3 Coralville Reservoir sedimentation 29
3.2 Motivation 30
3.3 Methodology 31
3.4 Numerical simulation 31
3.4.1 HEC-ResSim model 31
3.4.2 Downstream constraints 32
3.4.3 Assumptions/limitations 32
3.4.4 Model validation 33
3.5 Results and discussion 34
3.5.1 Impact of dredging 34
3.5.2 Impact of dredging and operational changes 36
3.5.3 Impact of downstream operational constraints 36
3.5.4 Impact of major flood pool elevation 38
3.5.5 Predicted impact of future sedimentation 39
3.6 Summary 40

CHAPTER IV: DEVELOPMENT OF FLOOD INUNDATION MAP LIBRARY FOR IOWA CITY, IOWA 68

4.1 Introduction 68
4.2 Motivation 68
4.3 Data collection 69
4.3.1 Study area 69
4.3.2 Bathymetry 69
4.3.3 Topography 70
4.3.4 Digital elevation models 71

4.3.5 Existing HEC-RAS model....72
4.3.6 Bulk flow data....73
4.4 Numerical simulation....73
4.4.1 Numerical methods....74
4.4.2 Boundary conditions....74
4.4.3 Assumptions....75
4.5 Results....75
4.5.1 Development of inundation map library....75
4.5.2 Web-based inundation map library....76
4.6 Summary....77

CHAPTER V: DEVELOPMENT OF A COUPLED 1D/2D HYDRAULIC MODEL FOR WATERLOO/CEDAR FALLS, IOWA....90

5.1 Introduction....90
5.2 Data collection....90
5.2.1 Study location....90
5.2.2 Overview....91
5.2.3 Bathymetry....91
5.2.4 Topography....92
5.2.5 Land use....92
5.2.6 Structural elements....92
5.2.7 Digital elevation model....93
5.2.8 Water surface elevation surveys....95
5.2.9 Bulk flow data....96
5.2.10 Summary....97
5.3 Numerical simulation....97
5.3.1 Numerical methods....98
5.3.2 Boundary conditions....99
5.3.3 Modeling of bridges....100
5.3.4 Modeling of low head dams....100
5.3.5 Simulation run-time....101
5.3.6 Model calibration....102
5.3.7 Model application....105
5.3.8 Investigation of levee closures....105
5.4 Summary....107

CHAPTER VI: SUMMARY AND RECOMMENDATIONS....124

6.1 Discussion....124
6.2 Future work....126

BIBLIOGRAPHY....128

APPENDIX A: CURRENT CORALVILLE RESERVOIR OPERATIONS PLAN....132

APPENDIX B: HISTORIC CORALVILLE RESERVOIR ELEVATION-STORAGE CURVES....135

APPENDIX C: CORALVILLE RESERVOIR REGULATION HISTORY....136

APPENDIX D: 1983 CORALVILLE RESERVOIR OPERATIONS....137

APPENDIX E: 1964 CORALVILLE RESERVOIR OPERATIONS....138

APPENDIX F: 2008 FLOOD WATERLOO/CEDAR FALLS HIGH WATER MARKS.....141

LIST OF TABLES

Table 2.1. The standard step procedure used to solve the energy equation. 24

Table 4.1. Uncertainty associated with the hydrographic survey instrumentation. 80

Table 4.2. Manning's 'n' values and calibrated 'n' values. 82

Table 4.3. Ayres Associates low-flow calibration results 83

Table 4.4. Ayres Associates high-flow calibration results of the HEC-RAS model. 84

Table 5.1. Distributed Manning's ‘n’ roughness coefficients based on NCLD classifications. 115

Table 5.2. High flow calibration roughness parameters and simulation results. 116

Table 5.3. Additional high flow calibration scenarios and simulation results. 117

Table A.1. Current Coralville Reservoir operations plan 132

Table F.1. High water marks following 2008 flood for Waterloo and Cedar Falls. 141

LIST OF FIGURES

Figure 2.1. Muskingum routing method storage wedge. 23

Figure 2.2. Diagram demonstrating terms in the energy equation relating two river cross-sections.....23

Figure 2.3. Schematic of finite difference grid. 24

Figure 2.4. Sweep procedure used with time-centering. 25

Figure 2.5. MIKE FLOOD allows coupling of 1D hydraulic models to a 2D computational mesh using standard, lateral, and structure links. 26

Figure 3.1. Coralville Reservoir regulates approximately 3,115 square miles of the Iowa River basin. 42

Figure 3.2. Observed reservoir pool elevation, inflow, and releases during the 2008 flood.....43

Figure 3.3. Active constraints during the 2008 flood. Some constraints were disregarded due to the pool elevation being within the major flood pool. 44

Figure 3.4. Changes in storage (ac-ft) for different elevation ranges below the spillway elevation through time. 44

Figure 3.5. Sediment fluxes and reservoir trapping efficiency for Coralville Reservoir 45

Figure 3.6. Volumes associated with the 2008 flood. 45

Figure 3.7. Flood storage remaining below the spillway according to pool elevation. The extent of the sedimentation is demonstrated by the deviation of storage curves from the original capacity in 1958. The storage in the upper elevations of the reservoir has remained relatively unchanged. 46

Figure 3.8. Comparison of model simulations using 2008 event, 1999 elevation-storage curve and 2001 operations plan with observed data. Difference in releases can be attributed to the inability to replicate decisions made using forecasted river stages and discharges. 47

Figure 3.9. Simulation utilizing a modified form of the 2001operations plan to replicate the observed release decisions. This modified operations plan is only applicable to the 2008 event, and was not used to evaluate the impacts of dredging. 48

Figure 3.10. Comparison of simulation of 1993 flood to observed data. 49

Figure 3.11. Simulation using 2008 flood event, 2001 operations plan, 2001 conservation pool, and varied storage curves.....50

Figure 3.12. Simulation using 2008 flood event, 2001 operations, and varied storage curves and conservation pools 51

Figure 3.13. Simulation using 1993 flood event, 2001 operations, and varied storage curves and conservation pools 52

Figure 3.14. Simulation using 2008 flood event, varied historical operations, storage curves, and conservation pools 53

Figure 3.15. Simulation using 1993 flood event, varied historical operations, storage curves, and conservation pools 54

Figure 3.16. Simulation changing the maximum summer release from 6,000 cfs to 8,000 cfs. 55

Figure 3.17. Simulation demonstrating disregarding of the Burlington river stage constraint. 56

Figure 3.18. Simulation disregarding of the Lone Tree river stage constraint. 57

Figure 3.19. Simulation disregarding of the Wapello river stage constraint. 58

Figure 3.20. Simulation disregarding all downstream river stage constraints and increasing the maximum summer release from 6,000 cfs to 8,000 cfs. 59

Figure 3.21. Prescribed releases for current (el. 707 ft) and alternate major flood pool elevations. 60

Figure 3.22. Simulation evaluating the effect of changing the major flood pool elevation using the 2008 event. 61

Figure 3.23. Simulation evaluating the effect of changing the major flood pool elevation using the 1993 event. 62

Figure 3.24. Depiction of the sedimentation in different elevation ranges during periods between reservoir storage capacity surveys 63

Figure 3.25. Linear regression of total sediment below el.720 through years of operation 64

Figure 3.26. Forecasted elevation storage relationships obtained by using a linear regression of total storage lost below el. 720, and shifting the 1999 storage curve 65

Figure 3.27. Simulation evaluating the effect of predicted sedimentation using the 2008 event. 66

Figure 3.28. Simulation evaluating the effect of predicted sedimentation using the 1993 event. 67

Figure 4.1. Study area showing the location of the stream gage and model extents. 79

Figure 4.2. (above) single-beam echosounder, (below) multi-beam echosounder. 81

Figure 4.3. USGS stream gage (005454500) rating curve for Iowa River at Iowa City. 85

Figure 4.4. Ayres Associates rating curve for lower corporate limits of Iowa City, IA. 85

Figure 4.5. Depiction of model scenario runs and boundary conditions. 86

Figure 4.6. Example inundation shape, river stage: 31.5 ft, discharge: 40,900 cfs. Inset shows gradual inundation of bridges as a result of the addition of bridge decking elevations in the post processing DEM. 87

Figure 4.7. Example of an inundation depth raster, river stage: 31.5 ft, discharge: 40,900 cfs. Inset shows gradual inundation of bridges as a result of the addition of bridge decking elevations in the post processing DEM. 88

Figure 4.8. Example NWS AHPS inundation map library for Colorado River at Bastrop, TX. (A) inundation layers (B) 7 – day river stage forecast hydrograph (C) FEMA flood maps (D) inundation depths. 89

Figure 5.1. Study area along the Cedar River. 108

Figure 5.2. Bathymetric survey locations and times. 109

Figure 5.3. 2006 National Land Cover Dataset of study area. 110

Figure 5.4. Comparison of approximated building footprints with 10-meter raster representation. 111

Figure 5.5. July 2009 hydrograph at Waterloo USGS gage station 05464000 during collection of bathymetry data. 112

Figure 5.6. Low flow calibration profile derived from bathymetric data. 112

Figure 5.7. High water marks from the 2008 flood. 113

Figure 5.8. 2008 flood hydrographs observed at several USGS gage stations. 114

Figure 5.9. Rating curve used for downstream boundary of study reach. 114

Figure 5.10. Lateral weir structure determined interpolated water levels and bed levels between MIKE 11 h points. 115

Figure 5.11. Relative differences between low flow calibration dataset and simulation results (simulation minus observed). 116

Figure 5.12. Comparison of initial calibration results of Simulation I to observed high water marks. 117

Figure 5.13. Comparison of initial calibration results of Simulation XIII to observed high water marks. 118

Figure 5.14. 2008 Flood inundation depths, FEMA 100 and 500-year flood boundaries. 119

Figure 5.15. Levee closure locations in downtown Waterloo, IA. 120

Figure 5.16. 2008 flood extent comparison of with and without levee closure scenarios. 121

Figure 5.17. Maximum water surface profiles for with and without levee closures when simulating the 2008 flood. 122

Figure 5.18. Design hydrograph used in development of levee closure plan. 122

Figure 5.19. The levee closure plan is organized by phases, which are based on discharge and stage at the Waterloo USGS gage. 123

Figure B.1. Elevation storage curves for Coralville Reservoir. 135

CHAPTER I: INTRODUCTION

During June 2008, a combination of saturated soil and intense rainfall, broadly distributed caused flooding that approached or exceeded 500-year levels throughout Iowa. Thousands of homes and businesses were damaged, disrupting the lives of many Iowans. Following the recession of flood waters, an effort to better understand floods and improve mitigation was initiated by university researchers and state agencies. Application of numerical flood modeling to improve flood preparedness is the focus of the present study. The study includes three components: analysis of a reservoir operations model, development of an inundation map library using a one-dimensional (1D) hydraulic model, and development of a coupled 1D/2D hydraulic model.

Coralville Reservoir, located just north of Iowa City, Iowa, regulates approximately 3,115 square miles of the Iowa River Basin, protecting many downstream communities. However, the reservoir's emergency spillway was activated during floods of 1993 and 2008, sending unregulated flow downstream. Sedimentation within the reservoir has become more apparent in recent years, affecting recreation and possibly compromising flood protection. Using a United States Army Corps of Engineers (USACE) Hydrologic Engineering Center Reservoir System Simulation (HEC-ResSim) model of Coralville Reservoir, the effects of sedimentation and operational changes on extreme flood events were investigated.

Unregulated discharge from Coralville Reservoir inundated Coralville, Iowa City and The University of Iowa campus during June 2008. Although volunteer efforts were substantial, community officials lacked sufficient information regarding flooding extent to direct evacuation and sandbagging efforts. In an attempt to mitigate future devastating effects of flooding in the region, this investigation utilized an existing 1D Hydrologic Engineering Center River Analysis System (HEC-RAS) model to develop a library of inundation maps. These maps will be available online to supplement the National

Weather Service (NWS) Advanced Hydrologic Prediction Service's (AHPS) river stage forecasts. Maps will estimate flood extents, rather than discrete river stages at a single location. The process will service as a prototype for creation of inundation map libraries for other communities.

Iowa communities of Cedar Falls and Waterloo also incurred damages during June 2008, when the Cedar River overflowed its banks. Some areas were protected by USACE levee systems and temporary sandbag levees. The objective of this effort was to develop an inundation model of the reach while incorporating the benefits of both 1D and 2D hydraulic models. This was accomplished using hydraulic modeling software developed by DHI. Model development included a 1D MIKE 11 of the river channel and a 2D MIKE 21 of the floodplain and then coupling both using MIKE Flood. This coupled model was used to investigate the role of levee closures in downtown Waterloo and to develop a plan to prioritize levee closure efforts. The model will also be used to develop a library of web-based static inundation maps to serve as a resource for citizens and community officials in assessing their flood risk.

CHAPTER II: LITERATURE REVIEW

The movement of flood waters through the landscape can be approximated using many different methods. Describing natural physical phenomena using numerical methods requires making broad assumptions to develop governing equations. While simple routing methods may be sufficient for approximating propagation of flood peaks through river channels, more complex hydraulic analyses may be necessary to incorporate effects of infrastructure or complex overland flow. Advanced models are capable of modeling more detailed physical phenomena, but this does not correspond to a decrease in uncertainty.

2.1 Reservoir routing

Storage of flood waters is governed by continuity, as shown in Equation 2.1.

$$\frac{\partial Q}{\partial x} + \frac{\partial A}{\partial t} = 0 \tag{2.1}$$

Applying Leibniz's rule and integrating over space, Equation 2.1 becomes Equation 2.2 (Jain 2001). Simplification yields Equation 2.3.

$$Q(x_2) - Q(x_1) + \frac{d}{dt}\int_{x_1}^{x_2} A dx = 0 \tag{2.2}$$

$$\frac{dV}{dt} = I - Q \tag{2.3}$$

Where V is storage volume, I is inflow discharge, and Q is outflow discharge. Equation 2.3 cannot be solved directly to find attenuated outflow Q. Instead, a storage function must be incorporated to relate discharge and storage terms, or a function to relate water surface elevation and control structure discharge. In the case of a reservoir operated by valve or gate structure, discharge can be a function of several factors other than storage or water level, such as time (Maidment 1992). In the case of reservoir routing, the *level*

pool routing method can be used to calculate an attenuated outflow hydrograph. Equation 2.3 is discretized using a finite difference scheme, as shown in Equation 2.4.

$$V_{i+1} - V_i = \frac{I_i + I_{i+1}}{2}\Delta t - \frac{Q_i + Q_{i+1}}{2}\Delta t \tag{2.4}$$

Where storage volume at the beginning and end of the *i*th time interval are V_i and V_{i+1}, respectively. The inflow values at the beginning and end of the *i*th time interval are denoted by I_i and I_{i+1}, respectively. The corresponding values of the outflow are Q_i and Q_{i+1}. The unknowns in Equation 2.4 are Q_{i+1} and V_{i+1}, which are isolated by multiplying through by 2/Δt and rearranging, as shown in Equation 2.5.

$$\left[\frac{2V_{i+1}}{\Delta t} + Q_{i+1}\right] = \left(I_i + I_{i+1}\right) + \left[\frac{2V_i}{\Delta t} - Q_i\right] \tag{2.5}$$

A relationship between $2V/\Delta t + Q$ and Q is required to solve Equation 2.5, which can be obtained from elevation-storage and elevation- outflow relations of the reservoir (Jain 2001). The routing procedure is then completed using an initial outflow Q_1 and determining a corresponding value of $2V_1/\Delta t + Q_1$ from the established curve. The value of $2V_2/\Delta t + Q_2$ is found from Equation 2.5, and the corresponding discharge Q_2, is obtained from the relationship between $2V/\Delta t + Q$ and Q. The procedure is then repeated in order to route the hydrograph downstream.

The accuracy of models utilizing the level pool routing method compared to more accurate distributed dynamic routing models, such as DAMBRK, was evaluated by Fread and Hsu (1993), who found that the error can be described by Equation 2.6.

$$E = \frac{100}{Q_{D_p}}\left[\sum_{i=1}^{N}\left(Q_{L_i} - Q_{D_i}\right)^2 / N\right]^{1/2} \tag{2.6}$$

Where Q_{Li} is the level pool routed flow, Q_{Di} is the dynamic routed flow, Q_{Dp} is the dynamic routed flow peak, and N is the number of computed discharges comprising the rising limb of the routed hydrograph. Fread and Hsu (1993) found that the error, E,

increases as reservoir mean depth decreases, reservoir length increases, time of rise of the inflow hydrograph decreases, and inflow hydrograph volume decreases.

Reservoir modeling using the level pool method is a simple process, but can become complicated if operational constraints are considered. For example, evaluation of downstream river constraints requires river routing to translate and attenuate the release hydrograph in order to determine controlled releases.

2.2 Hydrologic river routing

One of the most popular routing methods is the *Muskingum method* of hydrologic routing, first developed by McCarthy (1938), which is based on the propagation of a flood wave through a simplified river channel. With the arrival of a flood wave, the inflow will exceed the outflow within the simplified channel. Continuity dictates that a wedge of storage will form as a result of the difference in inflow and outflow, as depicted in Figure 2.1. As the flood wave leaves the channel, the outflow will exceed the inflow and a similar "negative" storage wedge will appear. The storage prism below the storage wedge maintains a constant volume throughout the propagation.

If the cross-sectional area is assumed to be proportional to the discharge, then the total volume of the prism and wedge can be calculated using Equation 2.7.

$$V = KQ + KX\left(I - Q\right) = K\left(XI + \left(1 - X\right)Q\right) \tag{2.7}$$

Where Q is discharge and coefficient K has the dimension of time. The value of K is approximately the travel time of the flood wave through the river channel. The coefficient X is a weighting factor that relates the influence of storage on inflow and outflow. The weighting factor is necessary for attenuating the flood wave and the subsequent flattening of the hydrograph (McCarthy 1938). The value of X can range from 0 for a reservoir to 0.5 for full wedge storage (Maidment 1992). Typical weighting factor values for natural streams range from 0 to 0.3. The values of X and K for a river

reach are determined by trial and error using observed hydrologic data. Both X and K are assumed to be specified and constant throughout the range of flow.

If storage volume is considered at time i and i+1, volume is then expressed as shown in Equations 2.8 and 2.9. Subtracting these equations yields the change in storage over a discrete time interval, as shown in Equation 2.10.

$$V_i = K\left[XI_i + (1-X)Q_i\right] \tag{2.8}$$

$$V_{i+1} = K\left[XI_{i+1} + (1-X)Q_{i+1}\right] \tag{2.9}$$

$$V_{i+1} - V_i = K\{[XI_{i+1} + (1-X)Q_{i+1}] - [XI_i + (1-X)Q_i]\} \tag{2.10}$$

Combining Equation 2.10 with the discretized form of the continuity equation (2.4) gives the attenuated outflow, $Q_{i+1,}$ as shown in Equation 2.11.

$$Q_{i+1} = C_0 I_{i+1} + C_1 I_i + C_2 Q_i \tag{2.11}$$

The Muskingum routing coefficients, C_0, C_1, and C_2 are given in Equations 2.12, 2.13, and 2.14, respectively. The summation of these quantities is unity.

$$C_0 = \frac{(\Delta t / K) - 2X}{2(1-X) + (\Delta t / K)} \tag{2.12}$$

$$C_1 = \frac{(\Delta t / K) + 2X}{2(1-X) + (\Delta t / K)} \tag{2.13}$$

$$C_2 = \frac{2(1-X) - (\Delta t / K)}{2(1-X) + (\Delta t / K)} \tag{2.14}$$

Routing of flood waves can be computed for several sub-reaches (N) such that the total travel time through the reach is K (U.S. Army Corps of Engineers 1990). The United States Army Corps of Engineers (1990) has established a criterion to determine the number of routing sub-reaches, as shown in Equation 2.15.

$$\frac{1}{2(1-X)} \le \frac{K}{N\Delta t} \le \frac{1}{2X} \tag{2.15}$$

The Muskingum routing method has been shown to produce unrealistic negative hydrograph values on rising limbs. This can be explained as a consequence of the form of storage equation employed and mathematical responses to a linear extrapolation of the weighted discharge (Perumal 1993). The method is not suitable for flashy hydrographs such as dam break scenarios (Maidment 1992). Physical properties of the river channel and obstructions that may contribute to backwater effects are not considered in the method.

Choudhury, et al. (2002) utilized the Muskingum method to route multiple hydrographs in a river network. Their model predictions outperformed all other reported hydrologic based routing models. A sensitivity analysis of their Muskingum coefficients revealed the existence of a unique set of parameter values to minimize error.

2.3 Steady gradually varied flow

Floodplain management is a program of corrective and preventative measures. Delineation of floodplains is one of the most important mitigation measures a community can employ. Communities agreeing to participate in the National Flood Insurance Program (NFIP) must adhere to strict guidelines regarding zoning, subdivision and building (Federal Emergency Management Agency 2009). Historically in the United States, flood plain delineations have been based on analysis of a simple hydraulic model with an assumption of steady gradually varied flow. Flow conditions are based on recurrence intervals corresponding to the 100- and 500-year floods for a given river reach.

Steady gradually varied flow water surface profiles are approximated by calculating water surface elevations at each cross-section using the energy equation, as shown in Equation 2.16. An iterative method known as *standard step* is a widely used method to solve for the total energy head at consecutive cross-sections (Chow 1959).

$$Z_2 + Y_2 + \frac{a_2 V_2^2}{2g} = Z_1 + Y_1 + \frac{a_1 V_1^2}{2g} + h_e \tag{2.16}$$

In the equation above, Z_1 and Z_2 are channel invert elevations, Y_1 and Y_2 are the water depths at each cross-section, V_1 and V_2 are average cross-section velocities, a_1 and a_2 are velocity weighting coefficients, h_e is the energy head loss, and g is the acceleration of gravity. A diagram showing the application of the energy equation is shown in Figure 2.2. The energy head loss term, h_e, combines frictional losses and expansion/contraction losses as shown in Equation 2.17.

$$h_e = L\bar{S}_f + C\left|\frac{a_2 V_2^2}{2g} - \frac{a_1 V_1^2}{2g}\right| \tag{2.17}$$

In the equation above, L is the weighted reach length, $\overline{S_f}$ is the representative friction slope, and C is the expansion/contraction loss coefficient. The weighted reach length, L, is calculated based on overbank flow lengths and overbank discharges, as shown in Equation 2.18. L_{lob}, L_{ch}, and L_{rob} are the reach lengths for the left overbank, channel, and right overbank, respectively. The parameters $\overline{Q}_{lob}$, $\overline{Q}_{ch}$, and $\overline{Q}_{rob}$ are the arithmetic mean of the discharges between cross-sections for the left overbank, channel, and right overbank, respectively. An expansion loss is assumed when the velocity head upstream is greater than the velocity head downstream. A contraction is assumed whenever upstream velocity head is less than downstream velocity head.

$$L = \frac{L_{lob}\overline{Q}_{lob} + L_{ch}\overline{Q}_{ch} + L_{rob}\overline{Q}_{rob}}{Q_{lob} + Q_{ch} + Q_{rob}} \tag{2.18}$$

The representative friction slope, $\overline{S_f}$, is calculated using the average conveyance method, shown in Equation 2.19.

$$\bar{S}_f = \left(\frac{Q_1 + Q_2}{K_1 + K_2}\right)^2 \tag{2.19}$$

Where Q_1, Q_2, K_1, and K_2 are weighted values based on cross-section subdivisions. Cross-Section subdivisions are determined based on changes in Manning's n values. For

a given subdivision, discharge, *Q*, and conveyance, *K*, can be calculated (in English units) using Equations 2.20 and 2.21, respectively.

$$Q = KS_f^{1/2} \tag{2.20}$$

$$K = \frac{1.486}{n} AR^{2/3} \tag{2.21}$$

Where *n* is the subdivision Manning's roughness coefficient, *A* is the subdivision flow area, and *R* is the subdivision hydraulic radius.

2.4 Unsteady flow routing

At the core of all unsteady flow routing computer simulations are the Navier-Stokes equations for an incompressible fluid. These fundamental fluid mechanics equations are derived using continuity given in Equation 2.22.

$$\frac{\partial p}{\partial t} + \frac{\partial u}{\partial x} + \frac{\partial v}{\partial y} + \frac{\partial w}{\partial z} = 0 \tag{2.22}$$

Using the differential equations of motion and continuity, the Navier-Stokes equations of fluid motion are developed, as shown in Equations 2.23 to 2.25.

$$\rho\left(\frac{\partial u}{\partial t} + u\frac{\partial u}{\partial x} + v\frac{\partial u}{\partial y} + w\frac{\partial u}{\partial z}\right) = -\frac{\partial p}{\partial x} + \mu\left(\frac{\partial^2 u}{\partial x^2} + \frac{\partial^2 u}{\partial y^2} + \frac{\partial^2 u}{\partial z^2}\right) + \rho g_x \tag{2.23}$$

$$\rho\left(\frac{\partial v}{\partial t} + u\frac{\partial v}{\partial x} + v\frac{\partial v}{\partial y} + w\frac{\partial v}{\partial z}\right) = -\frac{\partial p}{\partial y} + \mu\left(\frac{\partial^2 v}{\partial x^2} + \frac{\partial^2 v}{\partial y^2} + \frac{\partial^2 v}{\partial z^2}\right) + \rho g_y \tag{2.24}$$

$$\rho\left(\frac{\partial w}{\partial t} + u\frac{\partial w}{\partial x} + v\frac{\partial w}{\partial y} + w\frac{\partial w}{\partial z}\right) = -\frac{\partial p}{\partial z} + \mu\left(\frac{\partial^2 w}{\partial x^2} + \frac{\partial^2 w}{\partial y^2} + \frac{\partial^2 w}{\partial z^2}\right) + \rho g_z \tag{2.25}$$

Where ρ is fluid density, *x*, *y*, and *z* are Cartesian coordinates, *t* is time, *u*, *v*, and *w* are velocity components in the *x*, *y*, and *z* directions, respectively, *p* is pressure, μ is viscosity, and *g* is gravitational acceleration. While these governing equations are applicable in almost all situations, computational constraints typically dictate the degree of simulation detail achieved. Three-dimensional (3D) hydrodynamic modeling at the

reach scale is typically unjustifiable when parameters of interest (velocity direction and magnitude, inundation extent, and water depth) can be predicted using one-dimensional (1D) or two-dimensional (2D) computational fluid dynamics (CFD) (Bates and De Roo 2000; Piotrowski 2010).

2.4.1 One-dimensional numerical models

The most widely used approach to modeling fluvial hydraulics has been 1D finite difference solutions of the full Saint-Venant Equations (Bates and De Roo 2000). The Saint-Venant Equations are based on conservation equations of mass and momentum for a control volume, as shown in differential form in Equations 2.26 and 2.27.

$$\frac{\partial A}{\partial t} + \frac{\partial Q}{\partial x} = 0 \tag{2.26}$$

$$\frac{\partial Q}{\partial t} + \frac{\partial}{\partial x}(uQ) + gA\left(\frac{\partial h}{\partial x} - S_0\right) + gAS_f = 0 \tag{2.27}$$

Where Q is discharge, A is cross-sectional flow area, u is longitudinal flow velocity, h is flow depth, S_o is bed slope, and S_f is friction slope. 1D solutions of the full Saint-Venant Equations are derived based on several assumptions: the flow is one-dimensional, the water level across the section is horizontal, the streamline curvature is small and vertical accelerations are negligible, the effects of boundary friction and turbulence can be accounted for using resistance laws analogous to those for steady flow conditions, and the average channel bed slope is small so the cosine of the angle can be replaced by unity (Cunge, Holly and Verwey 1980).

Widely available software such as MIKE11 and HEC-RAS use the general form of the section-averaged Navier-Stokes equations. The basic forms of the equations used in MIKE11 are shown in Equations 2.26 and 2.27.

$$\frac{\partial Q}{\partial x} + \frac{\partial A}{\partial t} = q \tag{2.28}$$

$$\frac{\partial Q}{\partial t} + \frac{\partial\left(\alpha \frac{Q^2}{A}\right)}{\partial x} + gA\frac{\partial h}{\partial x} + \frac{gQ|Q|}{C^2 AR} = 0 \qquad (2.29)$$

Where Q is discharge, x is longitudinal channel distance, A is cross-sectional area, q is lateral inflow, t is time, h is flow depth, C is the Chezy coefficient and R is the hydraulic radius.

HEC-RAS has a similar approach except Manning's roughness is used to calculate friction losses instead of the Chezy coefficient (HEC 2010). The unsteady equations are solved by HEC-RAS using a four-point implicit scheme which requires that spatial derivatives and functions are evaluated at an interior point $(n+\theta)\Delta t$ (HEC 2010). Thus, values at the next time step are required for all terms in the general 1D equations. A system of simultaneous equations results from the implicit scheme. The effect of the implicit scheme allows information from anywhere within the reach to influence the solution. This discretization scheme requires much more computational effort than an explicit scheme, but it has improved numerical stability. Von Neuman stabilities analyses conducted by Fread (1974) and Liggett and Cunge (1975) found that the four-point implicit scheme is unconditionally stable for $0.5<\theta<1.0$ (HEC 2010).

MIKE 11 also utilizes an implicit scheme, but uses a six-point Abbott scheme in solving the general Saint-Venant Equations (DHI 2009). Computations are performed on a grid consisting of alternating discharge, Q, and water level, h points. Simulation times depend on the number of computational nodes, but are typically completed in several minutes. Computational efficiency is one of the major advantages of employing a one-dimensional numerical scheme.

An inherent assumption of 1D finite difference river modeling is that flow velocities are perpendicular to cross-sections. Additionally, water surface elevations are assumed constant for entire cross-sections. For river reaches containing backwater areas or naturally occurring diversion channels, these assumptions are frequently violated. For

out-of-bank flow, interaction with the floodplain results in highly complex fluid movement with at least two-dimensional properties. Flow at the channel-floodplain transition has been shown to develop a three-dimensional flow field due to intense shear layers (Bates and De Roo 2000).

Development of a one-dimensional hydraulic model requires user discretion in defining model geometry. Bates and De Roo (2000) found that subjectivity of cross-section placement is an important contributor to the overall accuracy of a 1D hydraulic model. In addition to directly determining overbank reach lengths, placement of cross-sections must be executed so that changes in conveyance due to expansions or contractions are accurately captured.

2.4.1.1 Boundary conditions

If a one-dimensional finite difference model contains *n* computational nodes, then there are *n* - 2 finite difference equations that can be developed. Therefore, two other equations are necessary to solve the system of equations. Two boundary conditions must be specified due to the hyperbolic behavior of the Saint-Venant equations (Cunge, Holly and Verwey 1980). The location of the boundary condition specification depends on the flow regime within the study reach. Supercritical flow regimes will require two boundary conditions specified at the upstream boundary. Subcritical flow regimes require one on the upstream boundary and one on the downstream boundary. Boundary conditions can consist of constant values of water surface elevation or discharge, time dependent values of water surface elevation or discharge, or a rating curve relating water surface elevation to discharge (Cunge, Holly and Verwey 1980). Values are typically taken from gage data, provided that the model boundaries are at gage locations. When model boundaries do not occur at gage locations, approximations using normal depth calculations can be completed. Flow depth is considered to be normal depth when uniform flow conditions exist. Since uniform flow conditions do not normally exist in the natural environment,

precautions must be taken when implementing this type of control (HEC 2010). The boundary condition derived from normal depth calculations should be placed a sufficient distance away from the area of interest so that accuracy of simulation results are not compromised.

2.4.2 Two-dimensional numerical models

Complex interaction of channel and floodplain flow fields make two-dimensional simulation codes more desirable than one-dimensional codes in many modeling situations (Horritt and Bates 2002). Continual improvements in computational resources and affordability have also increased implementation of two-dimensional modeling. Most widely used commercial two-dimensional codes utilize depth-averaged Navier-Stokes equations, commonly called the Saint-Venant shallow water equations, shown in Equations 2.28, 2.29 and 2.30.

$$\frac{\partial h}{\partial t}+\frac{\partial(hU)}{\partial x}+\frac{\partial(hV)}{\partial y}=0 \tag{2.28}$$

$$\frac{\partial(hU)}{\partial t}+\frac{\partial(hUU)}{\partial x}+\frac{\partial(VU)}{\partial y}=\frac{\partial(hT_{xx})}{\partial x}+\frac{\partial(hT_{xy})}{\partial y}-gh\frac{\partial z}{\partial x}-\frac{\tau_{bx}}{\rho} \tag{2.29}$$

$$\frac{\partial(hV)}{\partial t}+\frac{\partial(hUV)}{\partial x}+\frac{\partial(VV)}{\partial y}=\frac{\partial(hT_{xy})}{\partial x}+\frac{\partial(hT_{yy})}{\partial y}-gh\frac{\partial z}{\partial y}-\frac{\tau_{by}}{\rho} \tag{2.30}$$

Where h is flow depth, U and V are velocities in the x and y directions, T_{xx} , T_{xy}, and T_{yy} are depth-averaged turbulent stresses, z is the water surface elevation, and τ_{bx} , τ_{by} are bed shear stresses.

DHI's MIKE21 software utilizes similar equations to describe the conservation of mass and momentum in two horizontal dimensions, as shown in Equations 2.31, 2.32, and 2.33.

$$\frac{\partial \zeta}{\partial t}+\frac{\partial p}{\partial x}+\frac{\partial q}{\partial y}=\frac{\partial d}{\partial t} \tag{2.31}$$

$$\frac{\partial p}{\partial t}+\frac{\partial}{\partial x}\left(\frac{p^2}{h}\right)+\frac{\partial}{\partial y}\left(\frac{pq}{h}\right)+gh\frac{\partial \zeta}{\partial x}+\frac{gp\sqrt{p^2+q^2}}{C^2h^2}-\frac{1}{\rho_w}\left[\frac{\partial}{\partial x}\left(h\tau_{xx}\right)+\frac{\partial}{\partial y}\left(h\tau_{xy}\right)\right]=0 \quad (2.32)$$

$$\frac{\partial q}{\partial t}+\frac{\partial}{\partial y}\left(\frac{q^2}{h}\right)+\frac{\partial}{\partial x}\left(\frac{pq}{h}\right)+gh\frac{\partial \zeta}{\partial y}+\frac{gq\sqrt{p^2+q^2}}{C^2h^2}-\frac{1}{\rho_w}\left[\frac{\partial}{\partial y}\left(h\tau_{yy}\right)+\frac{\partial}{\partial x}\left(h\tau_{xy}\right)\right]=0 \quad (2.33)$$

Where h is water depth, d is time varying water depth, ζ is surface elevation, p and q are flux densities in x- and y-directions, C is Chezy resistance, g is acceleration of gravity, ρ_w is the density of water, x and y are Cartesian coordinates, t is time and τ_{xx}, τ_{xy}, and τ_{yy} are the components of effective shear stress (DHI 2009).

The MIKE21 Hydrodynamic solver utilizes an Alternating Direction Implicit (ADI) scheme to approximate the Saint-Venant shallow water equations (DHI 2009). The scheme makes a sweep in each direction and each individual grid line by using a Double Sweep (DS) algorithm, as shown in Figures 2.3 and 2.4. The system of equations are first solved in single-row sweeps, alternating between x and y directions. In the x-direction, continuity and x-momentum equations are solved, moving ζ from n to n + 1/2 and p from n to n + 1. For equations that require q, two previously solved values are used, n - 1/2 and n + 1/2 (DHI 2009).

In the y-direction, continuity and y-momentum equations are solved by moving ζ from n + 1/2 to n + 1 and q from n + 1/2 to n + 3/2. For equations that require p at n and n + 1, values calculated in the x-direction sweep are used (DHI 2009). For a given time step, x-direction sweep solutions are completed in the order of decreasing y-direction, or a down sweep, and the next time step in the order of increasing y-direction, or an up sweep. Summing the two directional sweeps results in time centering at n + 1/2 (DHI 2009).

2.4.3 Coupling of 1D/2D numerical models

Modeling of urban flooding has presented several challenges to using typical one- and two- dimensional numerical codes (Patro, et al. 2009). One-dimensional numerical

models are unable to resolve complex floodplain flow fields and require post-processing to produce realistic flood extents. Two-dimensional numerical models are unable to model structural elements that may produce super-critical or pressurized flow conditions. Consequently, recent urban flood modeling efforts have been focused on dynamically coupling one- and two-dimensional models to avoid these limitations (Frank, et al. 2001; Patro, et al. 2009). A one-dimensional numerical model of the river channel complimented by a two-dimensional model of the floodplain provides improvements in hydraulic modeling accuracy and computational efficiency. If an entire river reach is modeled using a one-dimensional model, then computational nodes within that portion of the two-dimensional mesh will not become active, improving computational efficiency. Several hydraulic models have successfully been coupled or are available in commercial packages: Lin et al. (2006) coupled ISIS and DIVAST, Delft-FLS, LISFLOOD-FP, SOBEK 1D2D and MIKE FLOOD.

MIKE FLOOD has been developed to accommodate several types of links between one-dimensional MIKE 11 and two-dimensional MIKE 21. These include the standard link, lateral link, and structure link as shown in Figure 2.5. Standard links are explicit and are able to link ends of a MIKE 11 branch with a MIKE 21 computational mesh. These types of links allow model boundary conditions to be controlled by a rating curve, which is useful when modeling unsteady conditions. The discharge contribution from a MIKE 11 branch affects the continuity and momentum equations in the MIKE 21 cell when linked with a standard link (DHI 2009). The link requires the MIKE 11 branch be one time step behind the MIKE21 mesh; therefore a discharge predictor is utilized for the time step $n + 1/2$, as shown in Equation 2.31.

$$\frac{\partial Q^{n+1/2}}{\partial t} = -\left(gA\frac{\partial H^{n}}{\partial x} + \frac{Q^{n}\left|Q^{n}\right|}{AC^{2}R} \right) \tag{2.31}$$

Where Q is discharge, t is time, g is acceleration of gravity, A is cross-sectional area, H is water level, x is longitudinal distance, C is the Chezy coefficient, and R is hydraulic radius. This predictor assumes that the roughness coefficient is controlling the flow.

Lateral linking of a MIKE 11 branch to a MIKE 21 mesh allows water to enter the floodplain laterally from the river channel. The linking method is explicit. The flow exchanged between the two models is controlled by a structural relationship such as a weir equation. Since one-dimensional hydraulic models like MIKE 11 do not consider cross-channel flow, momentum cannot be conserved across this type of link (DHI 2009).

Structural links are used to incorporate the effects of structural elements such as dams and bridges. This linking procedure is the most stable coupling method due to its implicit nature. The function of the link is to utilize the momentum calculated through a MIKE 11 branch to modify the momentum in adjacent MIKE 21 cells in order to represent the hydraulic effects of the structure (DHI 2009). Conservation of momentum is not guaranteed, so emphasis is placed on interrogating simulation results.

2.4.4 Numerical discretization

Hydraulic modeling of a continuous fluid with Navier-Stokes equations requires finding approximate solutions at discrete points in the space-time domain. Designation of points in the space-time domain is called discretization, which requires selection of node spacing and time step. Most commercial software packages express derivatives and integrals by discrete functions called finite difference schemes (Cunge, Holly and Verwey 1980). There are two basic finite difference schemes, which include explicit and implicit schemes. Explicit finite difference schemes compute flow variables at any point in the space domain at time level $n + 1$ based entirely on known data at a few adjacent points at time level n. Explicit methods are typically not utilized in hydraulic modeling due to stability concerns. Stability of the explicit numerical scheme depends on the Courant-Friedrichs-Lewy (CFL) condition, given in Equation 2.32. This criterion assures

that characteristic information cannot be passed farther than (n + 1, j) if computed from (n, j – 1) and (n, j + 1) and the time interval is less than $t_p - n\Delta t$, where t_p is the level of characteristic intersection (Cunge, Holly and Verwey 1980). This often requires the time step to be very small, which can become computationally intensive (Stoer and Bulirsch 2002).

$$\left| c\frac{\Delta t}{\Delta x} \right| \le 1 \ , c = (gh)^{1/2} \tag{2.32}$$

Numerical stability is improved considerably when an implicit finite difference scheme is employed. Implicit finite difference schemes solve a system of equations for the entire model domain using boundary conditions and equations for each grid point from the previous time step. This means that the conditions at any point in the domain can affect all other points, similar to the physical characteristics of river flow. Solving the system using a matrix or iterative technique requires significant computational resources, but an advantage of implicit schemes is they are unconditionally stable (Cunge, Holly and Verwey 1980). Thus, the CFL condition can exceed unity for certain situations when using an implicit scheme. Though the scheme is numerically stable and consistent and its solution may satisfy the difference system, it may not converge to a solution of the differential equations (Cunge, Holly and Verwey 1980). Although the CFL number can exceed 50 in certain situations, it should be as close to unity as computationally feasible to accommodate floodplain characteristics (Bates, Anderson and Hervouet 1995).

2.4.5 Sources of error

Inundation maps are the most useful results produced from flood simulations, but uncertainties must be considered because error is introduced throughout the development process. Currently, uncertainties are typically left unspecified when flood inundation maps are released (Bales and Wagner 2009). The cumulative effect of uncertainties

introduced during data collection, model development, numerical simulation, post-processing, and theoretical assumptions can render results inaccurate and ultimately misleading.

Data collection uncertainties include instrument measurement uncertainties and collection method uncertainties. Typical single-beam echosounder systems measure depth with an uncertainty of 1.0 to 18cm ± 0.1% depth, while multi-beam echosounder systems measure with an uncertainty of 0.6 to 1.0 cm. Another important consideration is inertial effects such as heave, pitch, and roll. Most single- and multi-beam systems include inertial correction systems mounted aboard the survey vessel. Work, et al. (1998) found that single-beam survey measurement error near the shoreline can be on the order of ±20cm when inertial effects are not accounted for. Piotrowski (2010) obtained similar results through comparison of single- and multi- beam data for the Iowa River in Iowa City, IA, and found error to range from -25 cm to 15 cm. Characteristics of the river bed affect the quality of echosounder measurements. River beds are dynamic and composed of heterogeneous materials and may return inaccurate soundings if unconsolidated (Huang, et al. 2002). Multi-beam soundings are emitted in a swath onto the bed surface. If these soundings have a large incident angle with the bed, larger bed features may hide smaller ones (Huang, et al. 2002).

Model roughness parameters and geometry are considered to be the most important factors in predicting inundation extent. Common modeling practice includes parameterizing roughness coefficients to calibrate to observed measurements while minimizing error between the observation and prediction (Aronica, Hankin and Beven 1998). This approach assumes that there is one optimum set of parameters to minimize this error; however, the non-linearity of flood models likely indicates the existence of several optimum parameter sets (Aronica, Hankin and Beven 1998). One method to determine these optimum parameter sets is to perform Monte-Carlo simulations while

utilizing the generalized likelihood uncertainty estimation (GLUE) procedure (Aronica, Hankin and Beven 1998) (Pappenberger, Beven, et al. 2004).

One of the most important data sources in the development of flood inundation models is topography. Currently, the highest resolution topographic data available is Light Detection and Ranging (LiDAR) derived, which typically has a horizontal resolution of 1m and vertical accuracy of ±15 cm (Mason, et al. 2003). These datasets mark a significant improvement over the USGS National Elevation Dataset 1/3 Arc Second DEMs, which have a resolution of approximately 10 m and vertical accuracy of approximately ±7 m (USGS 2008). Werner (2001) investigated the impact of DEM grid size on flood extent mapping when intersecting a water surface result from a 1D hydraulic simulation of 50 and 200 year floods in a study reach. The approach was to create DEMs with resolutions of 2.5, 5, 10, and 25 meters, and compare inundated area at different depths and total inundation area for a test reach. They found that inundation area increased 10% when DEM resolution increased from 2.5 m to 5 m during the 50 year event and 26% when DEM resolution increased from 5 m to 25 m during the 200 year event. The results of similar investigations would vary by river reach. For example, a channelized reach would demonstrate less grid sensitivity than one with a wide floodplain.

Inundation maps are typically created with a steady gradually varied flow assumption. The largest implication of this assumption is that the inundation area is over- predicted at higher discharges due to the time required to reach a steady condition. This time typically exceeds the duration and total volume of the peak discharge present in a flood hydrograph (Bales and Wagner 2009). A hydrograph that rises slowly would result in more inundation than a flash flood hydrograph. Bales and Wagner (2009) utilized a calibrated HEC-RAS model of the Tar River basin in North Carolina to demonstrate the effects of hysteresis on inundation during Hurricane Floyd in 1999. A plot of water elevation versus discharge revealed four different water surface elevations,

ranging from 9.71 to 11.45 m, for a discharge of 360 m^3/s. Selecting an inundation map from a library with a river stage increment of 0.35 m would have resulted in seven possibilities. The researchers also found that a water surface elevation of 13 m on the rising and falling limbs resulted in an inundation difference of 10%. An alternative to developing inundation maps with a steady flow assumption is to utilize real-time forecasting to estimate inundation. This approach would incorporate the effects of hysteresis in the delineation of flood extent (Bales and Wagner 2009). A significant challenge in developing this framework is constructing hydraulic models capable of running faster than a 1:1 ratio of simulation time to real time.

Disclosure of uncertainty along with inundation boundaries in mapping products would more clearly communicate flood risk. Smemoe, et al. (2007) developed a framework for evaluation and presentation of floodplain uncertainty maps. They created maps by running a hydrologic, hydraulic, and flood plain delineation model. Models were run repeatedly using stochastic probability distribution function values as input parameters, generating a series of flood boundaries. These boundaries were used to create a continuous inundation map showing uncertainties from 0 to 100 percent for a 100 year event.

2.5 Summary

Modeling of flood water movement can be accomplished by analyzing simplified versions of complex natural physical phenomena. The most basic flood modeling methods include reservoir and hydrologic routing, which do not include any physically-based hydraulic parameters. However, they are capable of approximating translation and attenuation of flood peaks through the landscape with some degree of accuracy (Fread and Hsu 1993).

Situations requiring physically based parameters such as floodplain delineation may be modeled using a steady gradually varied flow assumption. The standard step

method is used to iteratively solve the energy equation at consecutive cross-sections in order to find water surface profiles. Development requires cross-section geometries, roughness parameters, structural information, and knowledge of river reach flow paths. Simulation results are used to delineate floodplains and develop appropriate mitigation strategies.

Flooding is a dynamic process, and the modeling of its unsteady nature requires robust governing equations. Using equations of motion and continuity, the Navier-Stokes equations of an incompressible fluid are derived. Although flow is known to be highly three-dimensional in out of bank flow situations, parameters of interest can be obtained using simplified versions of the full Navier-Stokes equations. The section averaged Saint-Venant equations, the simplest version of the Navier-Stokes equations, are widely used in unsteady one-dimensional hydraulic modeling software. Development of a one-dimensional hydraulic model requires cross-section geometries, structural information, roughness parameters, boundary conditions, and sufficient calibration data. However, this modeling approach makes broad assumptions: water level is the constant across an entire cross-section and flow is perpendicular to cross-sections.

Improvements in computational efficiency and affordability have made more detailed simulations of the Navier-Stokes equations feasible. Depth averaging of the Navier-Stokes equations yields the Saint-Venant shallow water equations which can be numerically simulated using a standard desktop computer. MIKE 21 is a widely used commercial software package used to develop two-dimensional hydraulic models. Required data include a computational mesh, boundary conditions, and spatial distributed roughness parameters. A major limitation of typical two-dimensional numerical codes in urban flood modeling is the inability to correctly model submergence or overtopping of bridges.

To overcome the limitations of one-dimensional and two-dimensional hydraulic models, investigators have begun developing 1D/2D coupled models. A one-dimensional

model of the river channel is coupled with a two-dimensional model of the floodplain. Bates, et al. (2000) have shown that coupled models can accurately predict flooding at the reach scale when sufficient calibration data is available. An additional benefit of developing coupled models is that two-dimensional cells only become active when wet; hence, when flow stays within the one-dimensional model, simulation time is likely improved. MIKE Flood is a commercially available software package that provides many options for developing couple 1D/2D models.

Inundation maps are the most useful results produced from flood simulations, but because error is introduced throughout the development process, uncertainties must be considered. Collection of bathymetry data introduces instrument measurement error. The magnitude of error introduced is dependent on the sophistication of the echo-sounder system. Current model calibration practices include minimization of error between observations and simulation results. Model calibration can be improved using a more thorough process such as running Monte-Carlo simulations while utilizing the generalized likelihood uncertainty estimation (GLUE) procedure. The assumption of steady gradually varied flow neglects the effects of hysteresis and likely over predicts inundation. Disclosing modeling uncertainty along with inundation maps would more effectively communicate flooding threat.

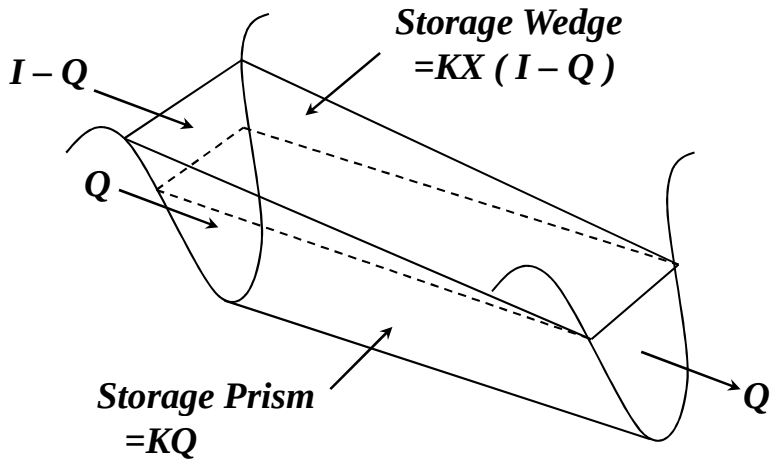

Figure 2.1. Muskingum routing method storage wedge.

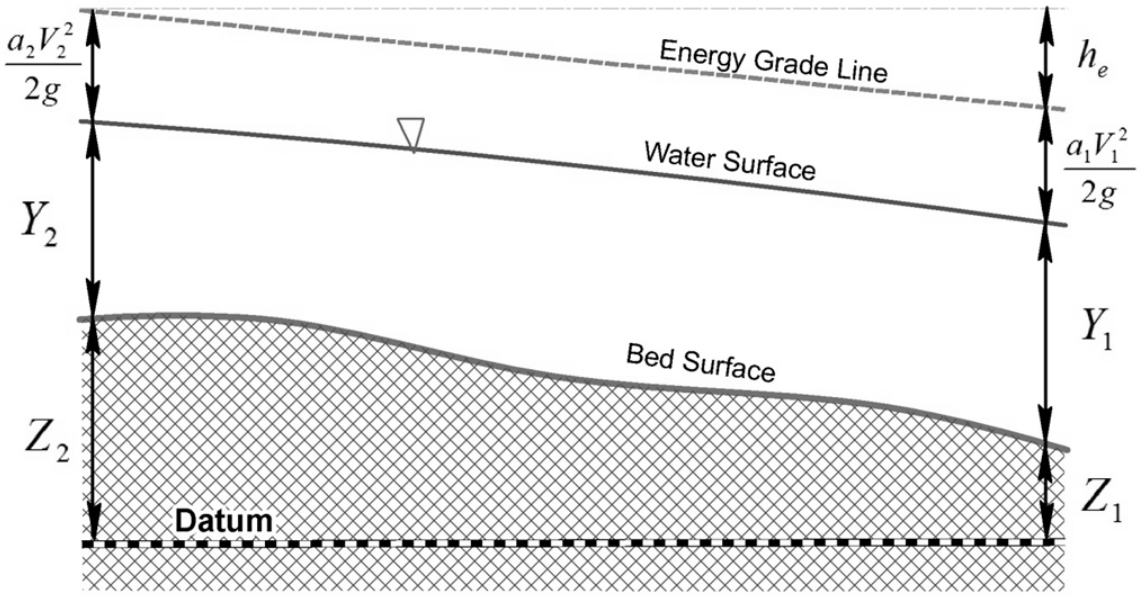

Figure 2.2. Diagram demonstrating terms in the energy equation relating two river cross-sections.

Table 2.1. The standard step procedure used to solve the energy equation.

	Standard Step Method
Step 1	Assume a water surface elevation at an upstream cross-section
Step 2	Based on the assumed water surface elevation, calculate the total conveyance and velocity head
Step 3	Using these values, friction slope and head loss are calculated
Step 4	Solve the energy equation for the water surface elevation at the upstream cross-section
Step 5	Compare the computed water surface elevation with the initial assumed value, continue iterating until values are within an acceptable tolerance

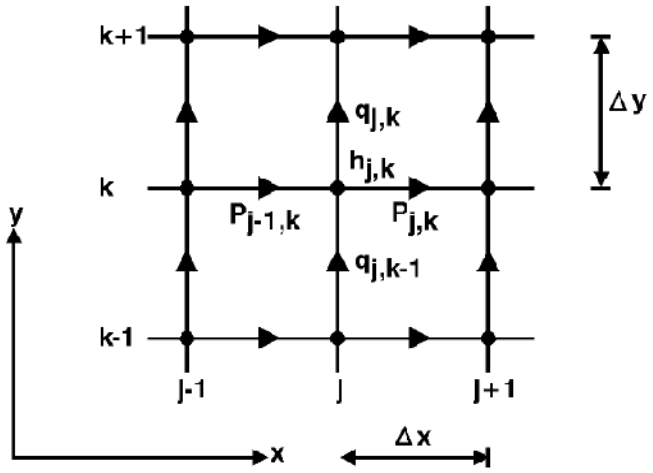

Figure 2.3. Schematic of finite difference grid.

Source: DHI. MIKE 21 Flow Model: Hydrodynamic Module Scientific Documentation. MIKE by DHI, 2009.

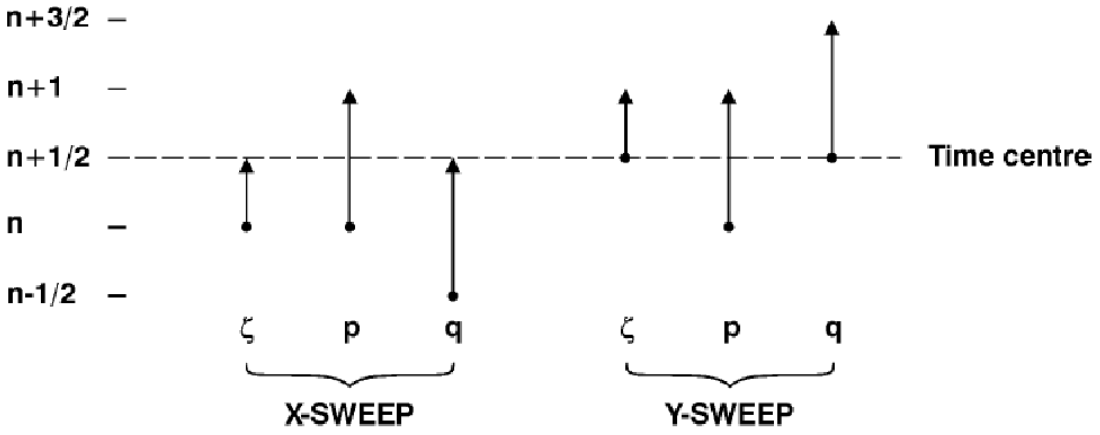

Figure 2.4. Sweep procedure used with time-centering.

Source: DHI. MIKE 21 Flow Model: Hydrodynamic Module Scientific Documentation. MIKE by DHI, 2009.

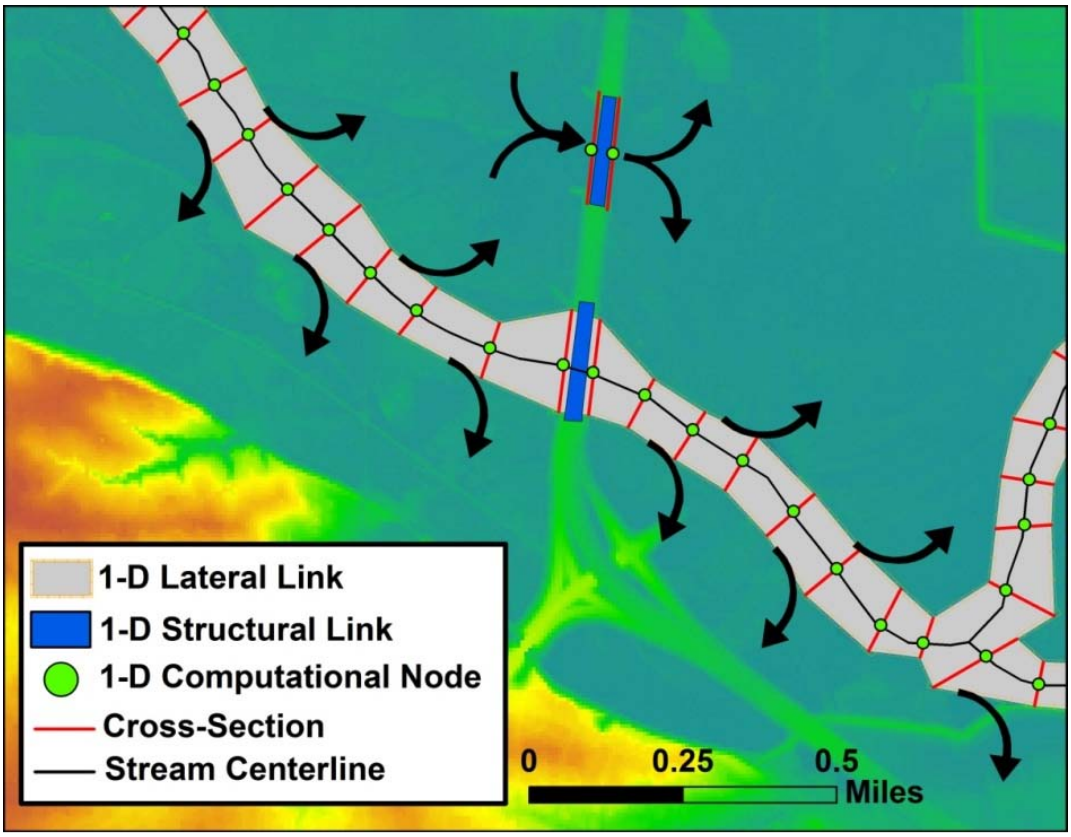

Figure 2.5. MIKE FLOOD allows coupling of 1D hydraulic models to a 2D computational mesh using standard, lateral, and structure links.

CHAPTER III: INVESTIGATION OF CORALVILLE RESERVOIR DURING HIGH FLOW PERIODS

Using a numerical model of Coralville Reservoir provided by The United States Army Corps of Engineers, operational changes and sedimentation effects were investigated for historic flood events. Operational changes included reverting to historic operation plans, major flood pool elevation modification, and relaxation of downstream river stage constraints. Sedimentation effects were investigated by modifying reservoir stage-storage relationships to approximate historic surveyed geometries. Future sedimentation effects were investigated by extrapolating historic trends since the commissioning of Coralville Reservoir in 1958.

3.1 Introduction

Coralville Reservoir was created in 1958 following the construction of the Coralville Dam on the Iowa River. The United States Army Corps of Engineers (USACE) commissioned the reservoir project to provide flood protection for downstream communities (Mutel, 2010). Secondary uses include augmenting flow during drought conditions, improving water quality, creating wildlife habitat, and providing recreational area (Mutel 2010). The reservoir has lost approximately 14% of its storage volume since 1958 and 11% since 1973 (Espinosa-Villegas and Schnoor 2009).

3.1.1 Study location

Coralville Reservoir is located in Johnson County, Iowa, just north of the communities of Coralville and Iowa City, as shown in Figure 3.1. The reservoir regulates 3,115 mi^2 of the Iowa River drainage basin, providing flood protection for many downstream communities including Coralville, Iowa City, Lone Tree, Wapello, and Burlington.

3.1.2 The 2008 Flood

To consider how dredging or operational changes at Coralville Reservoir may affect flood mitigation, it is beneficial to first examine release decisions made by the United States Army Corps of Engineers (USACE) during the spring of 2008. A plot showing observed pool elevation, reservoir inflow, and releases can be seen in Figure 3.2. The current Coralville Reservoir operations plan is included in Appendix A. Preceding the major flood event of June 2008, several spring rainfall events began to fill the reservoir. As a result, the use of flood control storage above the conservation pool began in mid-March. Operations from March to late April utilized the reservoir as it was intended: to lower the peak discharges of unregulated inflow. By using storage to reduce discharges to a maximum of 10,000 cfs during the spring, flooding was initially prevented in downstream communities. However, less storage was available for protection against the most significant rainfall event of 2008.

Releases from Coralville Reservoir are constrained by river stages occurring downstream on the Iowa and Mississippi Rivers. During spring 2008, the downstream constraints at Lone Tree, Wapello and Burlington were active several times, as shown in Figure 3.3. The releases were limited to a maximum of 1,000 cfs, and flood storage capacity was consumed during these periods to prevent flooding at these locations. During late April, the pool elevation was forecast to exceed the major flood pool elevation of 707 feet. Downstream constraints were then disregarded, and the releases were increased to 10,000 cfs. This continued through May until the pool fell below el. 707. The releases were then incrementally decreased to the summer maximum release of 6,000 cfs.

The reservoir inflow volume from March 1st to May 31st totaled approximately 1,600,000 ac-ft. The volume stored in the reservoir at the beginning of June was approximately 260,000 ac-ft., with 160,000 ac-ft. remaining below the spillway crest for flood control. The June event had an inflow volume of 1,300,000 ac-ft, roughly eight

times greater than the remaining storage volume. The remaining storage was quickly consumed and the emergency spillway went into operation on June 9th. The unregulated flow into the reservoir had a peak discharge of approximately 57,000 cfs (Mutel 2010). The peak outflow during the flood was 40,000 cfs, confirming that the reservoir had a significant attenuating effect on the flood hydrograph. The pool elevation peaked at el. 717 ft, which is significant because it corresponds to the upstream flood easements currently held by the USACE. After the pool elevation fell from el. 717 to below the spillway crest, el. 712, the gates regulating the discharge were left fully open to regain flood storage.

3.1.3 Coralville Reservoir sedimentation

Over its lifetime, the Coralville Reservoir has lost storage capacity to sedimentation. Using historical storage curves, found in Appendix B, it is possible to quantify the vertical distribution of storage lost since implementation of the reservoir in 1958. Figure 3.4 illustrates the changes in storage for different elevation ranges through time. This plot indicates that the reservoir storage lost from 1958 to the most current survey in 1999 has occurred primarily in the lower elevations of the reservoir. The cumulative storage lost below the spillway amounts to approximately 71,000 ac-ft, which is approximately 14% of the original 492,000 ac-ft of storage available below the spillway in 1958. The current sediment volume is likely somewhat larger than 71,000 ac-ft, considering the accumulation of additional sedimentation following 1999.

Espinosa-Villegas and Schnoor (2009) found that sedimentation accumulation was decreasing at a rate of 10.6×10^6 kg year^{-1}, which can be seen in Figure 3.5. The overall trap efficiency of the reservoir was 80.3%, as determined using suspended sediment concentrations in the inflow and outflow (Espinosa-Villegas and Schnoor 2009). They believed the changing accumulation was due to a decrease in trapping

efficiency and a decrease in incoming suspended sediment loads as a result of conservation practices.

Had an additional 71,000 ac-ft of storage been available during 2008, it would have been quickly consumed. For example, if all of this storage was available in the flood control zone, and the difference in inflow and outflow were 10,000 cfs, the storage would be used in 3.6 days. Figure 3.6 provides a perspective on the relative volumes of water and sediment associated with the 2008 flood.

Since a large portion of this sedimentation has occurred below the current conservation pool levels, much of the 71,000 ac-ft cannot be recovered for flood storage. Only 38,000 ac-ft of this sediment is currently above the lowest conservation pool elevation. Figure 3.7 depicts flood storage remaining below the spillway according to pool elevation. From this figure, it is apparent that sedimentation has affected storage up to el. 695, but it has had the most effect below el. 685. The full utilization of any dredged storage would require drastically lowering the conservation pool, which could negatively affect wildlife habitat and recreation.

3.2 Motivation

Flooding downstream from the Coralville Reservoir in 1993 and 2008 motivated stakeholders to explore ways of managing the reservoir sedimentation and operations. This study quantifies the impact of dredging and changes to the current Coralville Reservoir operations schedule on attenuation of major flood events. Model scenarios constructed from combinations of historic storage curves, historic operations plans, and significant hydrologic events that occurred in 1993 and 2008 are used to perform the evaluation. While this study seeks to characterize these impacts, feasibility will depend upon social, ecological, and financial factors identified by stakeholders in the lower Iowa River corridor. These may include time constraints, permitting, waste disposal, adverse wildlife or habitat effects, and cost.

3.3 Methodology

This study used an existing numerical model of Coralville Reservoir to evaluate changes in operations and storage capacity. In an effort to validate the model, the 2008 flood hydrographs were used in an attempt to reproduce observed releases. Using the flood simulation results as a baseline, storage and operational procedures can be modified in order to observe any improvements in flood attenuation. To determine the impact of dredging, several historical reservoir storage curves were utilized in different simulations and compared to the established baseline. The impact of downstream constraints was explored in an effort to determine any benefits relaxation may provide. Future sedimentation was predicted by extrapolating the historical trend in overall storage lost. Simulations utilizing predicted storage curves were executed and compared.

3.4 Numerical simulation

3.4.1 HEC-ResSim model

To evaluate changes in operations and storage capacity curves, a HEC-ResSim model of the Coralville Reservoir and associated downstream reaches was developed using an existing model provided by the USACE Rock Island District. HEC-ResSim software utilizes reservoir elevation-storage curves, inflow hydrographs, and user-defined operation rules. The historic reservoir elevation-storage curves and operations were also obtained from the USACE Rock Island District. The historic reservoir elevation-storage curves, shown in Appendix B, were developed from surveys conducted in 1958, 1964, 1975, 1983, and 1999. Appendices A, D, and E show the historic operational rules from 2001, 1983 and 1964, respectively. The 1993 and 2008 hydrographs used in the model were constructed from gaged time-series flow data obtained from the United States Geological Survey (USGS). The model included flow data for the Iowa River (downstream of Coralville Dam, at Iowa City, IA, at Lone Tree, IA, and at Wapello, IA), Clear Creek (at Coralville, IA), Rapid Creek (near Iowa City, IA) , English River (at

Kalona, IA), Old Man's Creek (near Iowa City, IA), the Cedar River (near Conesville, IA), and the Mississippi River (at Muscatine, IA and at Burlington, IA).

The HEC-ResSim software completes several tasks at each time step. The model determines the volume required to store the reservoir inflow and determines a corresponding rise in reservoir pool elevation based on a reservoir storage curve. A release discharge is determined based on adherence to the user defined operation plan. The magnitude of release prescribed by the operation plan is based any combination of reservoir pool elevation, downstream constraints, date, or reservoir inflow. If routing calculations indicate that a potential release will violate a downstream constraint, the release is decreased. After the reservoir pool elevation reaches a certain level, downstream constants are ignored for most reservoir operation plans.

3.4.2 Downstream constraints

The current reservoir operation manual, shown in Appendix A, treats Coralville/Iowa City, Lone Tree, Wapello, and Burlington as downstream constraints. The discharge constraint at Coralville/Iowa City is intended to prevent flash floods from other small tributaries. The other downstream constraints are based on river stages and change depending on time of year.

3.4.3 Assumptions/limitations

An important model consideration was reservoir inflow. A stream gage is located upstream of Coralville Reservoir at Marengo. However, it does not account for local drainage from the 320 mi^2 ungaged area between Marengo and the reservoir outlet. Reservoir inflow was therefore computed by summing the measured discharge at the stream gage immediately below Coralville Dam and the change in reservoir storage for each model time step.

Local inflows from ungaged areas downstream of Coralville Reservoir are not considered in the model. Ungaged flows may influence hydrographs downstream of

Coralville Reservoir. However, a complete and fully accurate reconstruction of historic flood events is not the goal of the present effort. The exclusion of local drainage downstream of the reservoir does not prevent the assessment of reservoir sedimentation and operations on flood mitigation.

3.4.4 Model validation

A simulation was configured in an effort to reproduce release decisions during the 2008 flood. The simulation utilized 2008 hydrographs, the most recent elevation-storage curve, and the 2001 operation plan. A comparison between simulated and observed hydrographs, shown in Figure 3.8, shows there are differences in releases several times during the simulation period. These occurred during mid-March, late April, and following the largest event in late June. During mid-March and late April, downstream constraints were active and observed releases were approximately 1,000 cfs. The model also responded to the downstream constraints, but released at higher discharges. This is likely a result of the model's use of observed, rather than forecasted hydrologic data. In spite of these operational differences, the model was able to replicate the observed peak discharge.

The operations plan used for the simulation shown in Figure 3.8 was modified to replicate the observed release decisions in an effort to demonstrate model validity. The operations were only altered only at points where the observed data differed from the operational rules. For example, deviation occurred when the primary outlet gates were left fully open to recover flood storage after the 2008 flood peak in late June. Model operations were altered during this period to reproduce this operation decision. The results from this simulation are shown in Figure 3.9. These modifications are only applicable to the 2008 event and are not valuable when comparing dredging and operational alternatives. Therefore, the modified operational rules depicted in Figure 3.9

were not used in further analyses. The simulated releases shown in Figure 3.8 were used as a baseline condition to evaluate any changes in storage and operation rules.

A simulation scenario was also configured in an effort to reproduce release decisions during the 1993 flood. This simulation utilized the 1993 event, the most recent elevation-storage curve, and the 2001 operations plan. A comparison between the simulated and the observed values, shown in Figure 3.10, indicates several discrepancies. The major discrepancies occur in late April, mid-July, early August, and early September. The discrepancy in late April is a result of the simulation's pool elevation being below the major flood pool while a downstream constraint remained active. The discrepancy in mid-July occurs at the peak discharge. The USACE partially closed the release gates to induce a surcharge, which ultimately lowered the peak discharge (Mutel 2010). As a result, the reservoir reached el. 717, which was higher than the peak elevation of el.715 produced by the simulation. The observed peak discharge was 25,000 cfs, while the simulated peak discharge was 27,500 cfs. The other discrepancies occurred when the gates were left open to regain flood storage after large peak discharges. The simulated releases shown in Figure 3.10 were used as a baseline condition to evaluate changes in storage and operation rules.

3.5 Results and discussion

3.5.1 Impact of dredging

This scenario is intended to demonstrate the impact of dredging alone. This scenario used the 2008 event, current operational rules, and conservation pool elevation, while varying the reservoir's stage-storage curve. Stage-storage relationships were modeled according to the historical curves shown in Appendix B. The 1999 storage curve was used as the base 2008 configuration. The simulation begins three months prior to June 2008, the last time prior to the 2008 event that the pool elevation equaled the conservation pool. This is an ideal initial condition for the model because once the pool

elevation reaches the conservation pool, any previous operations do not contribute to future pool elevation changes or releases. The results of this simulation are shown in Figure 3.11.

Additional storage from dredging was consumed in early May. Flow was limited to 1,000 cfs by an active downstream constraint from late April until early May when the pool elevations reached the major flood pool. Downstream constraints were then disregarded and releases were regulated by height above the major flood pool. Pool elevations reached the major flood pool level in the order of storage from least to greatest. All the trials in this scenario behaved similarly after reaching the major flood pool. The peak discharge for all trials was approximately 41,000 cfs, slightly higher than the observed discharge of 40,000 cfs.

To demonstrate the impact of conservation pool elevation alteration in addition to dredging, a simulation was configured to utilize the 2008 flood hydrographs and current operational rules while varying the reservoir's stage-storage relationship and conservation pool elevation. Each storage curve has a corresponding historical conservation pool that must be utilized to take advantage of additional storage capacity. Historic changes in the conservation pool are documented in Appendix C, and the results of this simulation are shown in Figure 3.12.

Dredging would allow downstream constraints to be observed for longer periods before the pool elevation would enter the major flood pool. This could possibly prevent some flooding in downstream communities from minor rainfall events. However, for extreme flooding events, dredging has no significant impact on the peak discharge.

Another scenario was designed to demonstrate the impact of dredging and conservation pool alterations with no changes to the current operations plan. This scenario used the 1993 event and the current operational rules while varying the reservoir's stage-storage relationship and conservation pool elevation. The results of this simulation are shown in Figure 3.13. Results were similar to those associated with the

2008 flood. Any additional storage was used in the early spring before the major event as a result of downstream constraints remaining active until additional storage is used. The behavior is nearly identical for all storage curves once simulated pool elevations reach the major flood pool.

3.5.2 Impact of dredging and operational changes

A scenario was designed to examine the impact of both dredging and operational changes at Coralville Reservoir on the 2008 flood event. Historic stage-storage curves and their corresponding operational plans were used to characterize potential benefits, as shown in Figure 3.14.

All of the simulations in this scenario produced an identical peak discharge slightly larger than the observed peak. The release procedure in Schedule C of the operations for 1983, 1975, and 1964 are such that the pool levels oscillate around the major flood pool elevation. This is a result of prescribed releases in Schedule C of the 1964 and 1983 operations, which lower pool elevation slightly below the flood control pool when the Lone Tree constraint of 5,000 cfs becomes active. The flow is then limited by active downstream constraints; consequently, pool elevation rises above the major flood pool once again.

A similar scenario was designed to examine the impact of both dredging and operational changes at Coralville Reservoir on the 1993 flood event. Historic stage-storage curves and their corresponding operational plans were used to characterize potential benefits. The results for this scenario, shown in Figure 3.15, also show the pool elevations oscillating at the major flood pool for the historic operations. There was no significant change in the peak discharge.

3.5.3 Impact of downstream operational constraints

A series of simulations were performed to evaluate the impact that adherence to downstream constraints had on reservoir releases during the 2008 flood and to assess

potential benefits of modifying constraints to improve major flood mitigation. Active downstream constraints during 2008 are shown in Figure 3.3. Constraints include the maximum summer release, and stage limitations at Lone Tree, Wapello, and Burlington. River stage constraints for Lone Tree, Wapello, and Burlington can be seen in the current operations plan located in Appendix A.

3.5.3.1 Maximum summer releases

A proposal to increase the maximum summer release from 6,000 cfs to 8,000 cfs was rejected by the downstream communities in 2001, as documented in Appendix C. Simulation results in Figure 3.16 characterize changes in 2008 flood discharges associated with an increased maximum summer release of 8,000 cfs. There was no significant change in peak discharge.

3.5.3.2 Burlington, Iowa Mississippi river stage constraint

Simulation results in Figure 3.17 characterize changes in 2008 flood discharges associated with disregarding the Burlington Mississippi River stage constraint in the current operations plan. There was no significant change in peak discharge.

3.5.3.3 Lone Tree, Iowa river stage constraint

Simulation results in Figure 3.18 characterize changes in 2008 flood discharges associated with disregarding the Lone Tree Iowa River stage constraint in the current operations plan. There was no significant change in peak discharge.

3.5.3.4 Wapello, Iowa river stage constraint

Simulation results in Figure 3.19 characterize changes in 2008 flood discharges associated with disregarding the Wapello Iowa River stage constraint in the current operations plan. There was no significant change in peak discharge.

3.5.3.5 Cumulative impact of all downstream constraints

Simulation results shown in Figure 3.20 disregard all downstream constraints to preserve reservoir storage. Results indicate a decrease of 2,000 cfs in the 2008 peak discharge. Relaxation of downstream constraints has the potential to augment the reservoir's impact on major flood events, but at the cost of increasing the frequency of annual flood damage from smaller events.

3.5.4 Impact of major flood pool elevation

Downstream constraints are currently disregarded when the reservoir pool reaches the major flood pool elevation of 707 ft. Alternate major flood pool elevations associated with both more aggressive and less aggressive reservoir operations were considered. The more aggressive trial used the major flood pool at el.700 ft, while the less aggressive trial used the major flood pool prior to 1991, el.710.4 ft. Changing the major flood pool elevation also required changing graduated releases in Schedule B of the current operations in Appendix A. These changes are shown in Figure 3.21.

3.5.4.1 2008 flood event

This scenario investigated how the 2008 peak discharge is affected by changing the major flood pool elevation. Simulation results are shown in Figure 3.22. Raising the major flood pool elevation had no effect on the peak discharge. However, the change resulted in additional flooding from a 15,000 cfs release following the small hydrologic event in late July. Lowering the major flood pool elevation from el.707 to el.700 and using the prescribed releases in Figure 20 decreased the peak discharge by approximately 3,000 cfs.

3.5.4.2 1993 flood event

This scenario used the 1993 event, the prescribed releases in Figure 3.21, and the current operations. Results in Figure 3.23 show there was a decrease in the minor peaks

as a result of changing the major flood pool from el. 707 to el. 700. With a lower major flood pool, active constraints were ignored in late April and more storage was available in July. However, there was no significant decrease in peak discharge in late July.

3.5.5 Predicted impact of future sedimentation

3.5.5.1 Predicted sedimentation

Predicting future sedimentation is challenging due to its event-driven nature. This is evident when comparing USACE surveys from 1983 and 1999, as shown in Figure 3.24. Approximately 40,000 ac-ft of sediment accumulated in the reservoir from 1983 to 1999. Approximately half of this sedimentation occurred below el. 685 ft, while the other half occurred above el. 690 ft. The distribution of sediment deposited above el. 690 ft did not follow the trend from the previous surveys. Historically, the majority of sedimentation occurred in the lowest elevations of the reservoir. The 1993 flood was likely a major contributor to the quantity and distribution of sedimentation that occurred during this period.

Future sedimentation was estimated using the historic elevation-storage curves. High levels of uncertainty associated with sedimentation estimates must be considered when interpreting simulation results. The most significant source of uncertainty is the lack of available survey data following the 2008 flood. As with the 1993 event, the 2008 flood likely deposited a large volume of sediment over a broad range of elevations.

Linear extrapolation of trends from historic elevation-storage curves was used to estimate future sedimentation. Figure 3.25 shows the data points used to establish a linear regression based on total sediment below el. 720. The 1999 elevation storage curve was translated to match the total volume of sediment predicted by the regression analysis. The results are shown in Figure 3.26. While linear extrapolation of historic trends neglects changes in trapping efficiency over time and likely over-predicts the

future sedimentation rate, the method provides a conservative estimate of the reservoir's lifetime.

3.5.5.2 2008 Flood with predicted sedimentation

This scenario is intended to evaluate the impact of possible future reservoir geometries on flood events similar to the 2008 flood. The simulation used the predicted elevation-storage curves from Figure 3.26 and the 1999 survey. The operations were assumed to remain unchanged, while the conservation pools were raised to el. 685 for 2020, el. 687.5 for 2040, and el. 690 for 2060 to accommodate wildlife habitat and recreation. The results for this scenario are shown in Figure 3.27. There is essentially no change in the peak discharge. For all scenarios considered, the reservoir enters the major flood pool in late April and early May, and downstream constraints are then disregarded. Additional sedimentation is shown to have some effect on how long downstream constraints can be observed.

3.5.5.3 1993 Flood with predicted sedimentation

This scenario evaluated the impact of sedimentation on events similar to the 1993 flood. Operations were assumed to remain unchanged, while the conservation pool was raised to el. 685 for 2020, el. 687.5 for 2040, and el. 690 for 2060 to accommodate wildlife habitat and recreation. Results for this scenario are shown in Figure 3.28. There is essentially no change in peak discharge. As with the 2008 event results, sedimentation affects how long downstream constraints are observed.

3.6 Summary

The volume of storage lost to sedimentation in Coralville Reservoir is small compared to the storage available. Additionally, the majority of the sedimentation has occurred below the current conservation pool, having little effect on the capacity of the reservoir to attenuate floods. Utilizing any storage recovered by dredging would require

lowering the current conservation pool, which may negatively impact recreation and wildlife habitat.

Dredging would provide limited additional flood protection against major floods similar to 2008. The large volume of water associated with such events rapidly consumes any additional storage gained from dredging. Both the 1993 and 2008 events occurred after exceptionally wet springs that consumed storage prior to the most severe events. Dredging may have a greater impact on smaller, more frequent flood events; however, additional analyses would be necessary to quantify such benefits and determine whether such measures would be economically justified.

Future sedimentation will have no effect on the peak discharges of events like 1993 and 2008 based on the predicted sedimentation. The additional sediment will affect the duration that downstream constraints are observed in order to prevent minor floods. Future sedimentation will also adversely affect the ability to augment flow during dry periods. A more recent survey would provide further information to help predict sedimentation and evaluate impacts on low flow augmentation.

The most effective method for managing a large flooding event is to maximize available storage preceding its occurrence. Using a more aggressive operations plan would increase available storage should a large event occur. However, the benefits demonstrated in the analyses described above are not substantial. Furthermore, aggressive operations would frequently flood downstream communities, in most cases unnecessarily. A flood frequency and economic assessment would provide information necessary to determine whether aggressive operational practices may provide an overall benefit to stakeholders downstream of Coralville Reservoir.

Figure 3.1. Coralville Reservoir regulates approximately 3,115 square miles of the Iowa River basin.

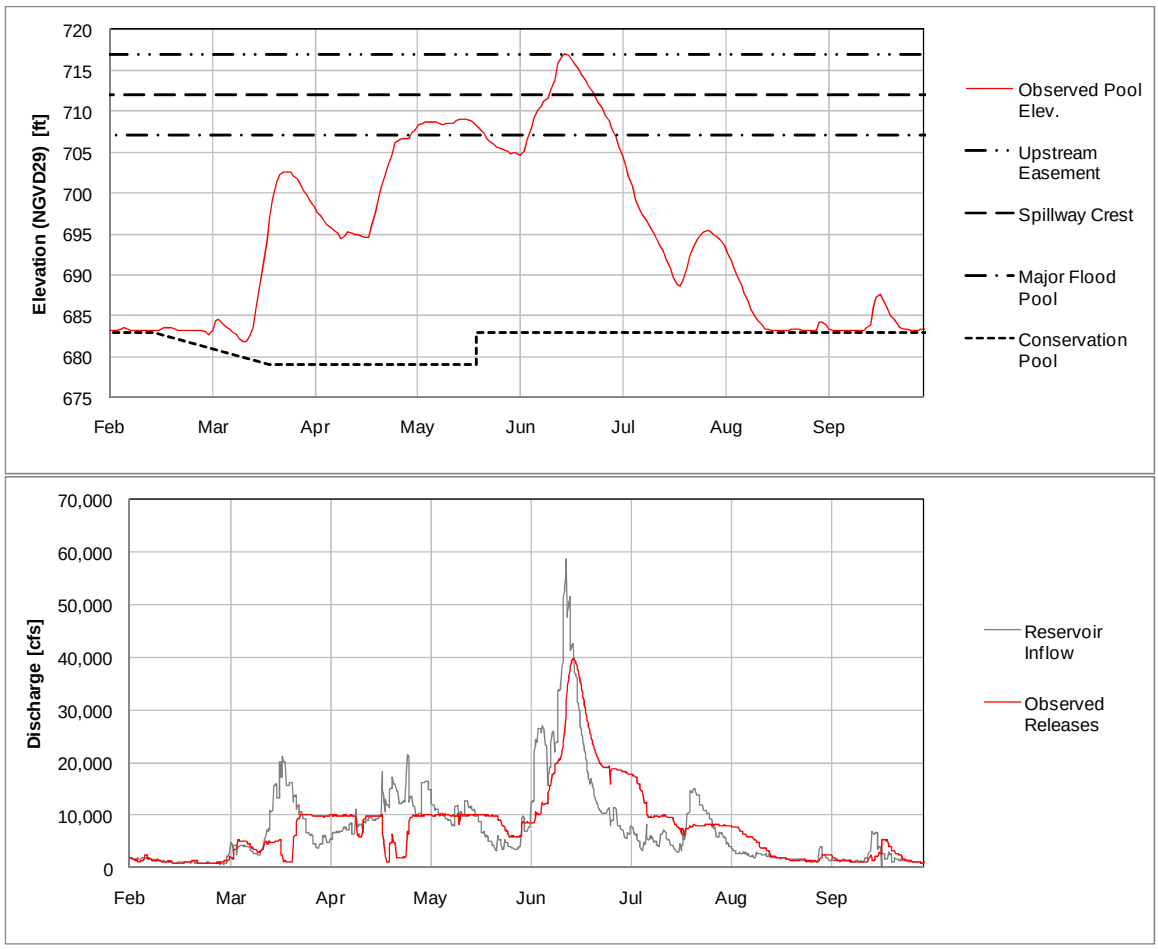

Figure 3.2. Observed reservoir pool elevation, inflow, and releases during the 2008 flood.

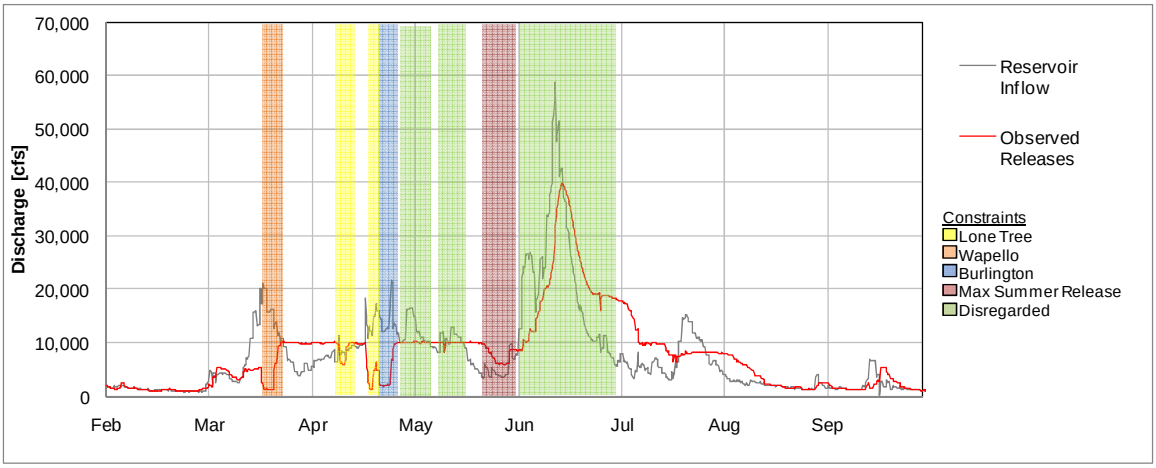

Figure 3.3. Active constraints during the 2008 flood. Some constraints were disregarded due to the pool elevation being within the major flood pool.

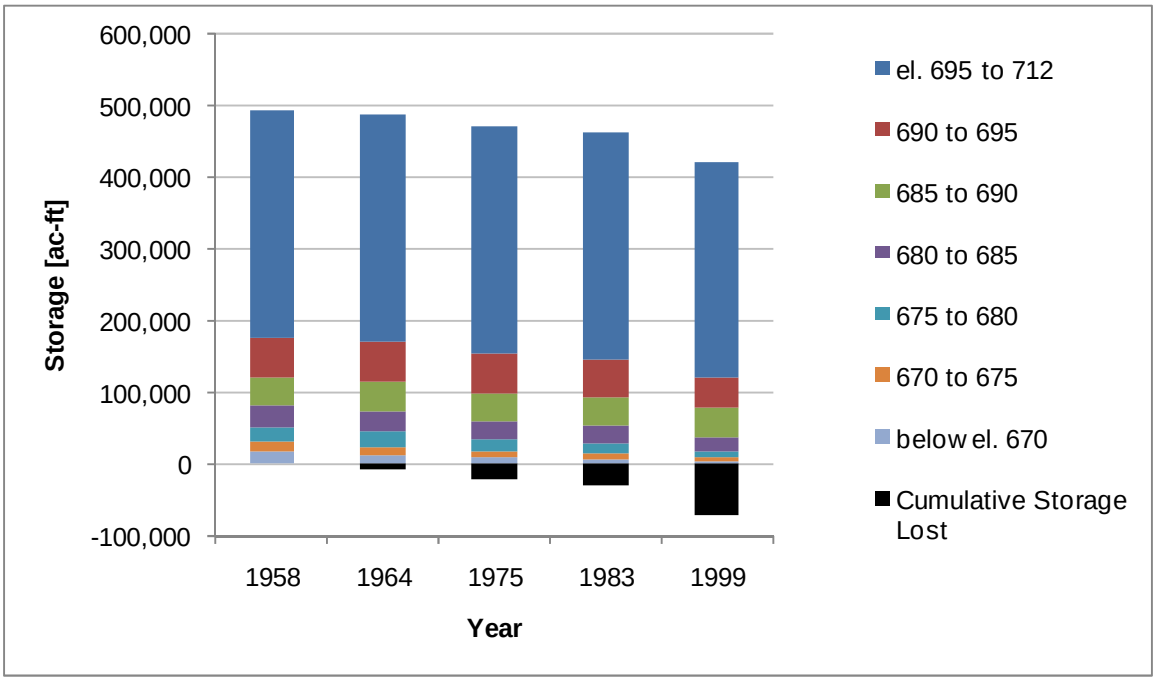

Figure 3.4. Changes in storage (ac-ft) for different elevation ranges below the spillway elevation through time.

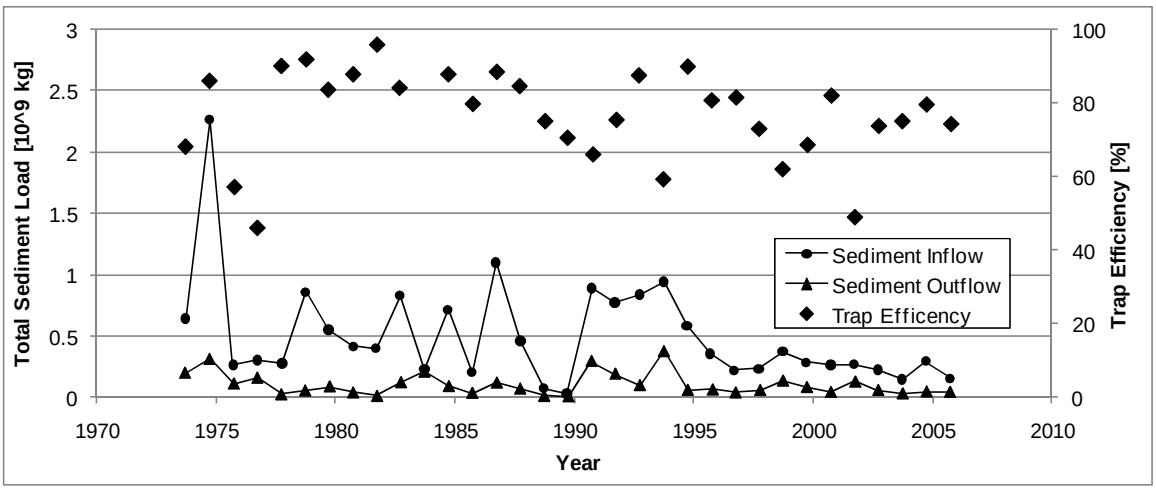

Figure 3.5. Sediment fluxes and reservoir trapping efficiency for Coralville Reservoir.

Source: Espinosa-Villegas, C.O., and J.L. Schnoor. "Comparison of Long-Term Observed Sediment Trap Efficiency with Empirical Equations for Coralville Reservoir, Iowa." *Journal of Environmental Engineering*, 2009: 518-525.

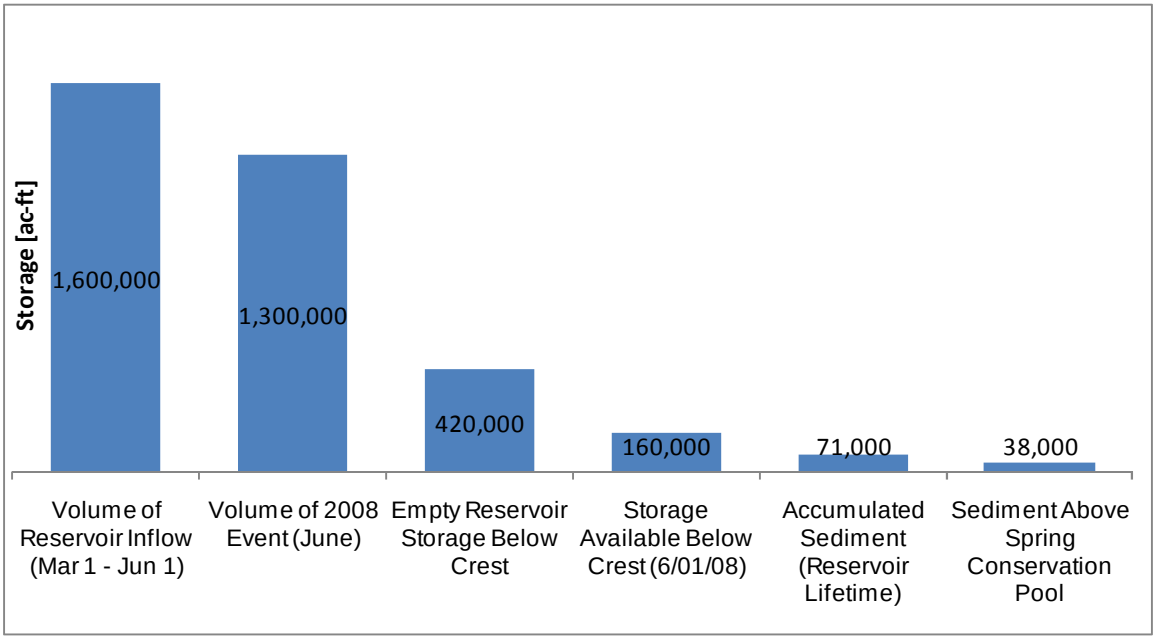

Figure 3.6. Volumes associated with the 2008 flood.

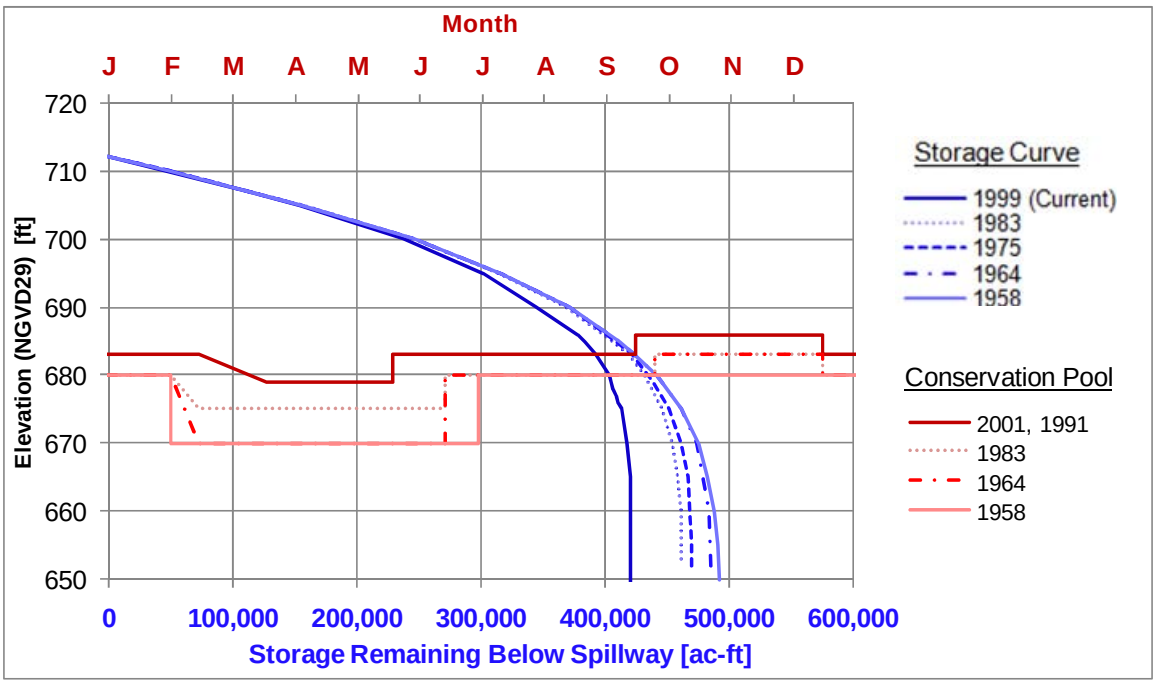

Figure 3.7. Flood storage remaining below the spillway according to pool elevation. The extent of the sedimentation is demonstrated by the deviation of storage curves from the original capacity in 1958. The storage in the upper elevations of the reservoir has remained relatively unchanged.

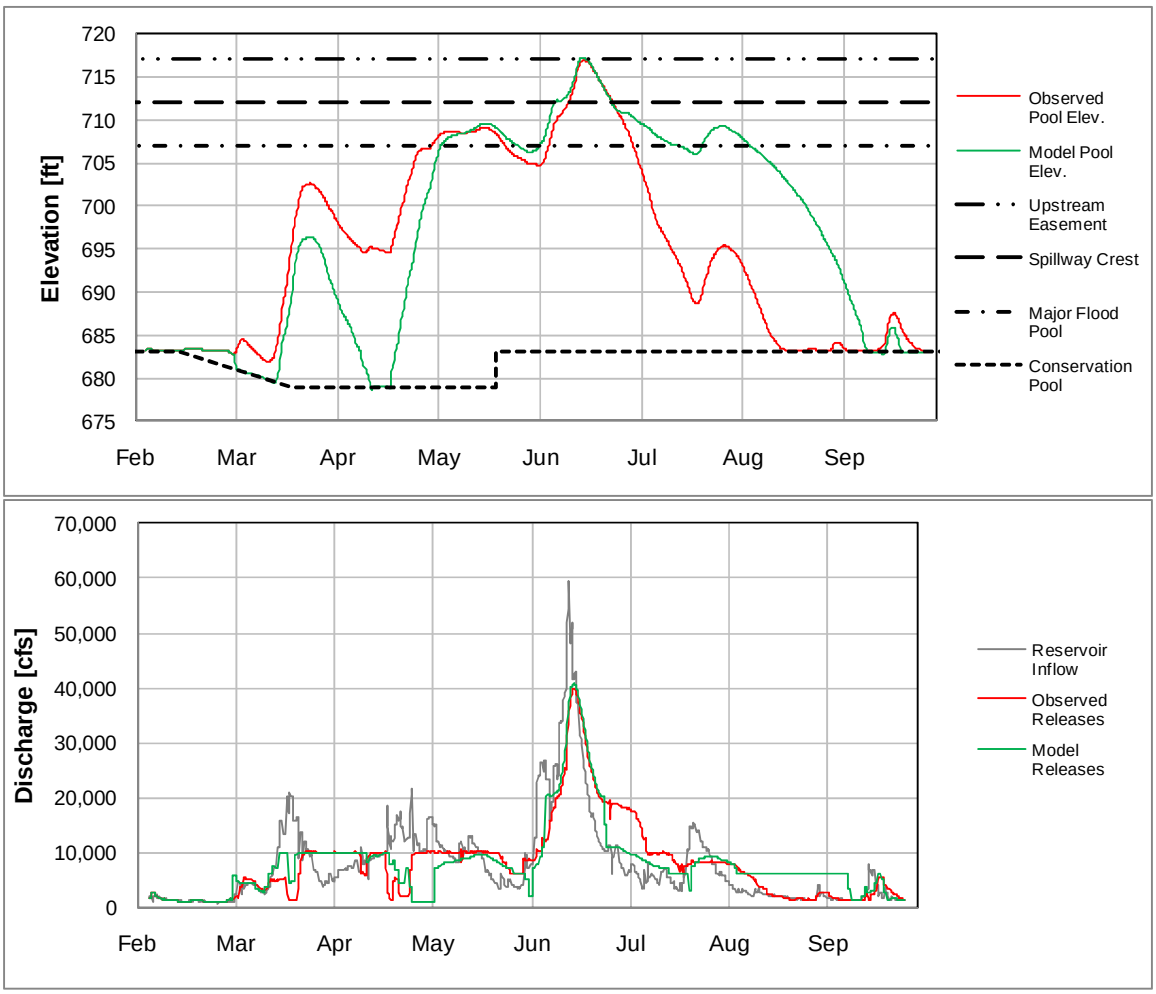

Figure 3.8. Comparison of model simulations using 2008 event, 1999 elevation-storage curve and 2001 operations plan with observed data. Difference in releases can be attributed to the inability to replicate decisions made using forecasted river stages and discharges.

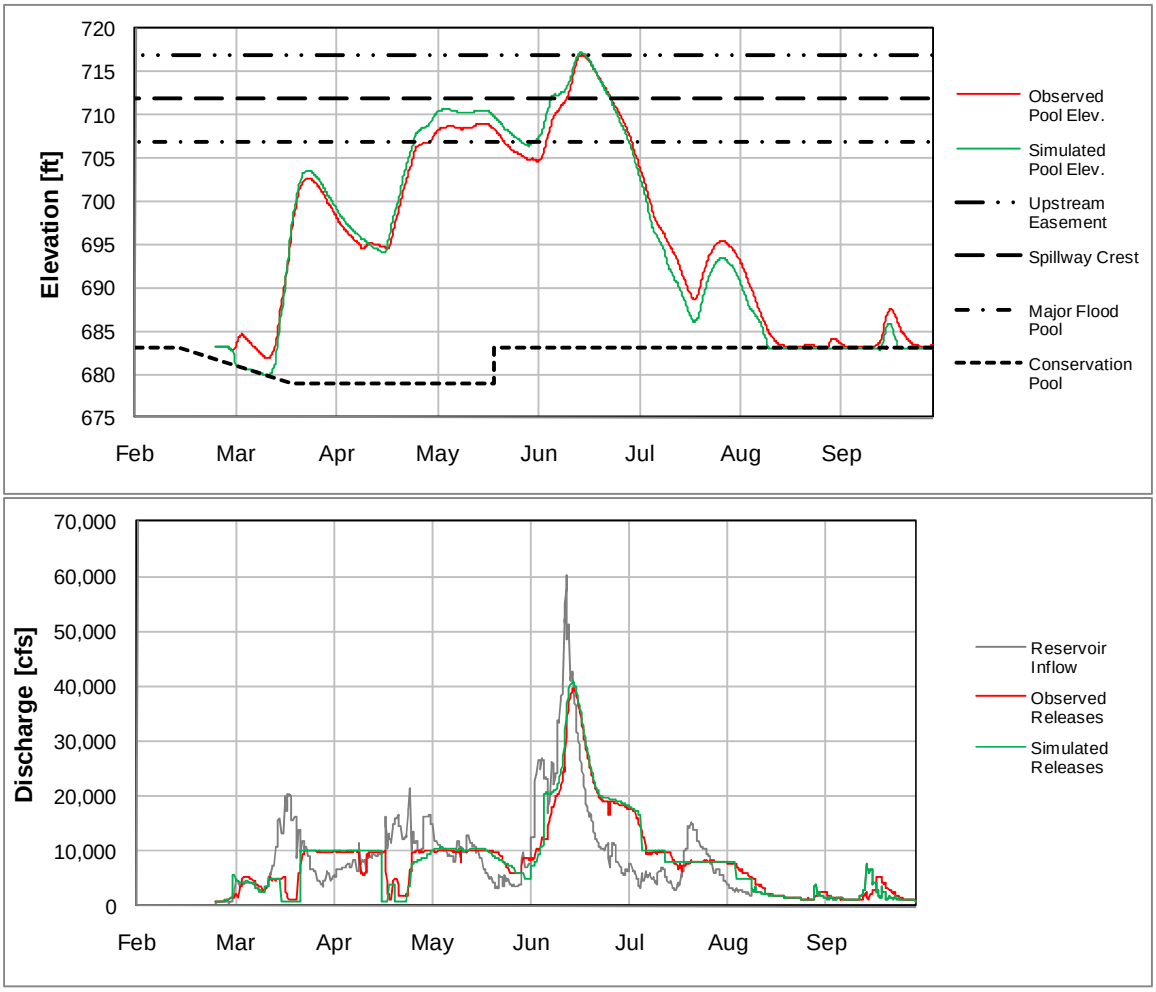

Figure 3.9. Simulation utilizing a modified form of the 2001operations plan to replicate the observed release decisions. This modified operations plan is only applicable to the 2008 event, and was not used to evaluate the impacts of dredging.

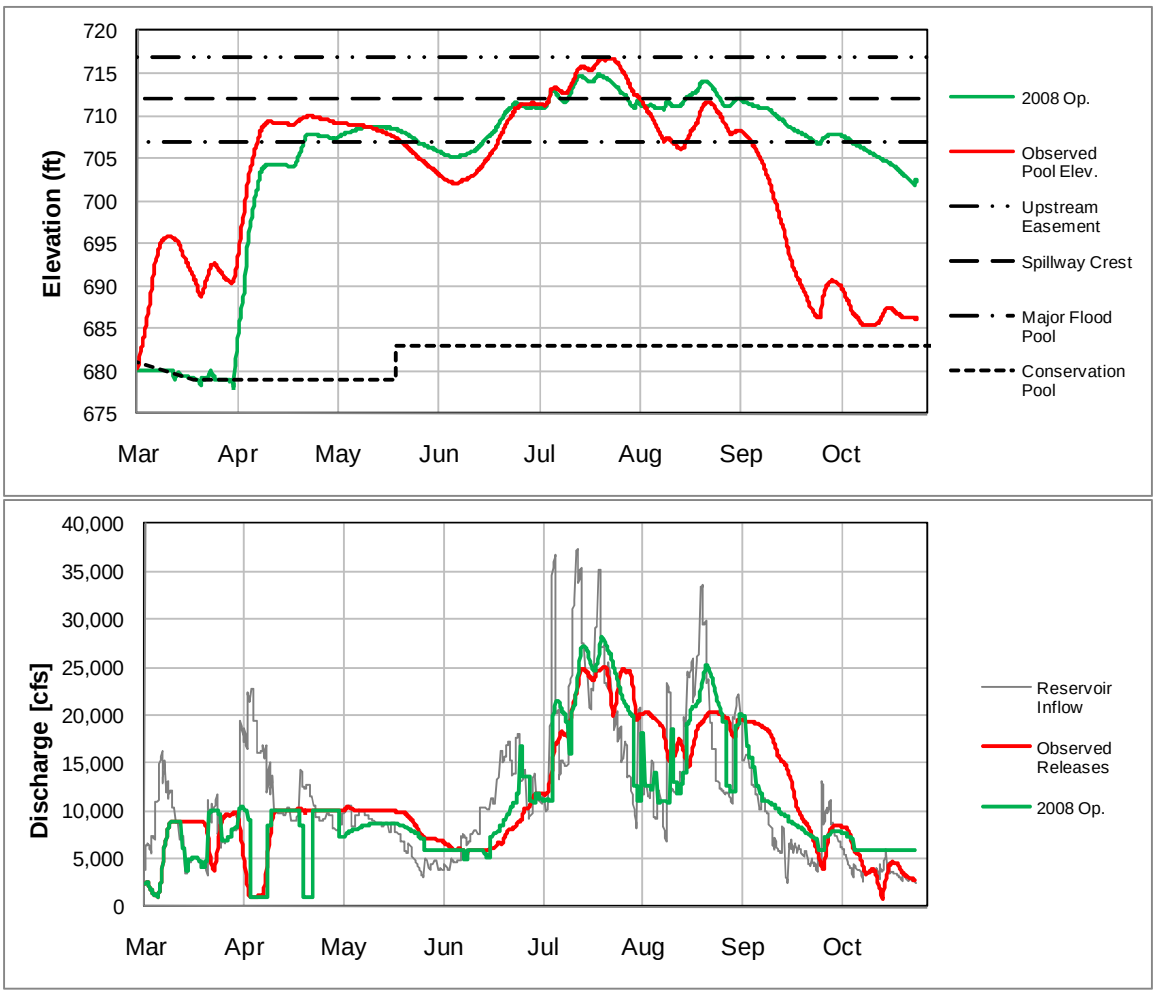

Figure 3.10. Comparison of simulation of 1993 flood to observed data.

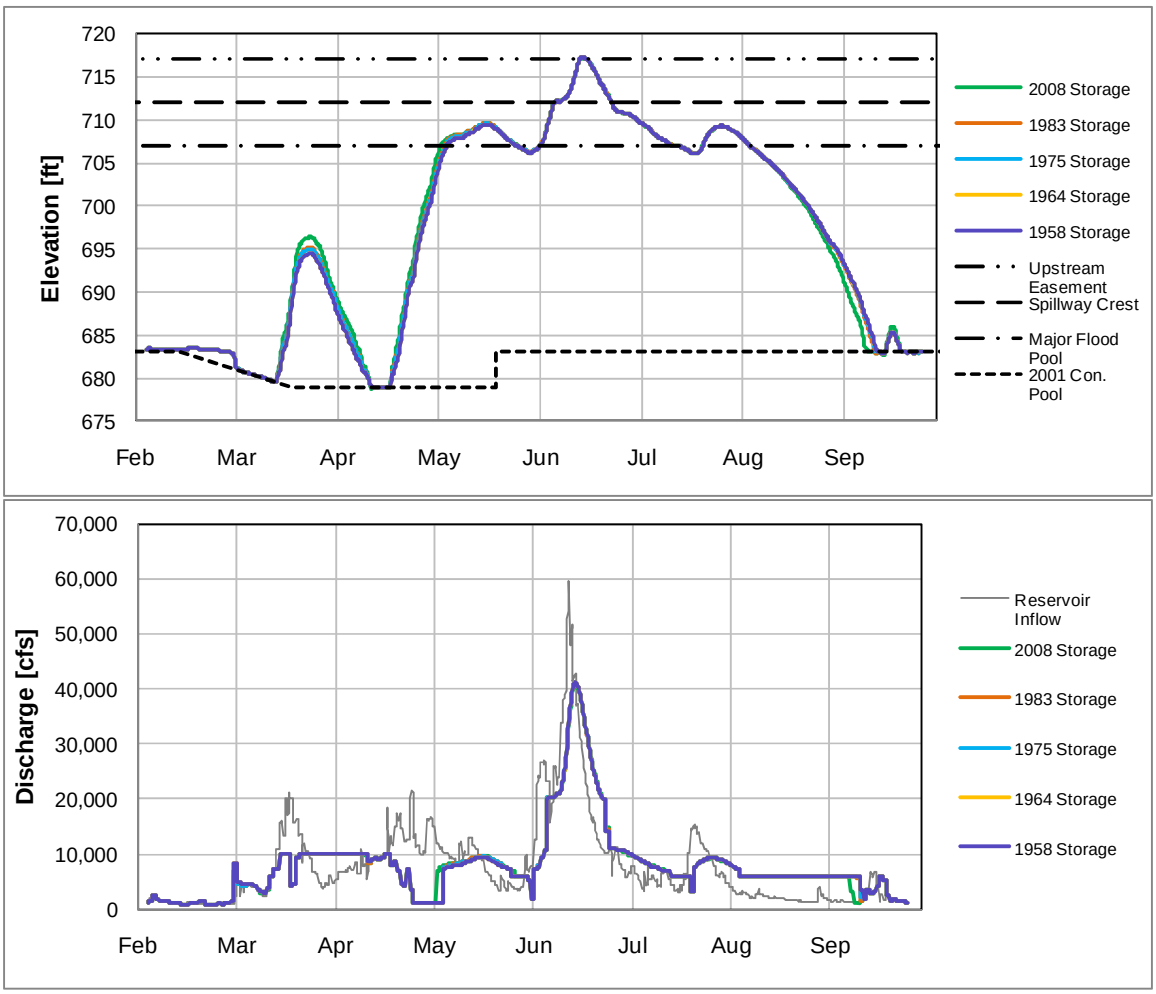

Figure 3.11. Simulation using 2008 flood event, 2001 operations plan, 2001 conservation pool, and varied storage curves

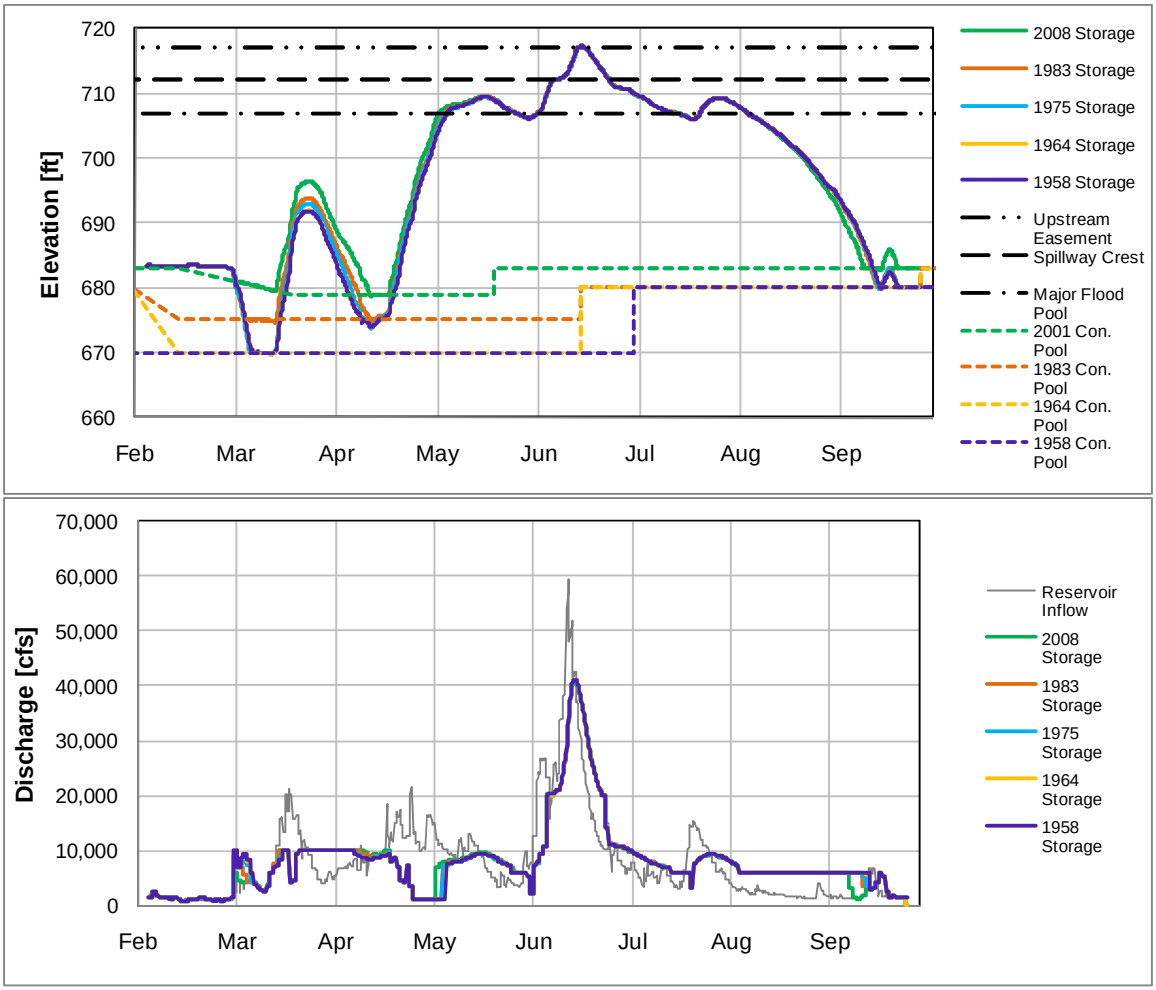

Figure 3.12. Simulation using 2008 flood event, 2001 operations, and varied storage curves and conservation pools

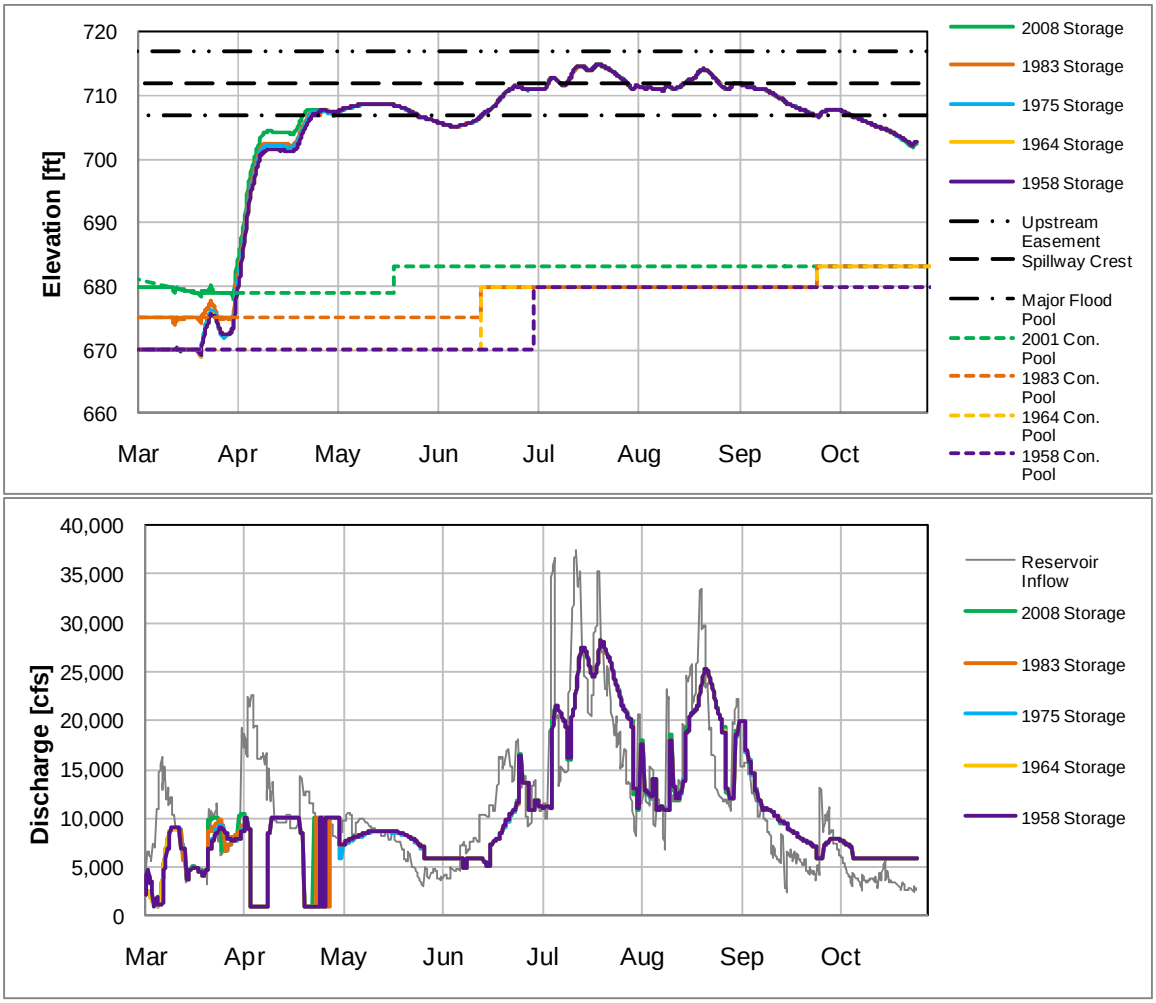

Figure 3.13. Simulation using 1993 flood event, 2001 operations, and varied storage curves and conservation pools

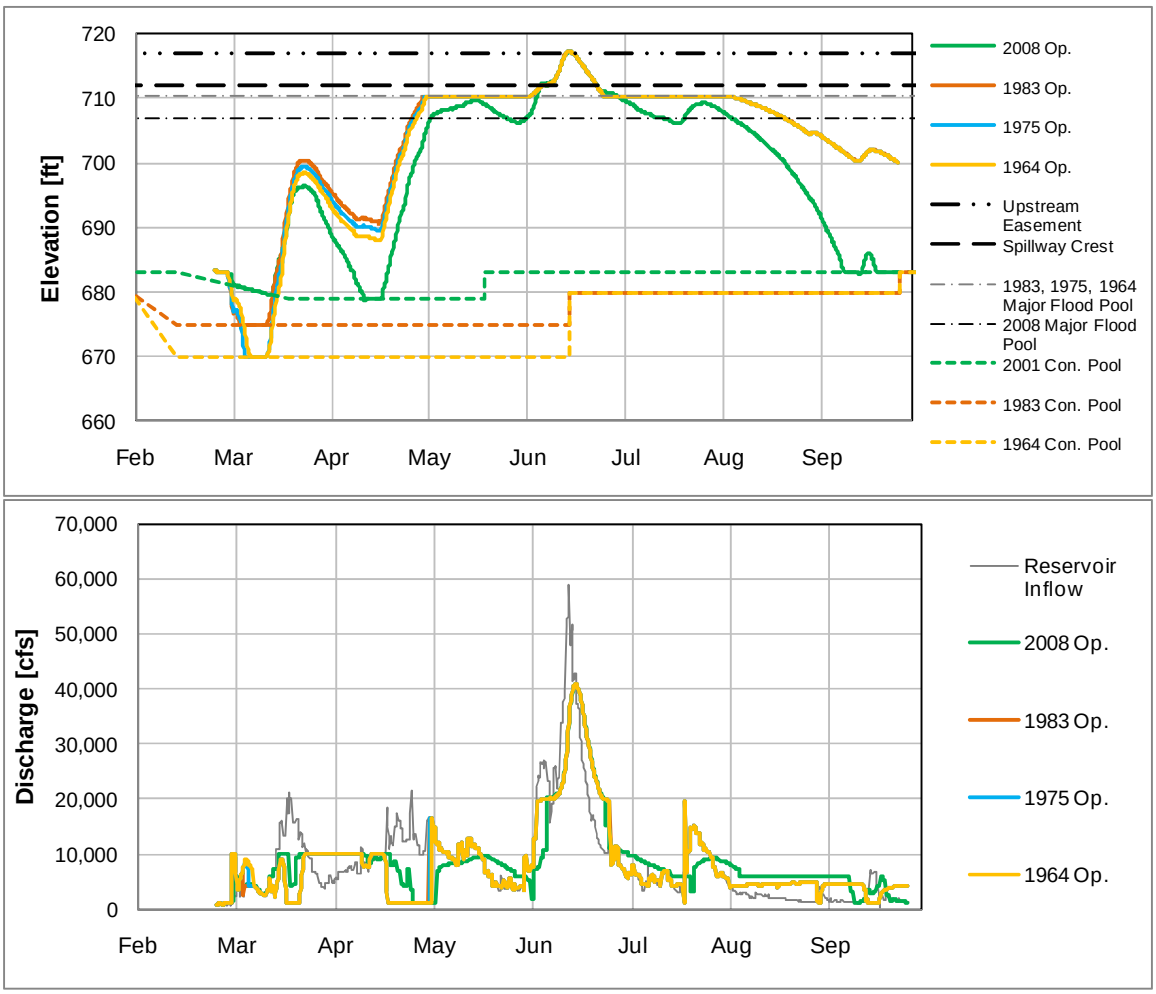

Figure 3.14. Simulation using 2008 flood event, varied historical operations, storage curves, and conservation pools

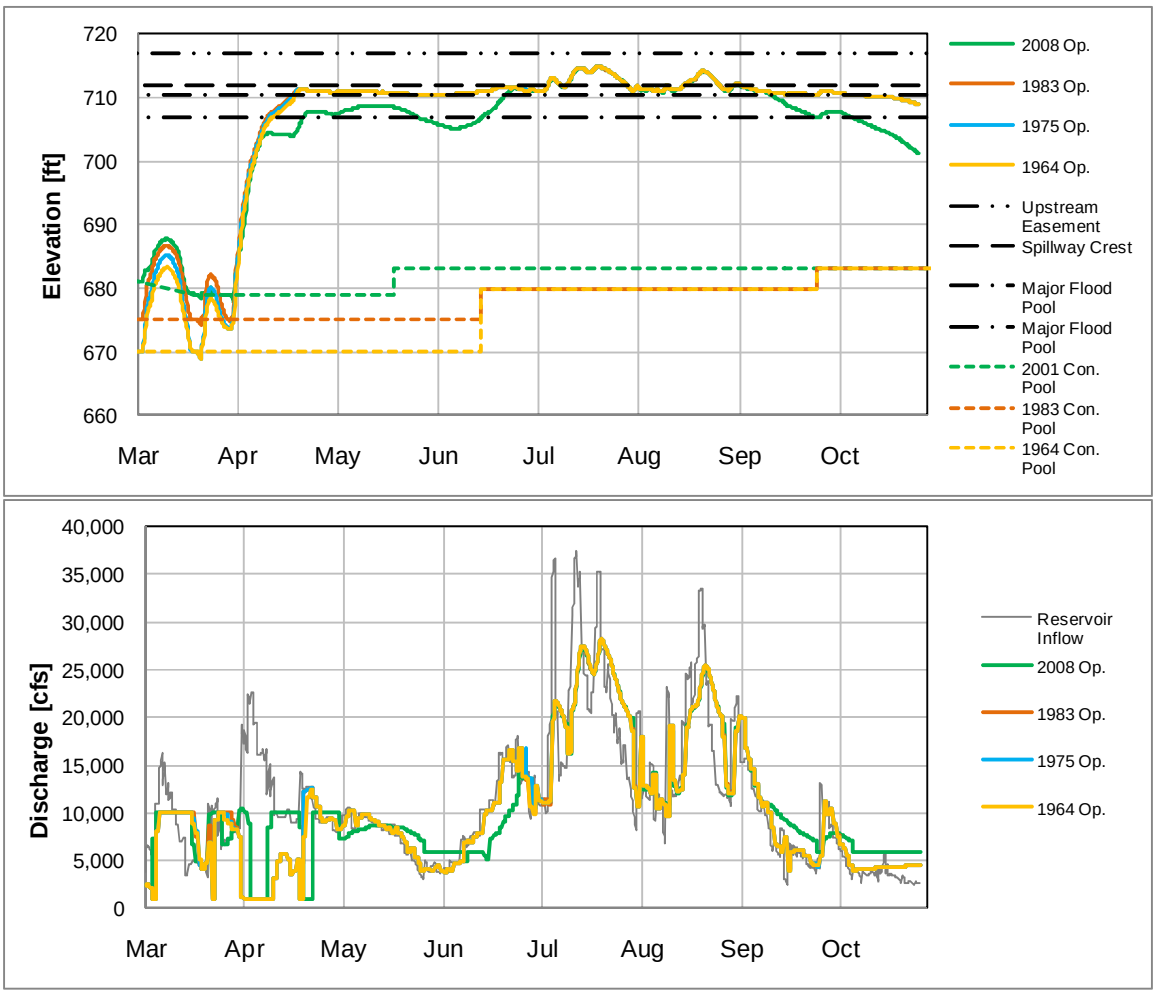

Figure 3.15. Simulation using 1993 flood event, varied historical operations, storage curves, and conservation pools

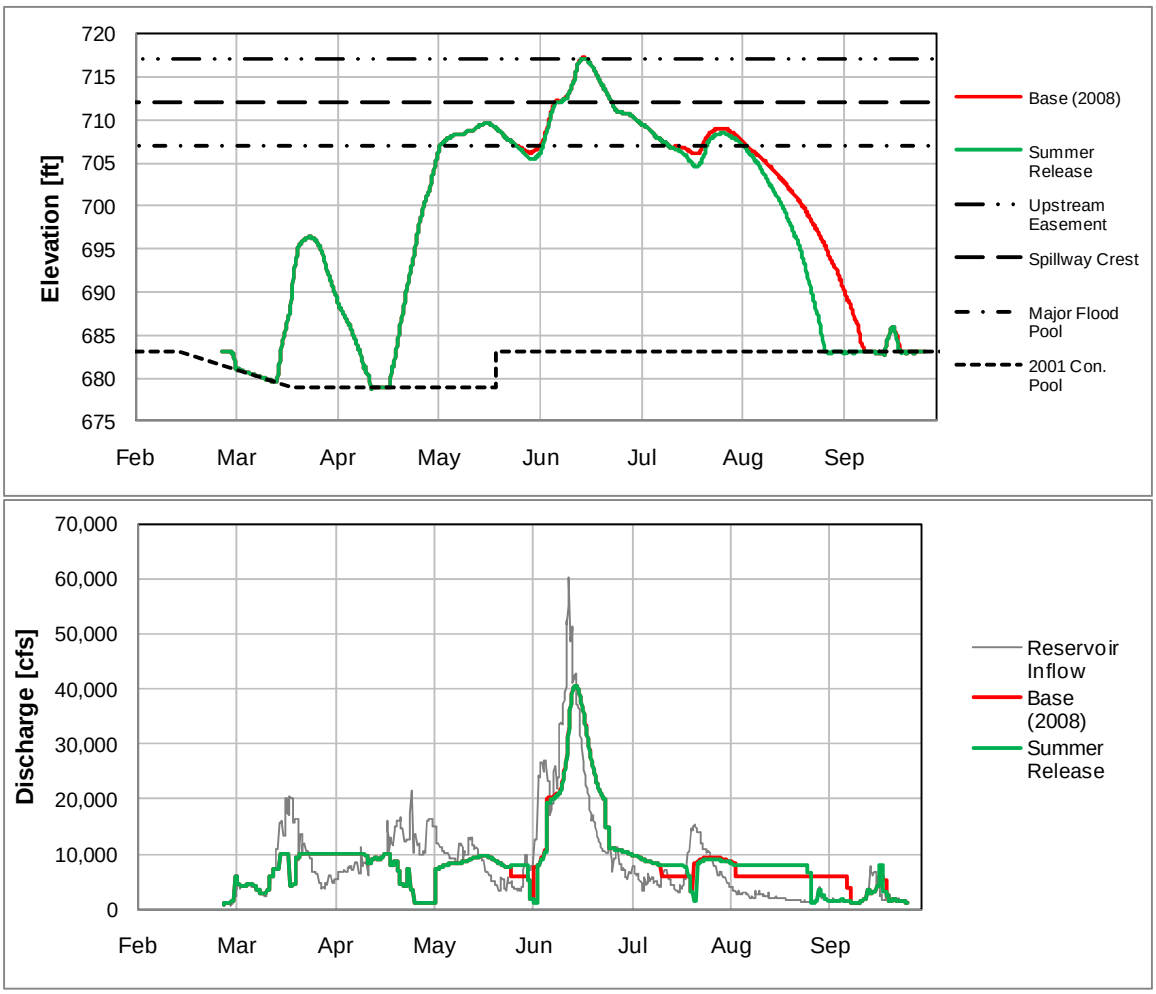

Figure 3.16. Simulation changing the maximum summer release from 6,000 cfs to 8,000 cfs.

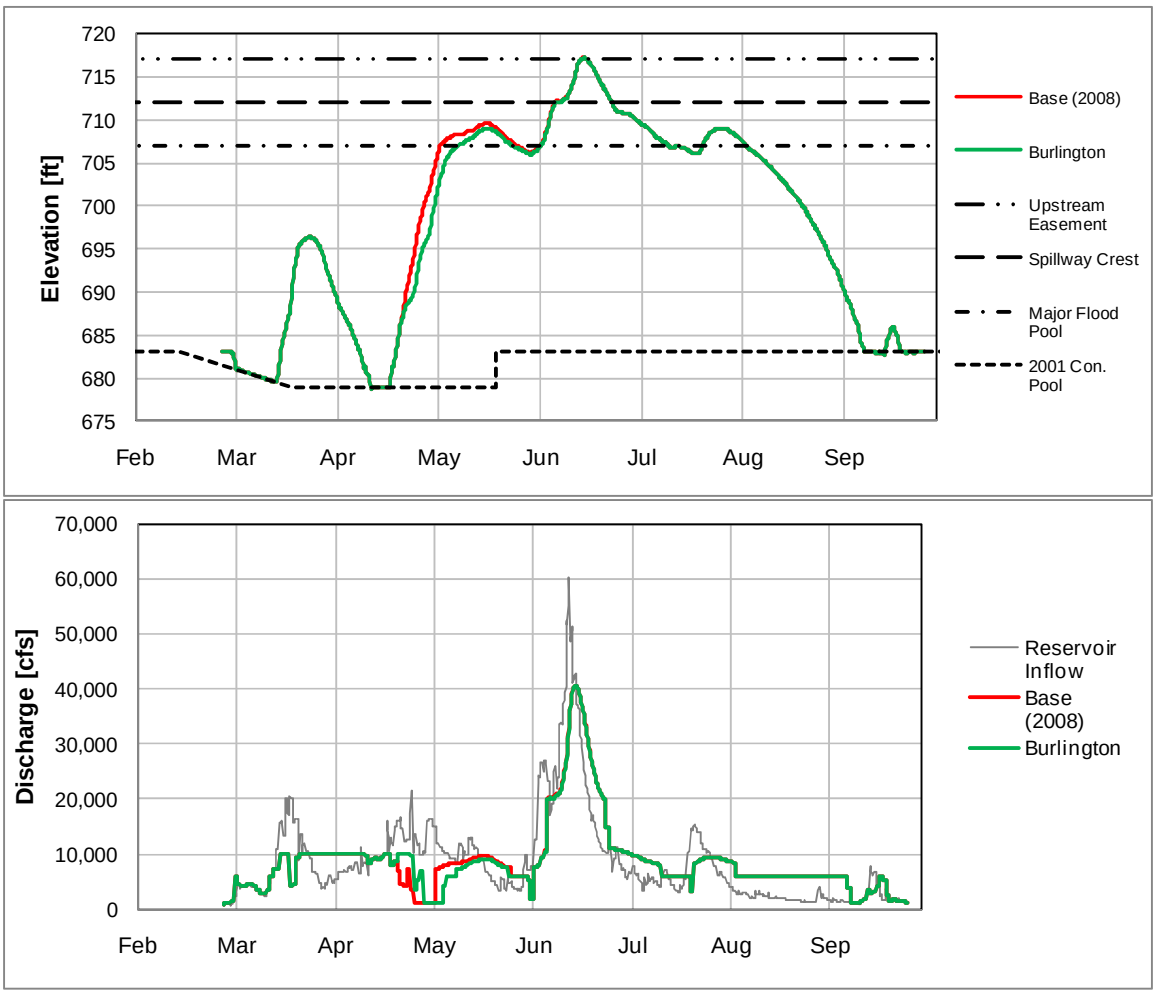

Figure 3.17. Simulation demonstrating disregarding of the Burlington river stage constraint.

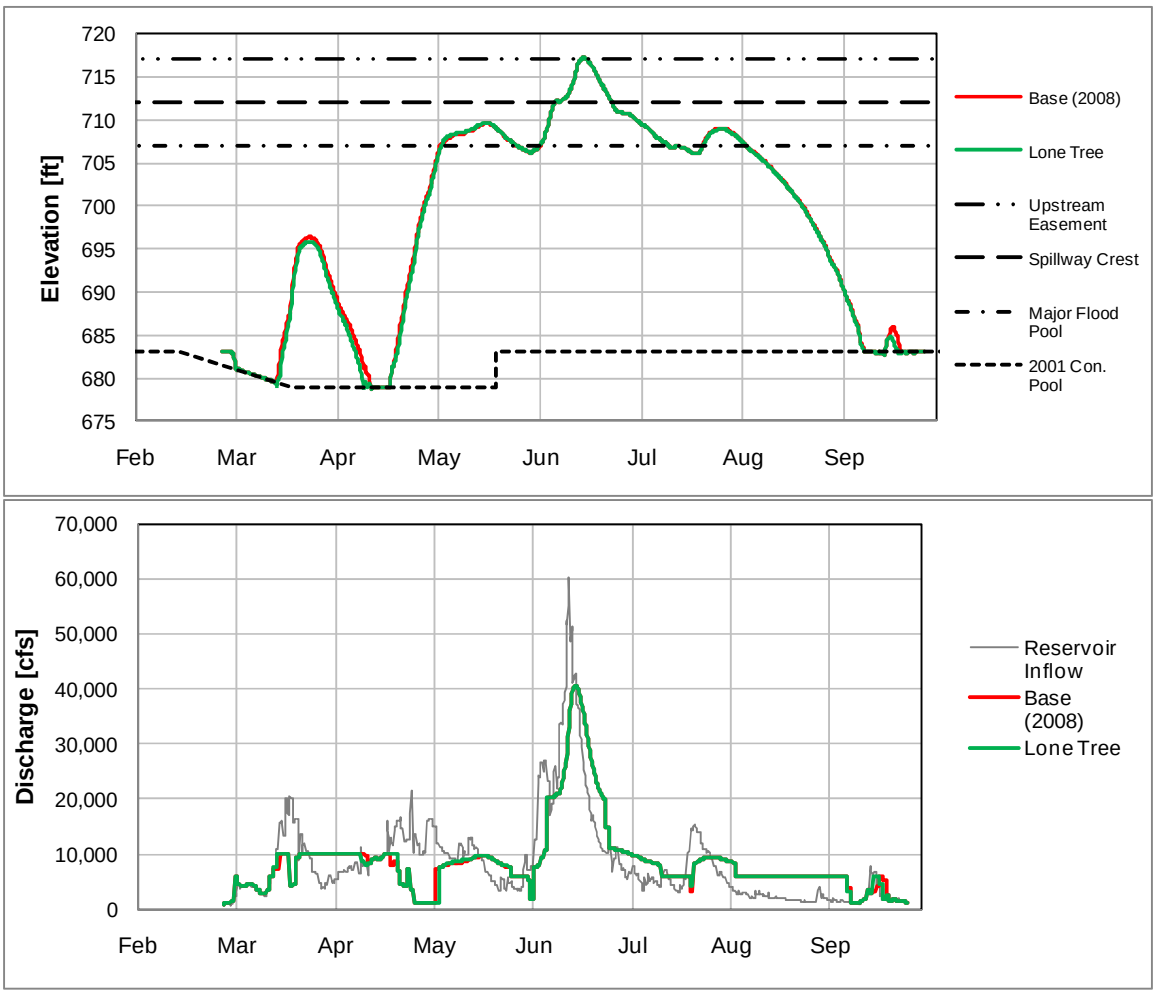

Figure 3.18. Simulation disregarding of the Lone Tree river stage constraint.

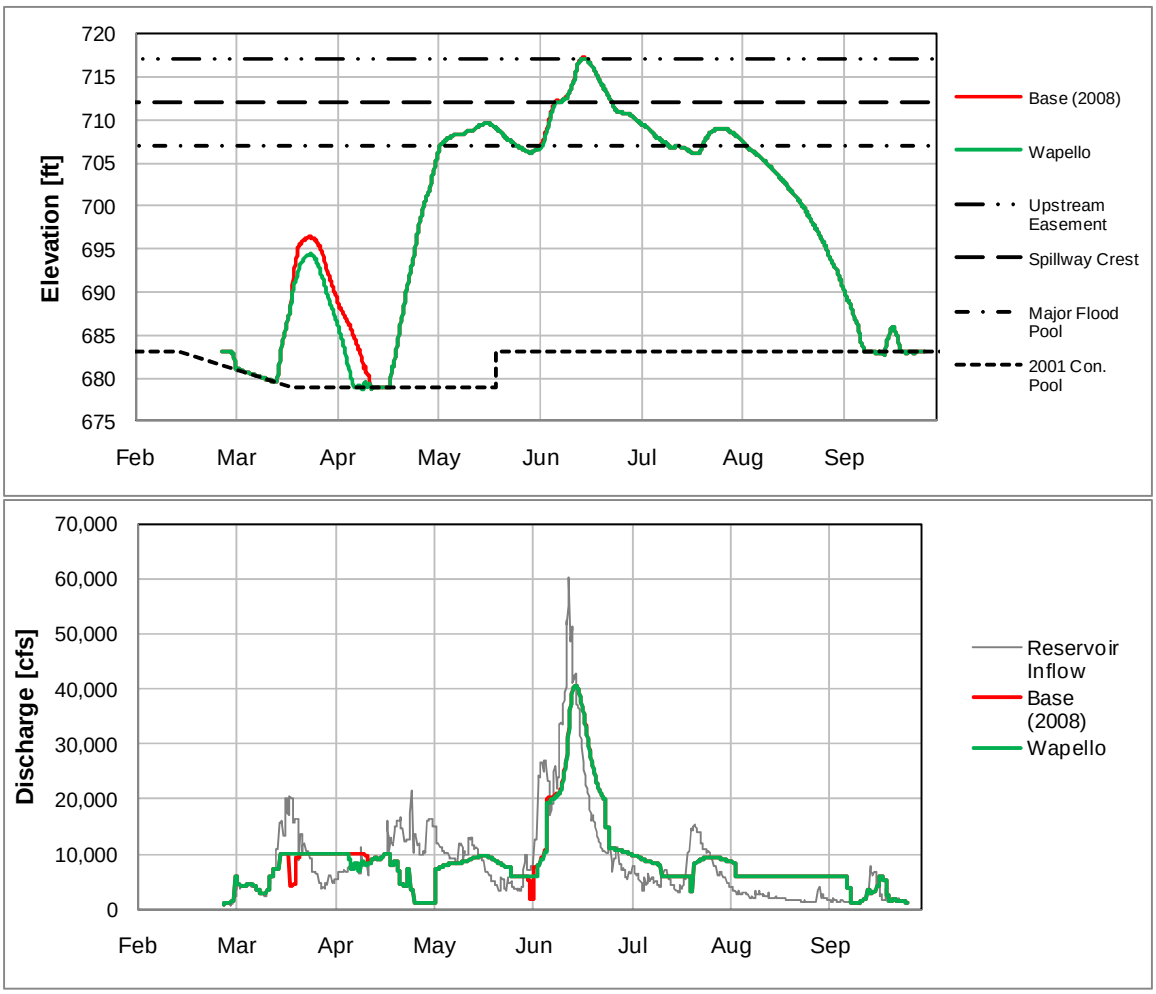

Figure 3.19. Simulation disregarding of the Wapello river stage constraint.

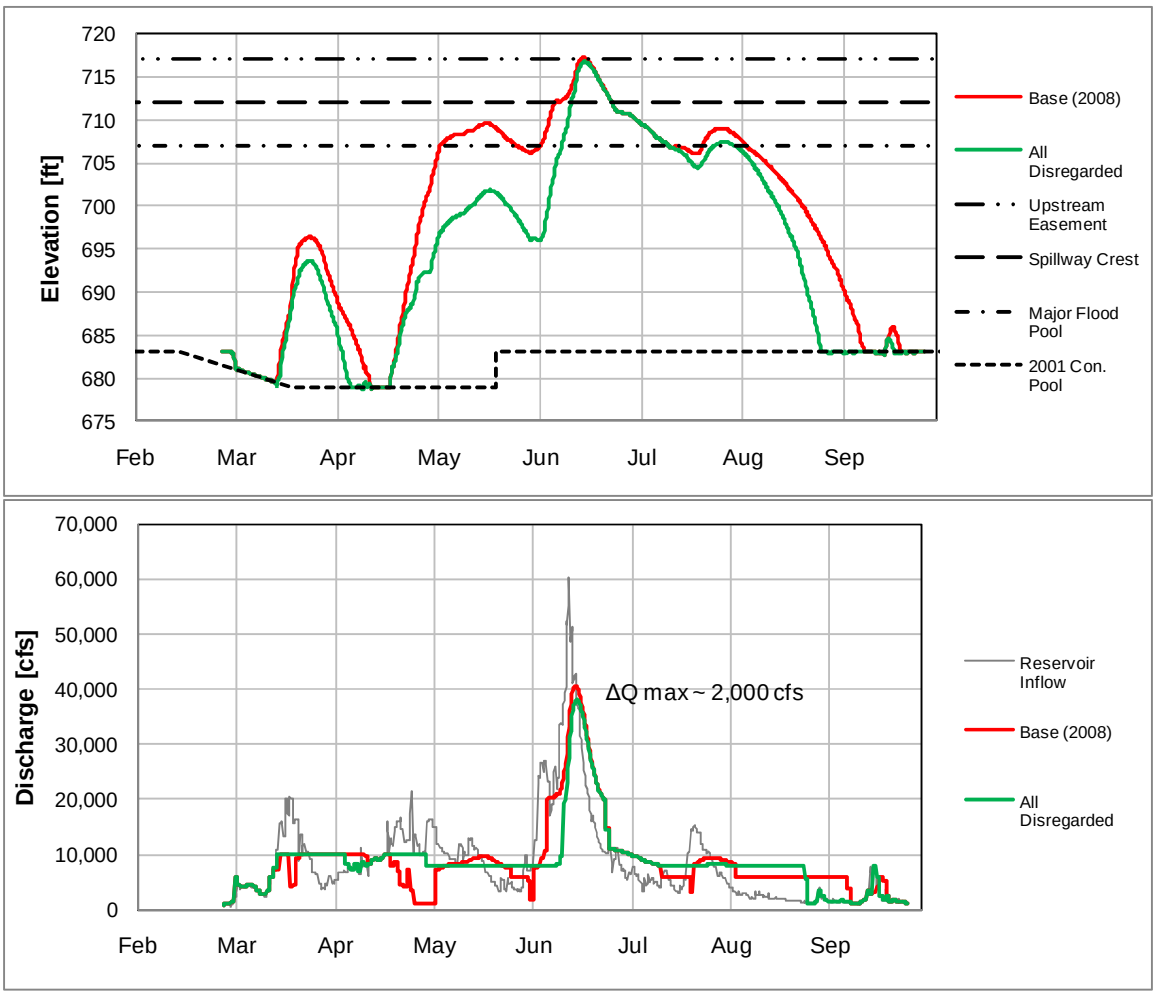

Figure 3.20. Simulation disregarding all downstream river stage constraints and increasing the maximum summer release from 6,000 cfs to 8,000 cfs.

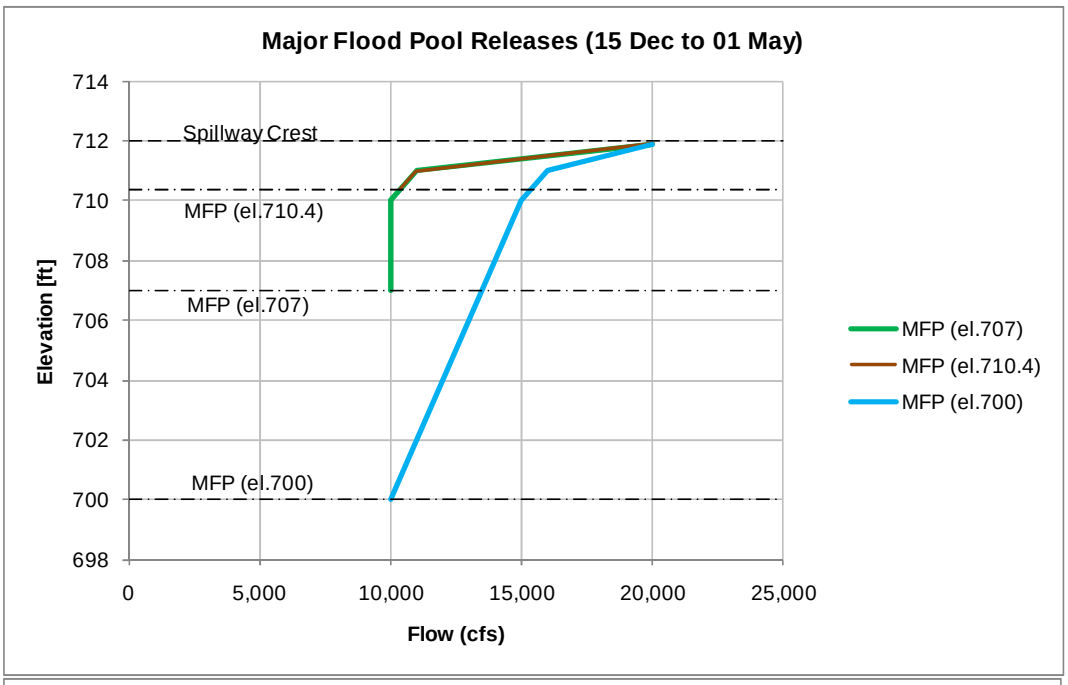

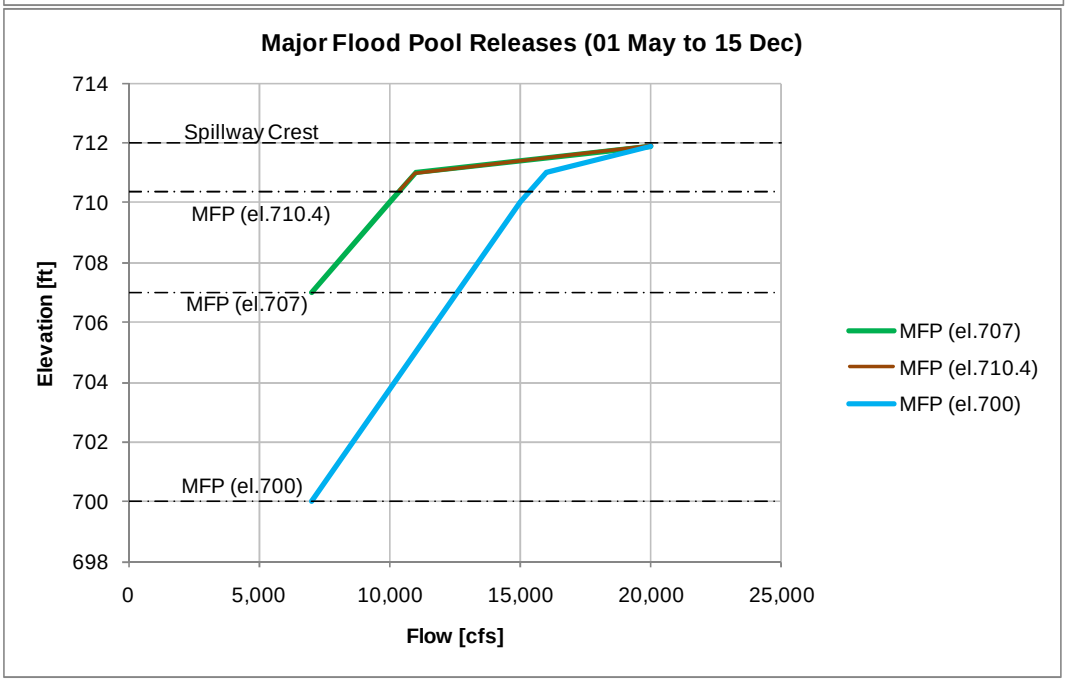

Figure 3.21. Prescribed releases for current (el. 707 ft) and alternate major flood pool elevations.

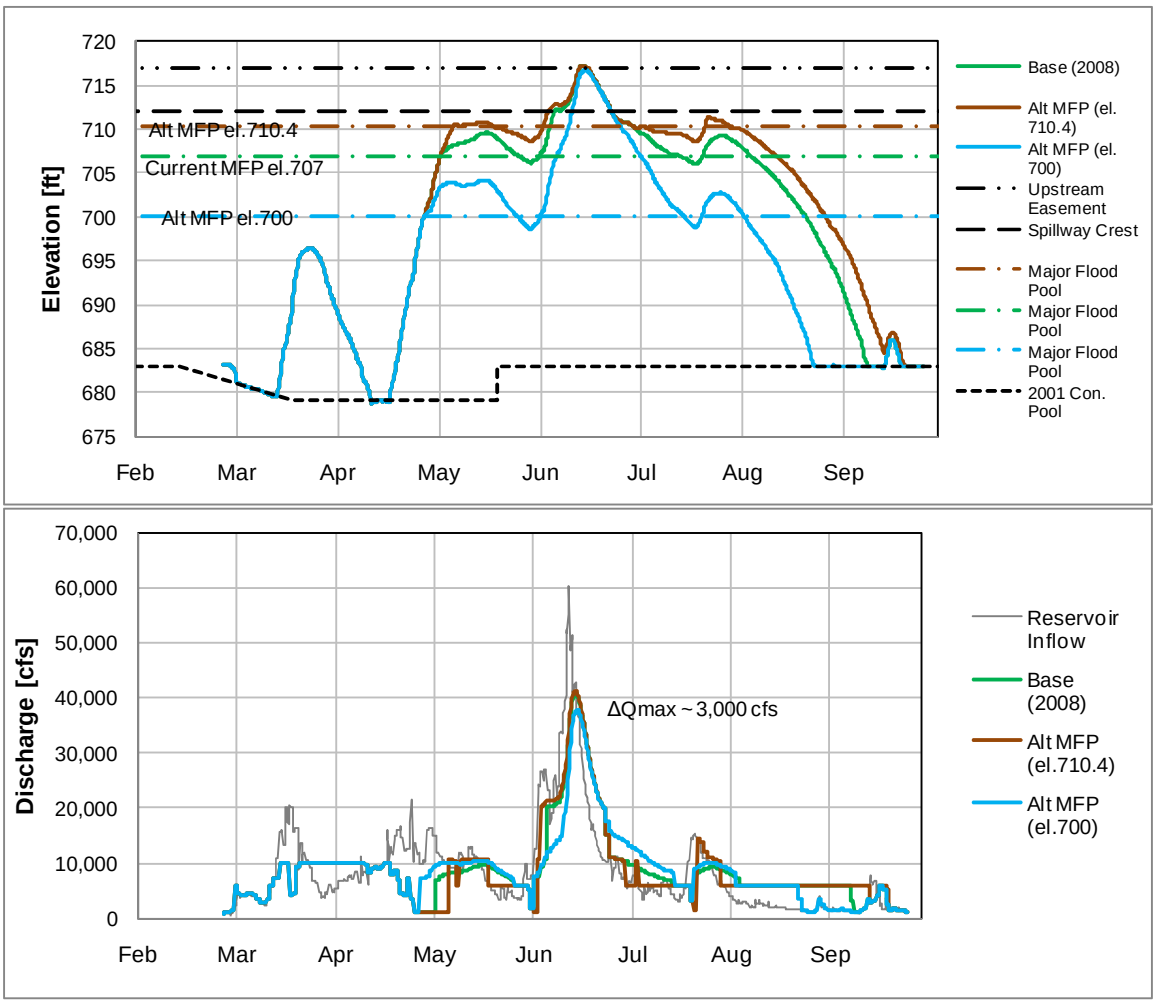

Figure 3.22. Simulation evaluating the effect of changing the major flood pool elevation using the 2008 event.

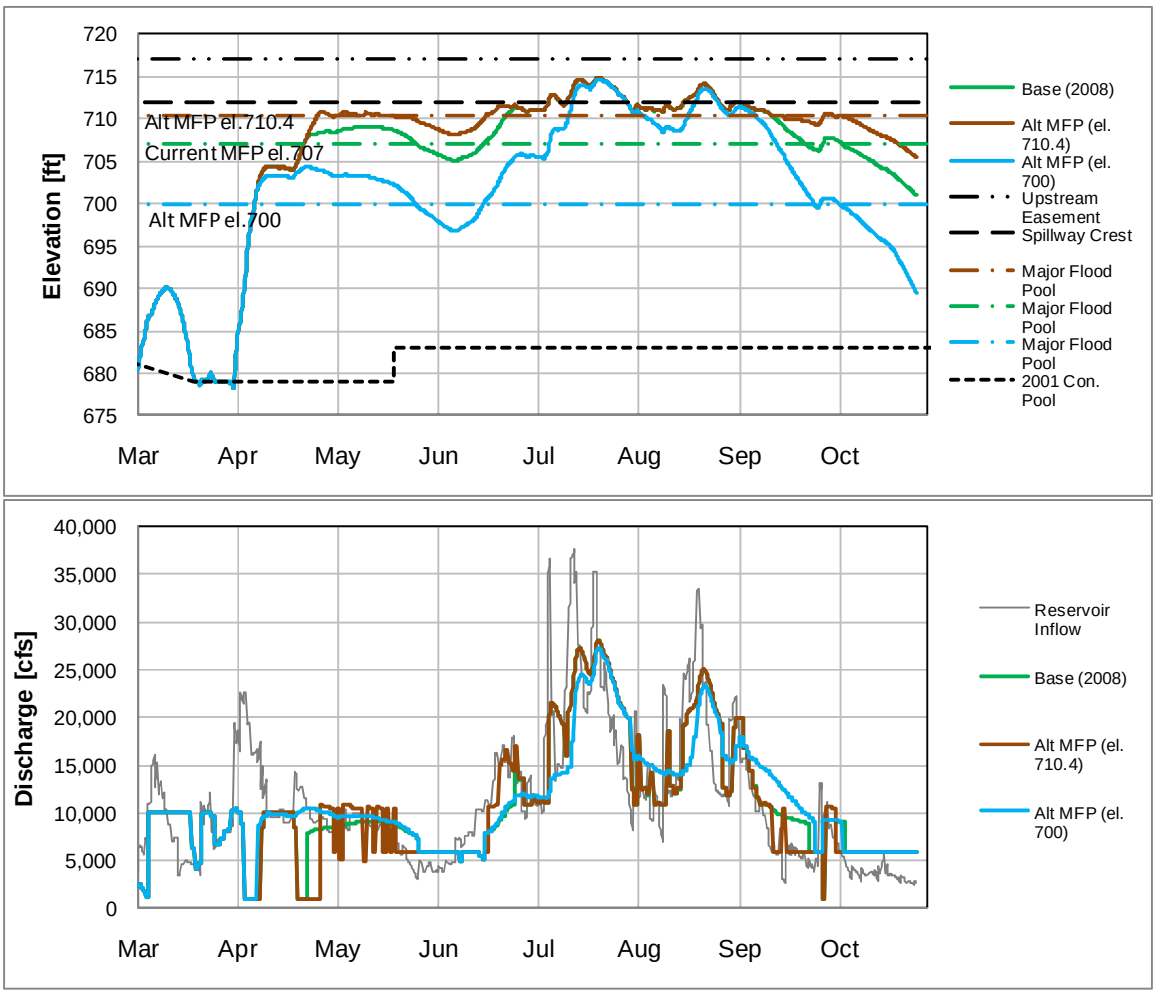

Figure 3.23. Simulation evaluating the effect of changing the major flood pool elevation using the 1993 event.

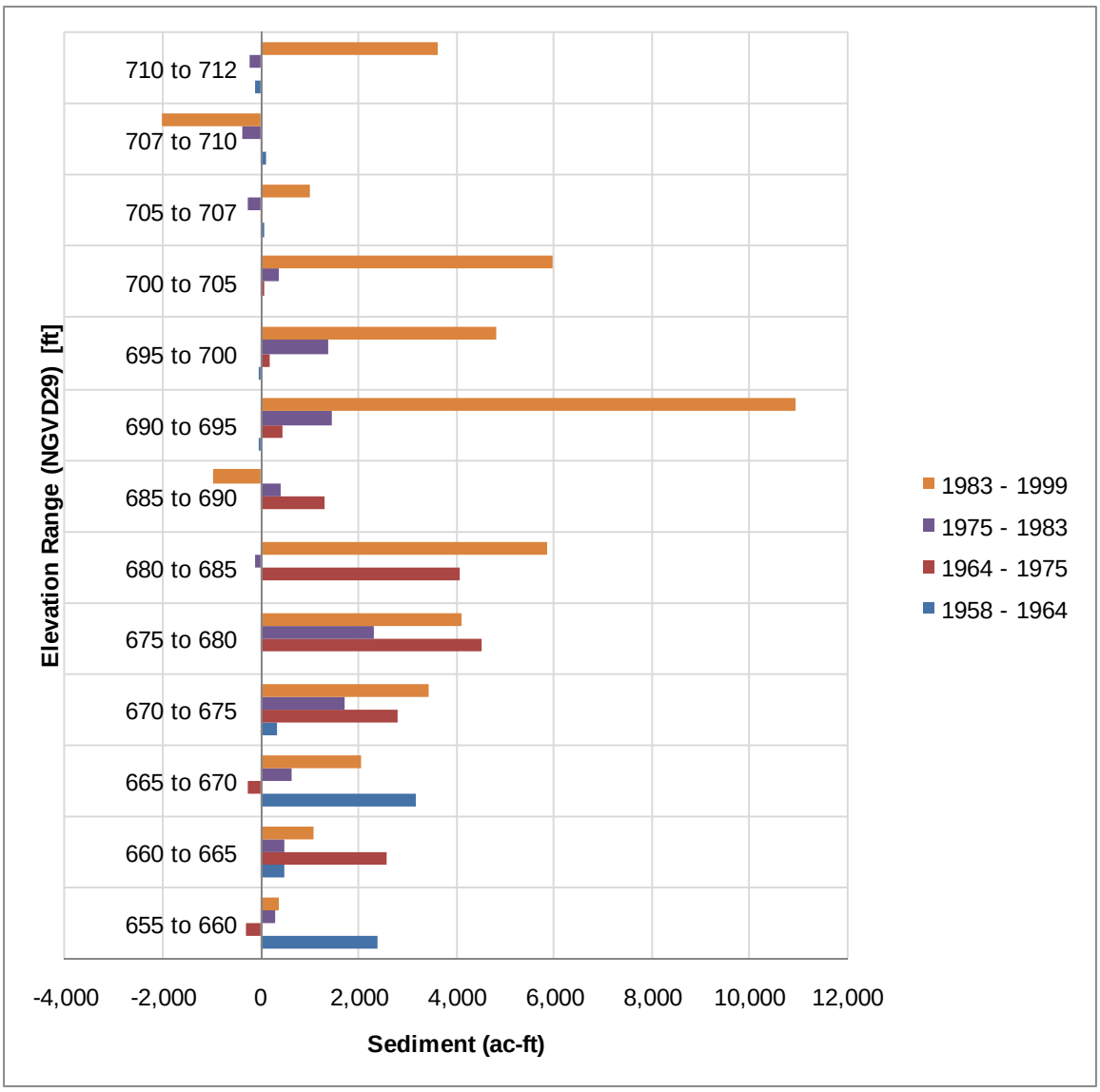

Figure 3.24. Depiction of the sedimentation in different elevation ranges during periods between reservoir storage capacity surveys.

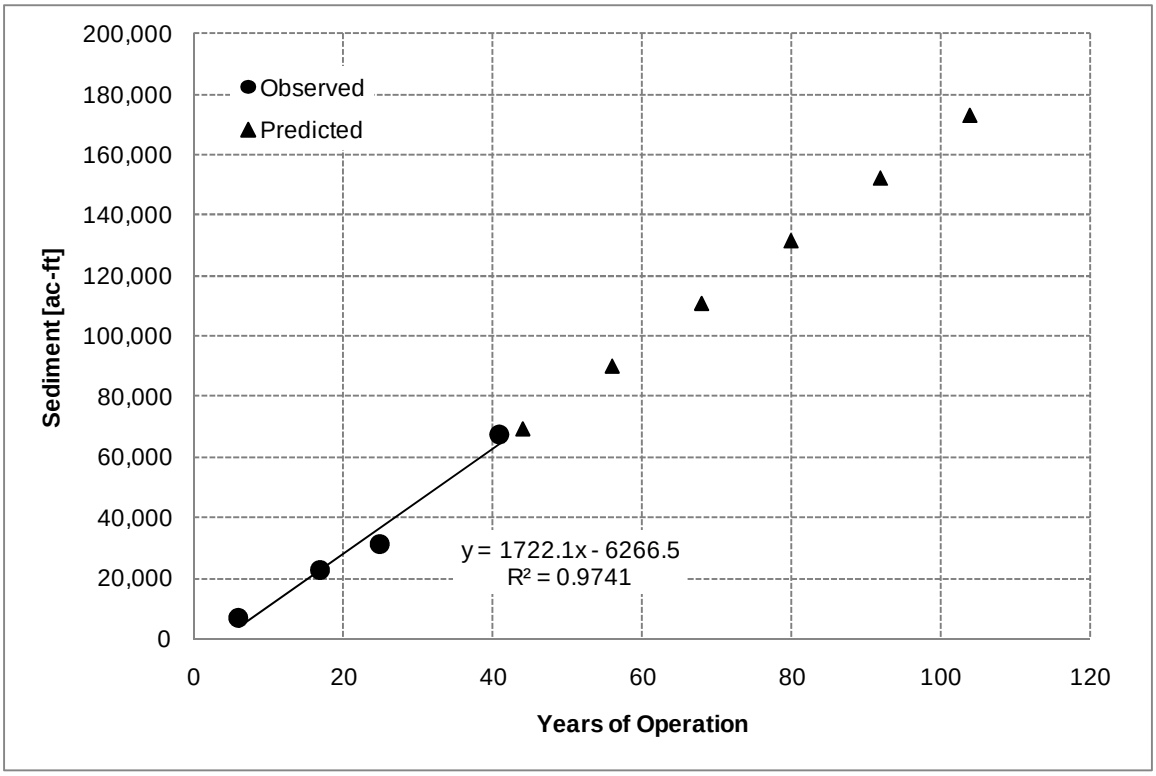

Figure 3.25. Linear regression of total sediment below el.720 through years of operation

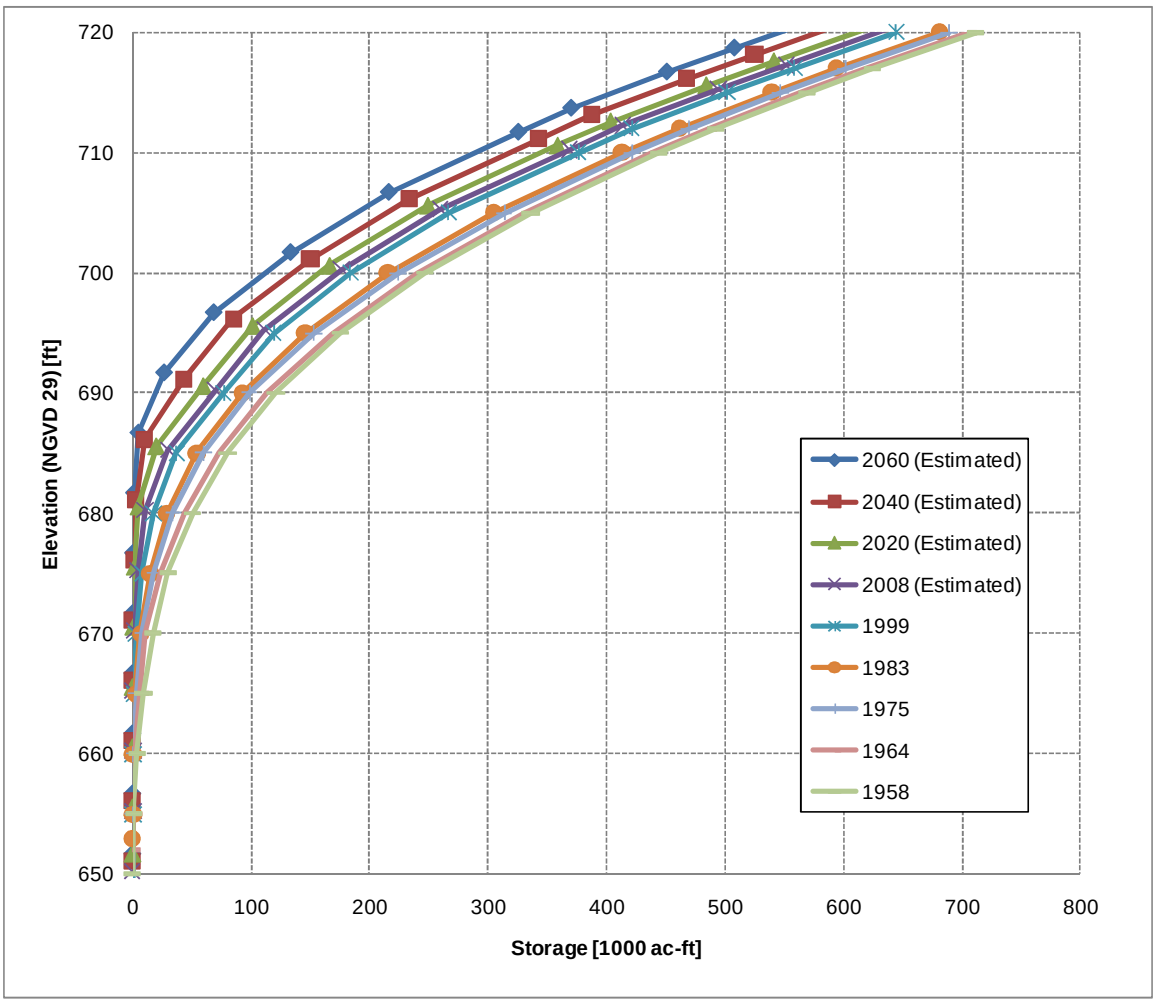

Figure 3.26. Forecasted elevation storage relationships obtained by using a linear regression of total storage lost below el. 720, and shifting the 1999 storage curve.

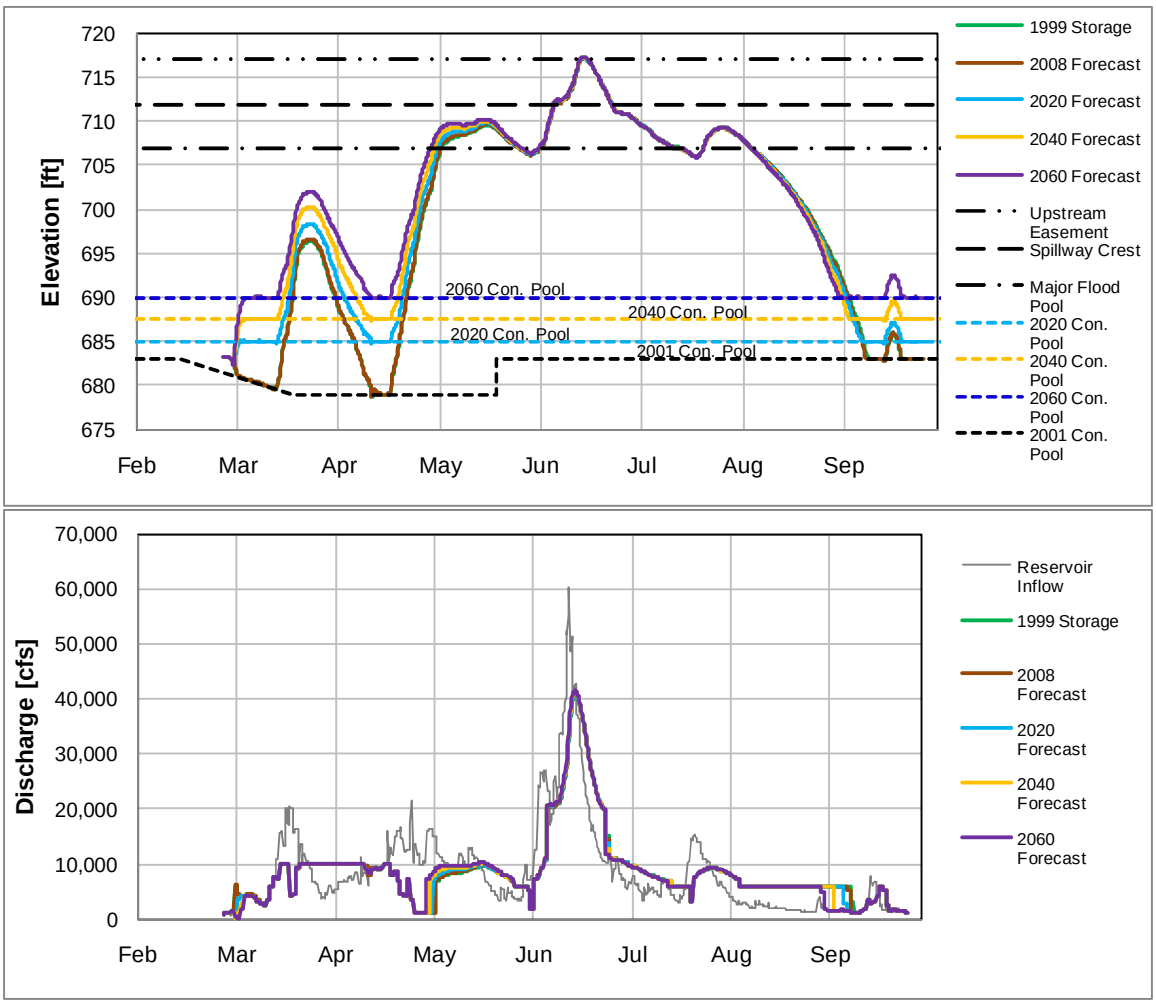

Figure 3.27. Simulation evaluating the effect of predicted sedimentation using the 2008 event.

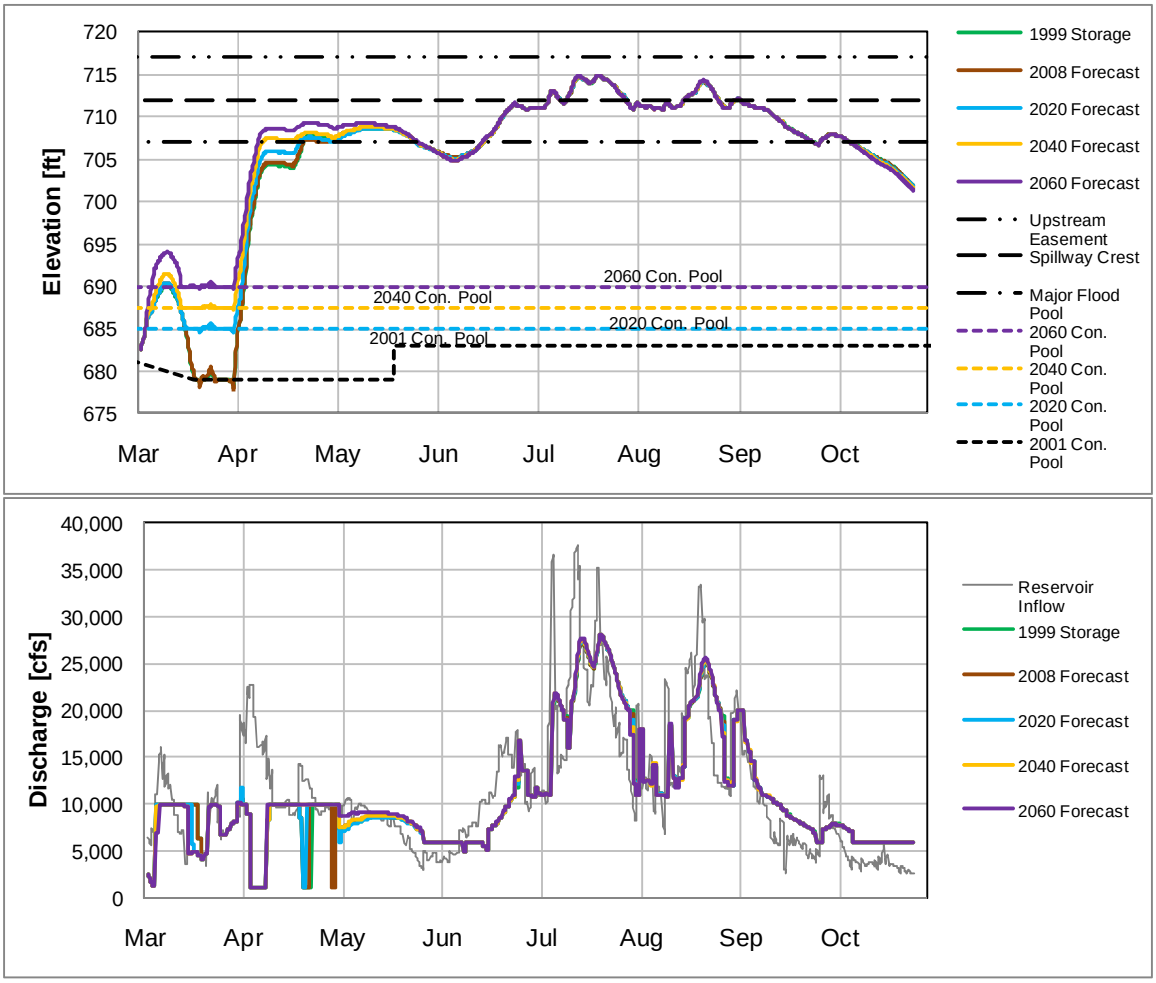

Figure 3.28. Simulation evaluating the effect of predicted sedimentation using the 1993 event.

CHAPTER IV: DEVELOPMENT OF FLOOD INUNDATION MAP LIBRARY FOR IOWA CITY, IOWA

This investigation utilized an existing one-dimensional HEC-RAS model to develop a library of inundation maps in an attempt to mitigate future devastating effects of flooding in the Iowa City/Coralville area. These maps will be available online to supplement the National Weather Service (NWS) Advanced Hydrologic Prediction Service's river flood forecasts, allowing researchers to provide an estimation of flood extent rather than having to rely on discrete predictions at the Iowa City river gage.

4.1 Introduction

The Iowa River inundated the cities of Coralville and Iowa City during the floods of 2008, causing millions of dollars in damages to homes, businesses, and university buildings. Typically, Coralville Reservoir regulates river flow through these communities, providing a high level of protection. However, preceding the flood of 2008, smaller rainfall events within the watershed consumed available reservoir flood storage. As a result, the emergency spillway was overtopped sending unregulated discharge through downstream communities. Flood mitigation efforts were concentrated on areas known to be vulnerable, but the magnitude of the flood of 2008 revealed many deficiencies in flood preparedness.

4.2 Motivation

Historically, the National Weather Service (NWS) has provided river forecasts for community officials and citizens. Forecasts of river stage are typically issued for stream gage locations with a maximum lead time of one week. While the lead time is generous, the discrete spatial distribution of the forecasts at stream gages is difficult for the general public to assimilate. The creation of highly detailed inundation map libraries to be used in conjunction with forecasts at river gaging stations would help to effectively

communicate a possible threat of flooding. The purpose of the work described herein is to develop inundation maps for Iowa City, Iowa, that will be delivered to NWS and made available on the Advanced Hydraulic Prediction Service (AHPS) website.

4.3 Data collection

4.3.1 Study area

The study area is located in Johnson County and encompasses approximately 6 miles of the Iowa River downstream of the Coralville Dam, as shown in Figure 4.1. This reach of the Iowa River flows just to the east of Coralville, Iowa before bisecting the University of Iowa campus in the heart of Iowa City, Iowa. A United States Geological Survey (USGS) stream gage is located in the middle of this reach and serves as a reference for all of the mapping products. Tributary flows include contributions from Clear Creek, which is gaged, and also from Ralston Creek, which is ungaged. There are twelve bridges and two low-head dams located in the study reach.

4.3.2 Bathymetry

Single-beam depth measurements were collected using survey-grade Odom Hydrographic HT100 single-beam sonar. The device was deployed from the side of an 18 foot tunnel hull boat (Piotrowski 2010). Georeferencing was accomplished by using a Trimble R8 real-time kinetic (RTK) GNSS fixed a known distance above the single beam sonar head. Recording and synchronization of depth soundings and geo-referenced positions of the survey head were accomplished using the software package HYPACK 2008 (Piotrowski 2010). A control point was established using the Johnson County, Iowa GNSS control network.

Bed elevations were calculated by subtracting the depth measurement and the distance between the sonar head and Trimble R8 unit from the time-average elevation reading from the Trimble R8 unit (Piotrowski 2010). This calculation method assumes

that the survey assembly is oriented normal to the water surface, and that the Trimble R8 unit is always directly above the sonar head. These assumptions are often violated due to the pitching, heaving, and rolling of the survey watercraft. Piotrowski (2010) determined the uncertainty associated with each of the instruments used in data collection based on the manufacturers' estimates, as shown in Table 4.1.

Multi-beam bathymetric data were later gathered to supplement single-beam sonar near bridge piers and other locations featuring complex bed geometry. Multi-beam depth measurements were collected using a state-of-the-art RESON SeaBat 7125 echosounder. This instrument has the ability to emit 512 individual depth soundings in a swath configuration. A comparison of the multi-beam to single-beam data collection is shown in Figure 4.2. The multi-beam system is more sophisticated in terms of quality control due to an Applanix POS-MV inertial motion detection system, which corrects for the heading, pitch, roll, and heaving of the survey watercraft. The measurement uncertainties for the multi-beam devices are shown in Table 4.1.

4.3.3 Topography

Ayres Associates provided a digital terrain model (DTM) that was a compilation of several elevation datasets. The City of Iowa City, the City of Coralville, the USGS, and Ayres Associates provided topographic data. Both cities provided 2-foot contour maps that were developed in 2006. The USGS provided 10-foot contour maps for the upper portion of the study area, just south of the Coralville Dam. Ayres Associates developed a 1/2-foot contour map created using photogrammetric stereo compilation in November of 2008 for much of the study area (Piotrowski 2010). Higher resolution datasets were given priority over lower resolution datasets during the merging process.

4.3.4 Digital elevation models

4.3.4.1 DEM for numerical model development

Piotrowski (2010) utilized the DTM developed by Ayres Associates as a starting point for a digital elevation model (DEM) to be used to develop numerical models of the reach. The single- and multi-beam bathymetric data collected by IIHR – Hydroscience & Engineering were incorporated into the DTM to accurately describe the channel geometry. Low head dams were incorporated using plan sets provided by the City of Iowa City. Creek geometries near culverts were inserted into the DEM using interpolation of upstream and downstream cross-sections of culvert openings (Piotrowski 2010) . The City of Iowa City, City of Coralville, and University of Iowa provided geo-referenced polygons to delineate building foot prints within the study reach. Building elevation data were not available, so footprint polygons were extruded using a constant of 3 meters. The finished 1-meter resolution DEM was utilized to develop a two-dimensional hydraulic model by Piotrowski (2010) and was also utilized by Ayres Associates (2009) to develop a one-dimensional hydraulic model.

4.3.4.2 DEM for post processing

An alternate DEM was developed for post processing of hydraulic simulation results. This DEM included the terrain data provided by Ayres Associates, and bathymetric data collected by IIHR – Hydroscience & Engineering. Building data were excluded from this DEM to avoid undesirable artifacts in post-processing of simulation results. Bridge decking was incorporated into the DEM using Light Detection and Ranging (LiDAR) data collected by the National Center for Airborne Laser Mapping (NCLAM) during the falling limb of the 2008 flood hydrograph (Piotrowski 2010). When the quality of the LiDAR data was poor for extraction of bridge decking elevations, a triangular irregular network (TIN) representation was developed by

interpolating from one bridge abutment to another. The TINs were then converted to raster datasets and inserted into the 1-meter resolution post processing DEM.

4.3.5 Existing HEC-RAS model

Ayres Associates developed a validated one-dimensional HEC-RAS model of the Iowa River for the University of Iowa flood mitigation program. Model geometric data were obtained by extracting data from the DEM that was created for numerical model development that is discussed in Section 4.3.4.1. Several geometries were created to maintain accurate model calibration over a range of flow conditions throughout the study reach. Model geometries with different roughness coefficients and effective flow areas are used for flows less than 30,000 cfs, greater than 30,000 cfs, greater than 45,000 cfs, and greater than 55,000 cfs.

Cross-section spacing was approximately 600 feet throughout the reach. Due to the number of bridges and low head dams, a high density of cross-sections was used; however, the number of cross-sections is well within an acceptable range for a model of this type (Ayres Associates 2009).

Initial Manning's 'n' roughness values were selected based on engineering judgment, field investigations, and established literature (Ayres Associates 2009). Roughness values for the main channel ranged from 0.027 to 0.04 and 003 to 0.12 for overbank areas, as shown in Table 4.2. Calibration was completed using bankfull water surface elevation data taken on March 19th, 2009 and surveyed high water marks collected following the 2008 flood by the City of Iowa City, The University of Iowa, and Shive – Hattery Architecture, Engineering Design Services (Ayres Associates 2009). Ayres Associates (2009) was able to calibrate the hydraulic model within a high level of accuracy utilizing these two datasets, as shown in Table 4.3 and Table 4.4. The average difference between the simulated water surface profile and 2008 flood high water marks after calibration was 0.09 ft. The average difference between the simulated water surface

profile and the surveyed bankfull profile was 0.05 ft. Simulation results from the 2008 flood were validated using LiDAR collected on the falling limb of the 2008 flood.

The existing HEC-RAS model was utilized to develop a library of inundation maps. NWS AHPS standards dictate that tributary backwater effects should be excluded; therefore, the existing HEC-RAS model was clipped to avoid backwater effects from Clear Creek, as shown in Figure 4.1. The furthest upstream cross-section is located just downstream of the Iowa River Power (IRP) dam, at river station 39,528.

4.3.6 Bulk flow data

Boundary conditions were based on rating curves obtained at the Iowa City USGS stream gaging station (005454500) and at the lower corporate city limit of Iowa City. For the purpose of creating a robust inundation map library, the rating curve at Iowa City USGS gaging station was extrapolated to 55,000 cfs, as shown in Figure 4.3. The rating curve for the lower corporate limit of Iowa City, shown in Figure 4.4, was developed by Ayres Associates using a FEMA flood insurance study of Johnson County (FEMA 2007).

4.4 Numerical simulation

Several steady gradually varied flow simulations were completed using a modified version of the HEC-RAS model developed by Ayres Associates. Discharges were based on 0.5 feet river stage intervals taken from the established rating curve for the Iowa River USGS gaging station 005454500. Boundary conditions were also taken from the USGS gaging station, and a rating curve was developed at the lower corporate limit of Iowa City using FEMA studies. One of four HEC-RAS geometry files was utilized depending on the magnitude of the discharge, as described in section 4.3.5.

4.4.1 Numerical methods

Steady flow simulations were completed using an altered version of a HEC-RAS model developed by Ayres Associates. The iterative standard step method was used to solve the energy equation between cross-sections, including bridges. Calculation of friction slope was completed using average conveyance method. Typical cross-section contraction and expansion loss coefficients were 0.1 and 0.3, respectively. Contraction and expansion loss coefficients just upstream or downstream of bridges were 0.3 and 0.5, respectively. The flow regime was assumed to be subcritical throughout the reach.

Discharges used in steady state simulations ranged from a bankfull condition of 7,180 cfs to 55,000 cfs, which is greater than the 2008 flood peak discharge of 41,000 cfs. Using a river stage interval of 0.5 feet at the Iowa City USGS gage, the total number of steady state simulation scenarios was thirty-five.

4.4.2 Boundary conditions

Steady flow simulation requires upstream and downstream boundary conditions. Simulations assumed subcritical flow in the study reach; and therefore only a known discharge at the upstream boundary and a known water surface elevation at the downstream boundary were required. The elevation-discharge relationship at the downstream boundary was determined using a rating curve, shown in Figure 4.4, developed by Ayers Associates (2009) from FEMA flood insurance study data. For a given flow at the Iowa City USGS gaging station, a corresponding water surface elevation was estimated at the lower corporate limit of Iowa City using this curve. Model scenarios are depicted in Figure 4.5. The two sets of data are paired based on stage, with each pair representing a model scenario. Each river stage on the x-axis intersects a point corresponding to an upstream discharge boundary condition (left y-axis) and a point corresponding to a downstream water surface elevation boundary condition (right y-axis). The rating curve given in Figure 4.3 is used as an internal boundary condition at the

cross-section corresponding to the location of the gage. An intended river stage at the Iowa City USGS gage is used as the criteria to determine upstream and downstream boundary conditions.

4.4.3 Assumptions

All simulations assumed steady gradually varied flow. The flow regime through this reach was assumed to be subcritical. Flow contributions from Clear Creek, Ralston Creek, and localized rainfall runoff were neglected. The energy equation was assumed to accurately describe the hydraulic effect of bridges even at high flow, or when the bridge was overtopped. The original HEC-RAS model was calibrated using geometric files that included a cofferdam, sandbags, and HESCO barriers that were in place during the 2008 flood.

4.5 Results

Simulation results from HEC-RAS were processed using ArcGIS. It was necessary to edit the simulation results to conform to NWS AHPS quality control standards. Inundation shapes and depth rasters will be hosted on the NWS AHPS in the future.

4.5.1 Development of inundation map library

Simulated water surface profiles were exported from HEC-RAS as georeferenced data stored in XML format. Data from these XML files were converted to triangular irregular network (TIN) representations using the HEC-GeoRAS utility for processing geospatial data in ArcGIS. TIN surfaces were then converted to raster grids and intersected with a 1-m resolution DEM developed for post processing. The DEM did not include buildings, but it did include bridge decking, as discussed in Section 4.3.4.2.

The post processing DEM incorporated bridge elevation data in order to realistically calculate inundation depths and delineate flooding extents. Bridge elevation

data were imported from LiDAR survey data when available. When bridge elevation data were not available in the LIDAR data set, a TIN was constructed by interpolating between deck elevations near bridge abutments. Bridge TINs were then converted to raster grids and incorporated into the initial DEM raster.

Intersecting water surfaces profile rasters with the post processing DEM raster yielded a raster grid that contained positive cell values if inundated and negative cell values if not inundated. Positive values were reclassified as a constant value, while negative inundation values were reclassified as "nodata." This reclassified dataset was converted to a generalized inundation polygon shapefile. These shapefiles were then manually edited to conform to the requirements of the NWS quality control standards. Most of these edits included removing or merging any "ponded" areas less than 250 ft in diameter with the main channel and removing any "islands" less than 250 ft in diameter from the shapefile. Edited polygon shapefiles were then used as analysis masks to extract inundation depth rasters from the original intersections of the water surface profile raster and the post processing DEM. The cell size of these inundation depth rasters was increased from 1-m to 5-m in order to accommodate the web hosting constraints of the AHPS website. Examples of an inundation shape and inundation raster are shown in Figure 4.6 and Figure 4.7, respectively. The addition of bridge decking elevations in the post processing DEM shows the gradual inundation of bridges.

4.5.2 Web-based inundation map library

The NWS AHPS will host the inundation shapes and depth rasters on a website dedicated to river forecasts and warnings for the Iowa River at Iowa City, similar to the example of the Colorado River at Bastrop, TX which is shown in Figure 4.8. The mapping interface will allow users to select different inundation levels and zoom in to view the accessibility of bridges and roads. An option will allow users to view approximate inundation depth based on the position of the mouse cursor on the map. A

tab will provide a 7- day river stage forecast hydrograph for the Iowa City stream gage, users will then be able to select an appropriate inundation map corresponding to the forecast. Federal Emergency Management Agency (FEMA) digital flood insurance rate (DFIRM) maps will also be available for the 100-year and 500-year inundation extents.

4.6 Summary

This study presents the development of an inundation map library for a six-mile reach of the Iowa River through Iowa City. The development of the library was facilitated by the use of an existing validated HEC-RAS model of the Iowa River corridor that was developed by Ayres Associates. The model required bathymetric, topographic, hydrographic, and roughness values. Bathymetric data were collected by IIHR – Hydroscience & Engineering from July 2008 to October 2008 (Piotrowski 2010). Topographic data were collected by Ayres Associates following the 2008 flood. Hydrographic data were acquired from the City of Iowa City, Shive-Hattery, IIHR – Hydroscience & Engineering, and the USGS. Ayres Associates selected roughness values based on field investigations, established literature, and calibration data. The hydraulic model was validated using a high-resolution LiDAR dataset flown during the falling limb of the 2008 flood hydrograph.

Using the established rating curve at Iowa City USGS gage (005454500), thirty-five steady state discharges were determined based on 0.5 feet river stage increments. Boundary conditions were based on thirty-five discharges and an elevation-discharge relationship for the lower corporate limit of Iowa City developed by Ayres Associates based on FEMA studies. Inundation extent polygons and inundation depth rasters were generated using simulation results and a DEM developed specifically for post processing.

NWS AHPS will host the inundation shapes and depth rasters on a website dedicated to river forecasts and warnings for the Iowa River at Iowa City. The website will serve as a resource for citizens and community officials during flood emergencies,

enabling informed decisions concerning flood risk based on the highest quality flood forecast data available.

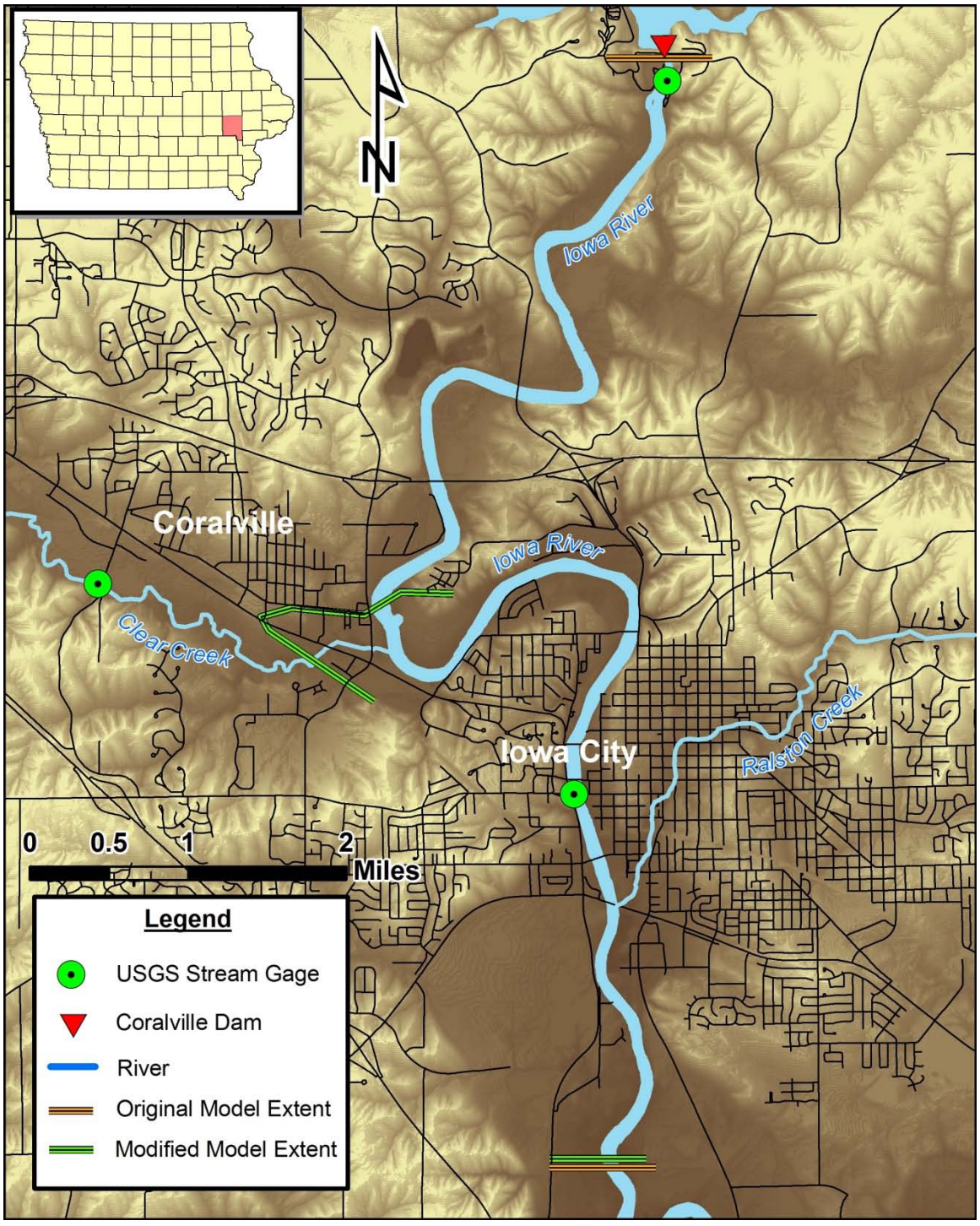

Figure 4.1. Study area showing the location of the stream gage and model extents.

Table 4.1. Uncertainty associated with the hydrographic survey instrumentation.

System Component	Measurement Type	Uncertainty*
Trimble R8 GNSS	Horizontal Position	10mm
	Vertical Position	20mm
RESON SeaBat 7125 multi-beam echosounder	Depth	6mm
Odom HT100 single-beam echosounder	Depth	10mm ± 0.01% depth
Applanix POS MV inertial positioning system	Roll and Pitch	0.010°
	Heave	50cm
	Position	20-100mm

Source: Piotrowski, Jesse A. Development of a High-Resolution Two-Dimensional *Urban/Rural Flood Simulation.* MS Thesis, The University of Iowa, 2010.

*Uncertainty values obtained from manufacturer fact sheets

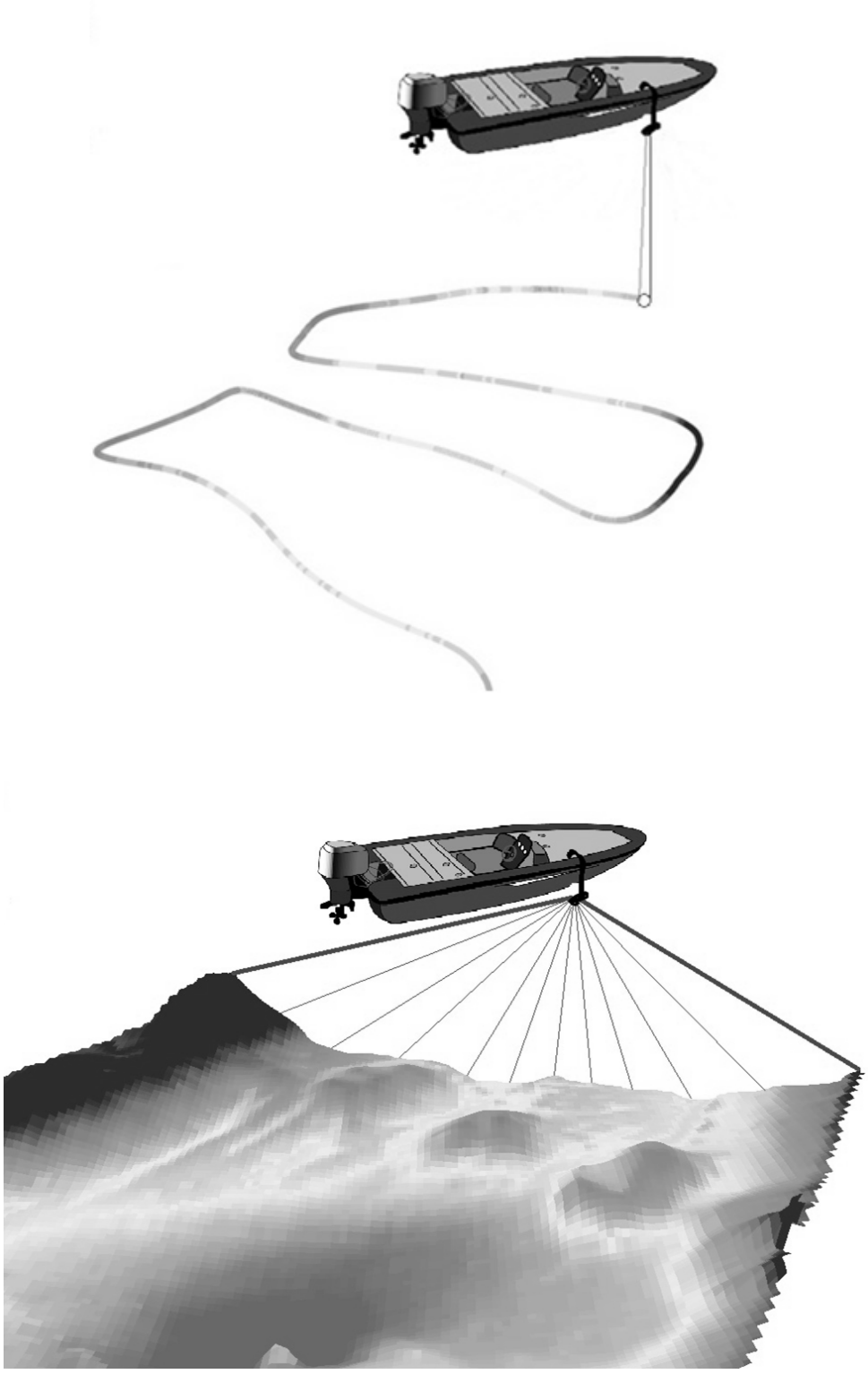

Figure 4.2. (above) single-beam echosounder, (below) multi-beam echosounder.

Table 4.2. Manning's 'n' values and calibrated 'n' values.

Location Description	Book	Book Description	Book Range	Book Average	Calibrated Value
Forest Area	Chow	Trees: Dense willows, summer, straight	0.11-0.20	0.15	0.12
Forest Area	Chow	Trees: Heavy stand of timber, a few down trees, little undergrowth	0.08-0.12	0.1	
Ponds	--				0.03
Steam banks: Weeds and some trees	Chow	Pasture: High Grass	0.03-0.05	0.035	0.035
Steam banks: Weeds and some trees	Chow	Brush: scattered brush, heavy weeds	0.035-0.07	0.05	0.065
Stream Bottom	Chow	Major Streams	0.025-0.06		0.027
Riprap Stream bottom					0.04
Brush: Weeds and some trees	Chow	Brush: scattered brush, heavy weeds	0.035-0.07	0.05	0.05
Pasture: High Grass	Chow	Pasture: High Grass	0.03-0.05	0.035	0.035
Trash Lot	---				0.08
Buildings modeled as blocked obstructions					0.035
Dense Buildings not modeled as block obstructions					0.08
Subdivision					0.08-0.12
Park	Chow	Pasture: short grass	0.025-0.035	0.03	0.03
Field	Chow	Pasture: short grass	0.025-0.035	0.03	0.03
Mining					0.045
Streets					0.03

Source: Ayres Associates. "*University of Iowa - Hydraulic Memorandum*." Iowa City, 2009.

Table 4.3. Ayres Associates low-flow calibration results.

Location Description	XS	Surveyed WSEL (ft)	Model WSEL (ft)	Difference (ft)
	10087	635.45	635.46	0.01
DS Railroad Bridge	12427	635.67	635.84	0.17
US Railroad Bridge	12509	635.8	635.88	0.08
DS Benton St Bridge	18093	636.42	636.59	0.17
US Benton St Bridge	18293	636.45	636.67	0.22
DS Railroad Bridge	18865	636.64	636.85	0.21
US Railroad Bridge	19025	636.8	636.96	0.16
DS Burlington St and Dam	20475	637.04	637.17	0.13
Gage – Iowa City	20798	637.175	637.38	0.21
US Burlington St and Dam	21265	642.18	642.41	0.23
US Railroad Bridge	22598	642.79	642.78	-0.01
	22731	642.79	642.78	-0.01
DS Memorial Footbridge	22864	642.84	642.79	-0.05
	23087	642.84	642.81	-0.03
	24280	643.04	642.98	-0.06
Hancher	25031	643.18	643.15	-0.03
	27911	643.67	643.84	0.17
	38643	645.73	645.77	0.04
US Iowa Power Footbridge	39593	652.72	652.35	-0.37
Over Weir at Iowa Power	39810	652.72	652.37	-0.35
	41497	652.68	652.43	-0.25
DS I-80 bridge	44983	653.05	652.87	-0.18
	44554	653.05	652.84	-0.21
DS Dubuque St bridge	51556	653.82	653.65	-0.17
US Dubuque St bridge	51702	653.97	653.69	-0.28
	63368	655.43	655.91	0.48
	66928	655.97	656.51	0.54
Gage- Coralville Dam	67099	655.905	656.49	0.59
			Model Average	0.05
			Campus Average	0.04

Source: Ayres Associates. "*University of Iowa - Hydraulic Memorandum.*" Iowa City, 2009.

Table 4.4. Ayres Associates high-flow calibration results of the HEC-RAS model.

Location Description	XS	Surveyed WSEL (ft)	Model WSEL (ft)	Difference (ft)
Napolean Lane	10087	643.9	643.14	-0.76
South Gilbert	14870	646.2	645.58	-0.62
HWY 6 – Downstream	16452	646.6	646.64	0.04
HWY 6 –upstream	16633	647.1	647.28	0.18
Benton	18293	647.5	647.77	0.27
Madison and Prentiss	19521	648.2	648.42	0.22
USGS Gage south of Hydraulics lab	20475	648.69	648.63	-0.06
UI Library	21850	651.3	651.12	-0.18
Between CRANDIC RR and Coffer Dam	22393	651.8	651.85	0.05
Art Building Temp (High Water Mark)	22731	652.7	652.75	0.05
IMU (High Water Mark)	22864	652.7	652.74	0.04
IMU (High Water Mark)	23087	652.7	652.87	0.17
Advanced Tech Lab (High Water Mark)	23315	652.7	652.94	0.24
Art West (High Water Mark)	23315	653.4	653.56	0.16
Art Building North	23556	653.3	653.12	-0.18
Canoe House (High Water Mark)	24670	653.4	653.37	-0.03
Voxman Music Building (High Water Mark)	24757	653.6	653.79	0.19
Voxman Music Building (High Water Mark)	25031	653.6	653.9	0.3
Between Hancher and Park	25814	653.9	654.2	0.3
Upstream of Park Road Bridge	26494	655.1	655.24	0.14
Mayflower (High Water Mark)	27911	655.4	655.63	0.23
Dubuque and Foster	28770	655.2	655.64	0.44
Normandy	33940	655.8	656.2	0.4
HWY 6 and Rocky Shore Drive	37462	657.4	657.16	-0.24
200ft North of Iowa River Power Dam	40118	658.8	658.2	-0.6
Corralville Reservoir USGS Gage	67099	667.84	667.65	-0.19
			Model Average	0.02
			Campus Average	0.09

Source: Ayres Associates. "*University of Iowa - Hydraulic Memorandum.*" Iowa City, 2009.

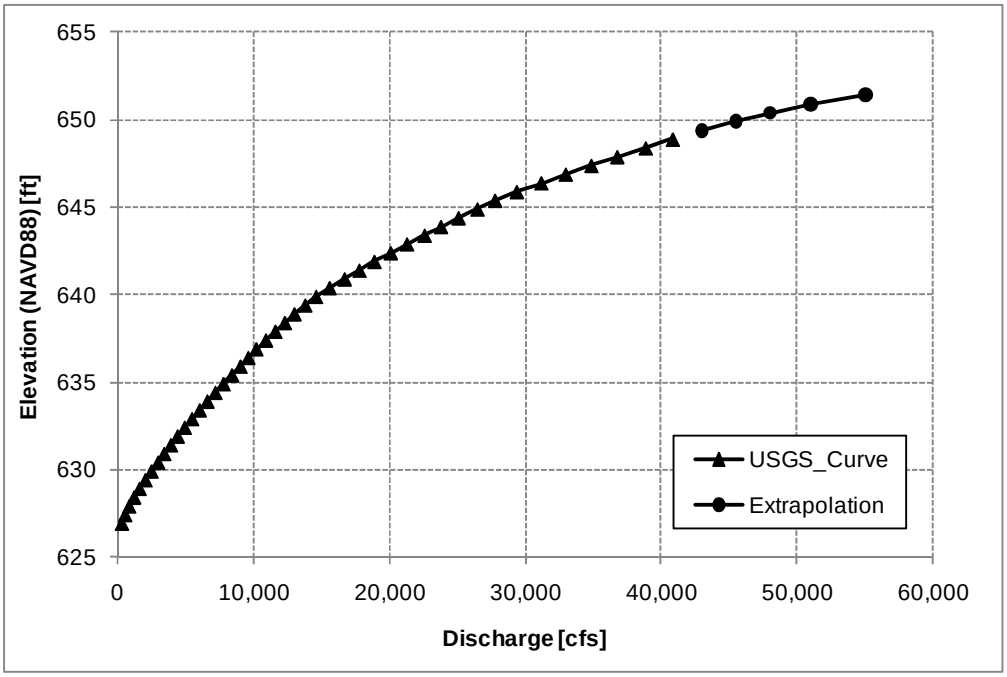

Figure 4.3. USGS stream gage (005454500) rating curve for Iowa River at Iowa City.

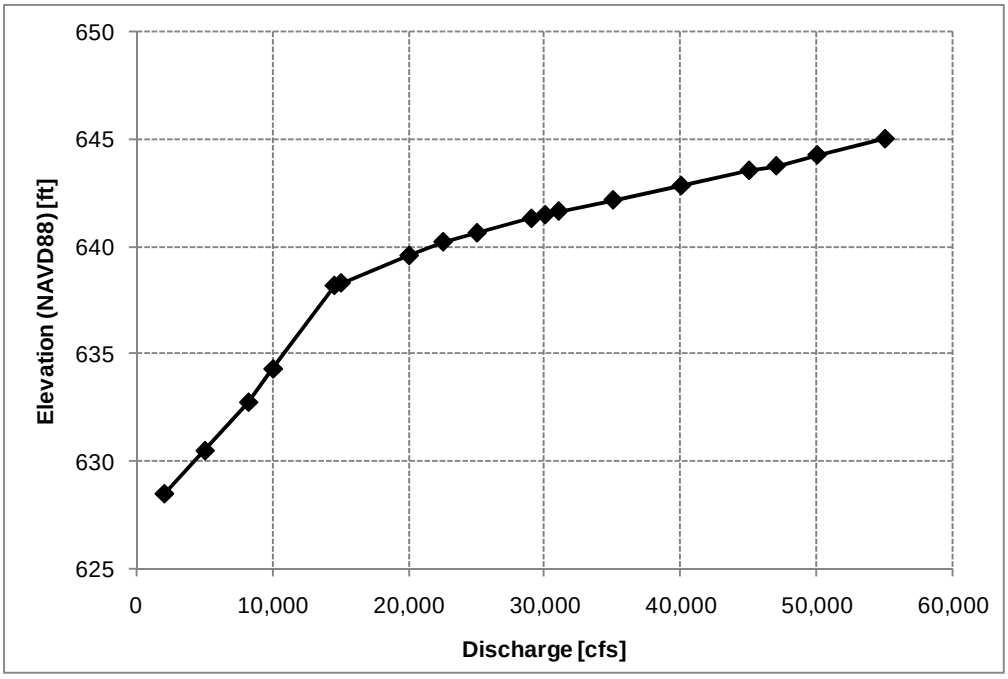

Figure 4.4. Ayres Associates rating curve for lower corporate limits of Iowa City, IA.

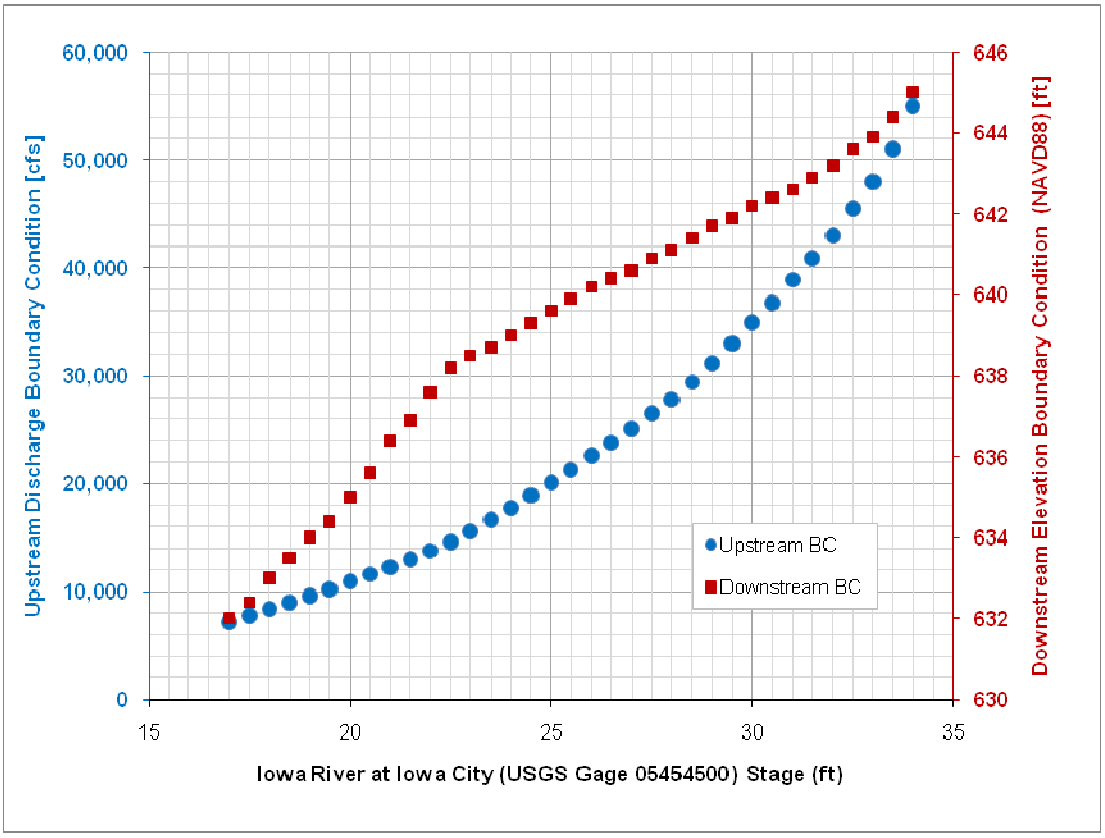

Figure 4.5. Depiction of model scenario runs and boundary conditions.

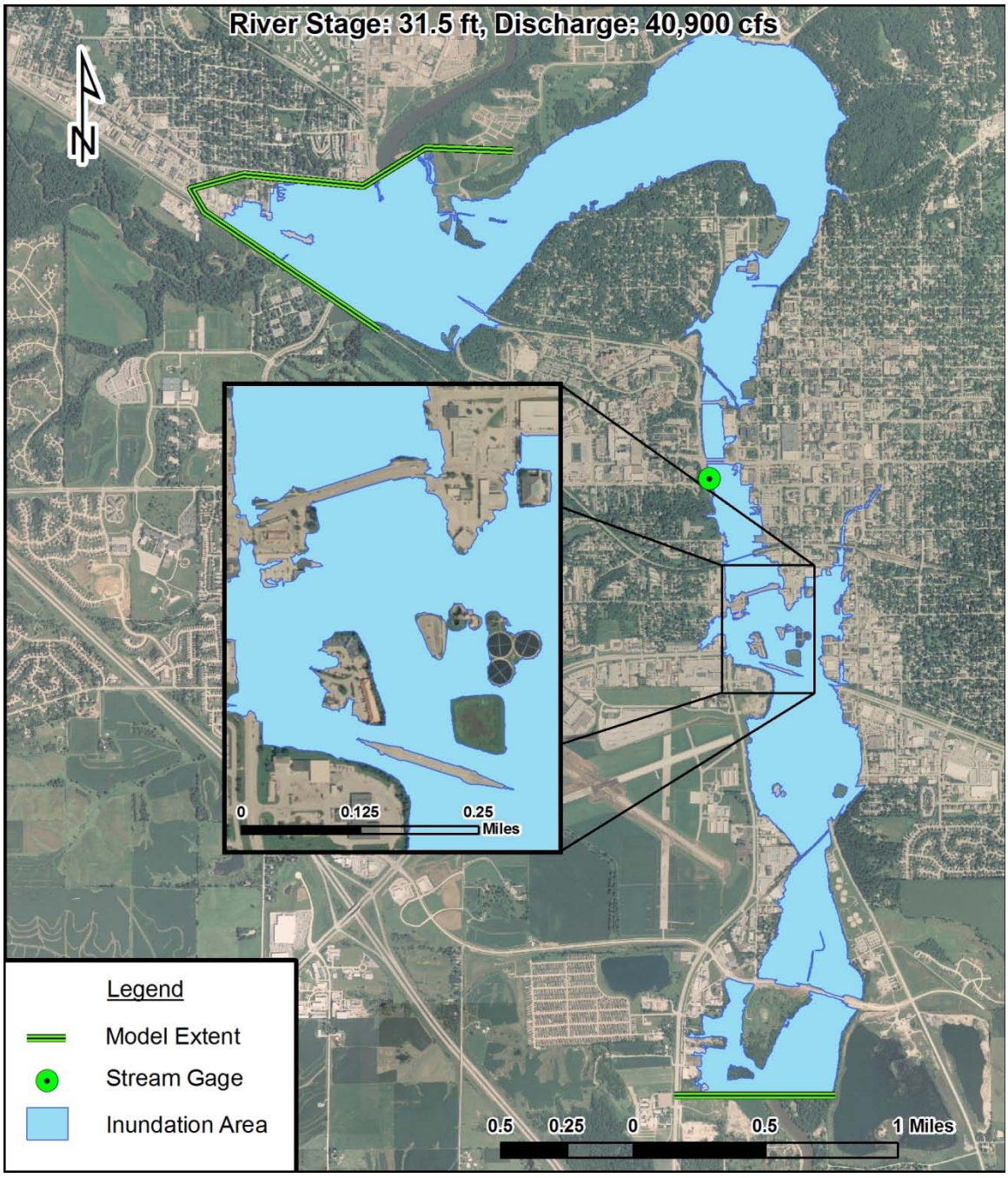

Figure 4.6. Example inundation shape, river stage: 31.5 ft, discharge: 40,900 cfs. Inset shows gradual inundation of bridges as a result of the addition of bridge decking elevations in the post processing DEM.

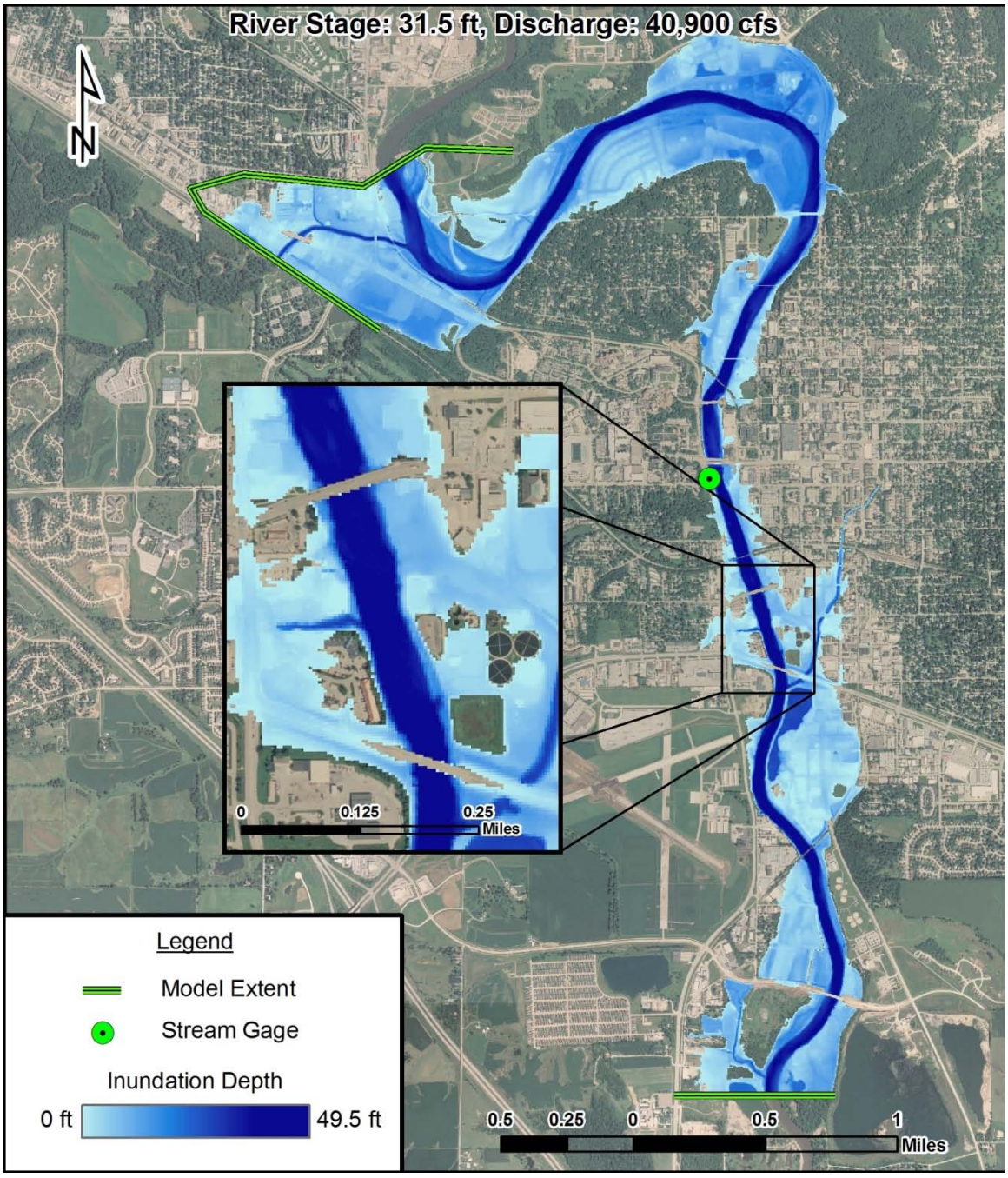

Figure 4.7. Example of an inundation depth raster, river stage: 31.5 ft, discharge: 40,900 cfs. Inset shows gradual inundation of bridges as a result of the addition of bridge decking elevations in the post processing DEM.

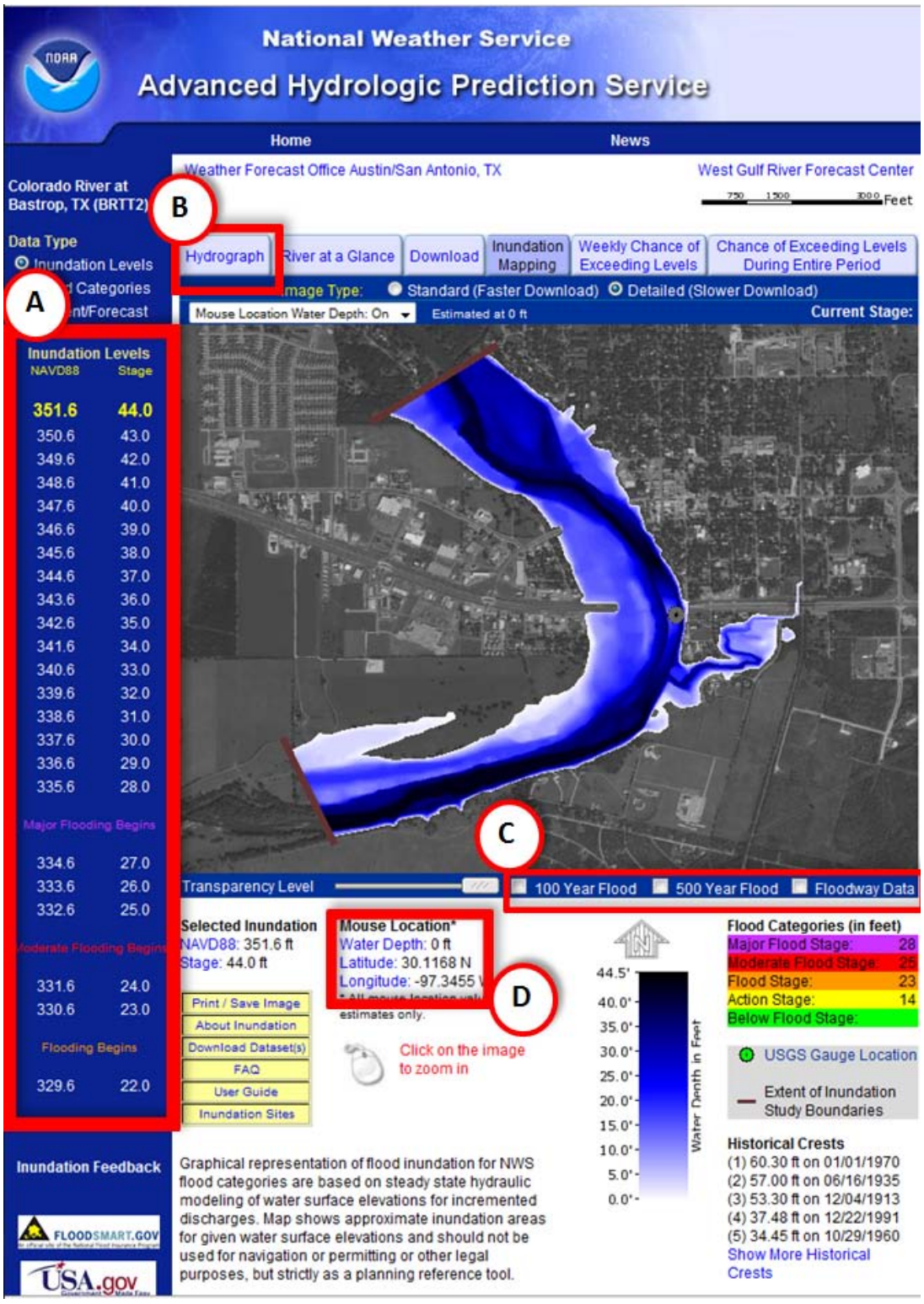

Figure 4.8. Example NWS AHPS inundation map library for Colorado River at Bastrop, TX. (A) inundation layers (B) 7 – day river stage forecast hydrograph (C) FEMA flood maps (D) inundation depths.

CHAPTER V: DEVELOPMENT OF A COUPLED 1D/2D HYDRAULIC MODEL FOR WATERLOO/CEDAR FALLS, IOWA

The objective of this effort was to develop an inundation model of a study reach while incorporating the benefits of both 1D and 2D hydraulic models. This was accomplished by developing a 1D hydraulic model of the river channel and a 2D hydraulic model of the floodplain and then coupling both using MIKE Flood. This model was utilized to investigate the role of levee closures in downtown Waterloo and to develop a plan to prioritize levee closure efforts. The model will also be used to develop a library of web-based static inundation maps to serve as a resource for citizens and community officials in assessing their flood risk.

5.1 Introduction

The flood of 2008 affected many communities along the Cedar River including Cedar Falls and Waterloo. Flood waters never overtopped any levees; however, despite a strong sandbagging effort (Ericson 2008), properties in downtown Waterloo suffered damages due to backed up storm sewers (Andersen 2008). Waterloo's extensive levee system requires the installation of levee closures when flood water reaches record levels, development of a plan to direct installation of levee closures would more efficiently utilize volunteer efforts.

5.2 Data collection

5.2.1 Study location

The study area includes the communities of Cedar Falls, Waterloo, and a portion of Evansdale, all of which are located along the banks of the Cedar River, in Black Hawk County, Iowa, as shown in Figure 5.1. The total drainage area is 5,146 mi^2 at USGS gaging station 05464000, located in downtown Waterloo. Four weir structures and nineteen bridges are within the seventeen miles of the study reach. An extensive levee

system has been constructed through Waterloo that has provided significant flooding protection, but it has also resulted in the channelization of the river. The river channel is much less defined upstream of Waterloo, consisting of many low lying wooded wetland areas. Just outside of these frequently flooded lowland areas are varying degrees of urban development. USGS gage 05463050 is located downstream of a low head dam in Cedar Falls. Farther upstream from Cedar Falls, the Cedar River has a braided channel pattern, consisting of numerous secondary channels and short circuits.

5.2.2 Overview

Data collection efforts included a bathymetric survey of the Cedar River and surveys of structural elements. The Iowa Department of Natural Resources (Iowa DNR), the City of Waterloo, and the United States Geological Survey (USGS) provided topographic data. The City of Waterloo, City of Cedar Falls, Iowa Department of Transportation (Iowa DOT), Union Pacific Railroad, CN Railroad, and United States Army Corps of Engineers (USACE) Rock Island District provided structural plan sets. A low flow calibration set was derived from bathymetry data. AECOM provided calibration data in the form of high water marks of the 2008 flood. The USGS provided bulk flow data such as rating curves and hydrographs used in calibration.

5.2.3 Bathymetry

Data collection methodology was nearly the same as those described in Section 4.3.2. Collection was initiated July 7th, 2009 and ended July 28th, 2009. Collection was postponed from July 10th to July 20th in anticipation of an event with a peak discharge of approximately 11,000 cfs. Collection locations and times are shown in Figure 5.2. Bathymetric data were not collected in reaches between dams or in close proximity to dams. Channel bed soundings were collected using a single-beam echosounder with 100 foot transect spacing. Real time corrections were received from the Iowa Department of Transportation (DOT) Real Time Kinematic GPS network (IA RTN) using a mobile

phone aboard the survey vessel. The mobile phone sent GPS corrections to the Trimble R8 unit via Bluetooth technology. Data analysis was executed the same way described in Section 4.3.2 to obtain channel bed elevation data.

5.2.4 Topography

Topographic data were compiled from several datasets of varying resolution and quality. The Iowa DNR provided a high-resolution airborne LiDAR dataset for the western half of Black Hawk County, which amounts to approximately half of the study area. This LiDAR dataset had a resolution of 1-meter and was the highest quality topographic data in the compilation. The City of Waterloo provided two-foot contour lines that were derived from an airborne LiDAR survey covering Waterloo city limits. A triangular irregular network was developed from the contour lines and then converted to a 1-meter raster grid. The USGS provided elevation data for Evansdale, a small portion of the study area not covered by LiDAR. The resolution of the USGS elevation data set was 10-meters and did not have the resolution or quality of the LiDAR products. These topographic datasets were used to create a digital terrain map (DTM), giving priority to the Iowa DNR dataset, then the City of Waterloo dataset, and finally to the USGS dataset.

5.2.5 Land use

Land use data were provided in the form of the 2006 National Land Cover Dataset (NLCD) by a consortium of US agencies (United States Department of Agriculture 2010). These data were classified in several land use categories, as shown in Figure 5.3, which served as a basis for selecting distributed roughness coefficients.

5.2.6 Structural elements

The City of Waterloo, City of Cedar Falls, Iowa DOT, Union Pacific Railroad, CN Railroad, and USACE Rock Island District provided plan sets describing levees,

flood walls, road embankments, bridges, and low-head dams that could obstruct flow. Field measurements were conducted when structural plans were unavailable.

5.2.7 Digital elevation model

The DTM created from a compilation of topographic data served as the basis for the creation of a digital elevation map (DEM). Bathymetric data collected by IIHR – Hydroscience & Engineering were incorporated into the DEM. Plan sets of structural elements such as levees and roadway embankments were digitized and also incorporated into the DEM.

5.2.7.1 Inclusion of bathymetry data

Bathymetric transect spacing of the single-beam echosounder collection was approximately 100 ft in the streamwise direction. Bathymetric data near river banks were removed, leaving only transect data in order to avoid creating any artificial bed features from interpolation between transects and near the banks.

Elevation points near the banks were extracted from the LiDAR data and merged with transects of bathymetric data. A TIN was generated from the merged bathymetry and bank elevation data. Three-dimensional polyline cross-sections were interpolated from the TIN surface at bathymetric transects. A new TIN of the channel bed was created from the three-dimensional polylines and converted to a raster grid. The raster grid was then inserted into the DEM, replacing unusable LiDAR elevation data of the water surface.

5.2.7.2 Inclusion of flood walls, levees, levee closures

Much of the levee system in the study area was covered by topographic data provided by the City of Waterloo. These data consist of 2-foot contour intervals derived from a LiDAR dataset. While levee embankment slopes are correctly depicted in the LiDAR, some levee crest elevations were incorrect by as much as two feet due to the

contour interval. Using as-built plan sets provided by the USACE Rock Island District, correct levee crest elevations were digitized and manually inserted into the DEM.

Floodwalls are located along the Cedar River in downtown Waterloo and near the wastewater treatment plant in Cedar Falls. In many places, the flood walls are small sections that connect earthen embankment levees. The resolution of both LiDAR datasets was insufficient to depict flood walls less than one meter wide. Additionally, any type of numerical mesh generated from the DEM was likely to have a resolution of 5 meters or greater. Therefore, existing floodwall elevations were determined from as-built plan sets. The floodwall widths were exaggerated in order to accommodate a coarser DEM resampling and inserted into the one meter resolution DEM.

Levee protection is discontinuous at most bridge crossings in downtown Waterloo. Levee gaps are typically filled using flood panels, gates, or sandbags in the event of a flood emergency. These gaps were present in the topography provided by the City of Waterloo, but were removed by interpolating between levee sections for purposes of calibration and accurately representing inundation. Further investigations of levee closures are presented in later sections.

5.2.7.3 Inclusion of buildings

Building foot prints within the flood plain were approximated and manually digitized using ArcGIS, LiDAR, and aerial photography. Elevation data were not available for any buildings in the study area, so a constant elevation of 272 meters NAVD88 as assumed for all buildings. It is likely that flow over the top of buildings would be insignificant compared to the flow around buildings. Resampling a 1-meter building elevation raster to a 10-meter raster produced building foot prints with only slight discrepancies, as shown in Figure 5.4. Buildings smaller than 10 meters in any dimension were not included in the DEM.

5.2.7.4 Modification of storage areas

The study reach includes several lakes and backwater areas that are located within or near George Wyth State Park between Cedar Falls and Waterloo just north of Cedar Falls. The DEM was modified to account for possible storage or conveyance through these areas. The LiDAR data in these inundated areas depicted an irregular water surface; therefore, a single water surface elevation was determined by averaging LiDAR data within the backwater or lake. A bed elevation for each area was approximated by subtracting one meter from the average water surface elevation. The estimated bed elevations for the backwater areas and lakes were then inserted into the DEM. Accounting for these areas should also more accurately depict the inundation extent.

5.2.8 Water surface elevation surveys

Bathymetry data collected for the study reach were also processed to obtain a low flow water surface profile to be used for calibration. Initially, the geospatial-position of the Odom survey head was determined by subtracting the elevation difference between the Trimble R8 unit and Odom survey head, 1.976 meters, from the geo-position of the Trimble R8 unit. The survey head was assumed to be submerged 0.1 meters below the water surface; therefore, this distance was also added to the geo-position of the Odom survey head to obtain water surface elevations.

The survey was conducted over six days during the month of July 2009. Ideally, there would have been a steady discharge throughout bathymetric surveying, but some valuable calibration data can still be extracted. Discharge data from USGS gage 05464000 at Waterloo shows a high flow period from July 10th - July 20th, as shown in Figure 5.5. Bathymetry was collected during three periods: July 7th –July 10th, July 20th – July 21st, and July 27th – July 28th. Since the discharge from July 7th – July 10th was approximately steady, the water surface profile obtained from these bathymetric surveys was considered one calibration dataset. The discharge was semi-steady from July 27th –

July 28th, so the data collected during this period were considered as another calibration set. The discharge from July 20th – July 21st was on the falling limb of a small event and was not used due to the existence of hysteresis. The other two periods that bathymetry data were collected were separated into individual datasets due to the fluctuation in discharge. The resulting low flow water surface profile is shown in Figure 5.6 along with survey collection dates.

A significant amount of uncertainty is introduced when developing these low flow calibration datasets. The pitch, roll, and heaving of the survey vessel were not measured during bathymetry collection. Therefore, the calculated geo-position of the survey head and water surface may have been less accurate depending on the movement of the survey vessel. This uncertainty must be considered in addition to the uncertainty of the Trimble R8 unit, which is 10mm in the horizontal and 20mm in the vertical directions.

A high flow calibration data set, included in Appendix F, was created using high water marks from the 2008 flood. Following the recession of flood waters, AECOM surveyed data points at locations shown in Figure 5.7. The locations of high water marks are concentrated along levees and flood walls in downtown Waterloo. Farther upstream, the locations are more widely spaced and continue just upstream of the low head dam in Cedar Falls. Additional flood protections, such as temporary sandbag levees, were in place throughout the 2008 flood, and may have affected high water marks.

5.2.9 Bulk flow data

Historical flow data for the Cedar River were obtained from online data archives hosted by the USGS (United States Geological Survey 2010). The 2008 flood hydrographs observed at Waterloo, Cedar Falls, and Black Hawk Creek USGS Gage Stations are shown in Figure 5.8. Cedar Falls gage station 05463050 does not have an established rating curve, but a comparison with Waterloo gage data reveals the 2008 flood hydrograph was likely routed downstream with little distortion. Black Hawk Creek

discharge contributions were small in magnitude when compared to the Cedar River. For this reason, the observed peak discharge at the Waterloo gage was used as an inflow hydrograph at the upstream model boundary for high flow calibration. A rating curve at the downstream boundary of the study reach was developed by assuming a normal depth for a range of flow rates, as shown in Figure 5.9. A downstream channel slope of 0.0008 and a Manning's roughness value of 0.032 were used to complete normal depth calculations.

5.2.10 Summary

Several sources of data were utilized to facilitate numerical simulation of flooding in Cedar Falls and Waterloo. Data collection included a single-beam bathymetric survey of the Cedar River through the study area. A DTM was generated using high resolution LiDAR provided by the Iowa DNR, contour lines derived from LiDAR provided by the City of Waterloo, and NED elevation maps provided by the USGS. Land use data was provided in the form of the 2006 National Land Cover Dataset, which is a product of a consortium of US agencies. Structural elements were digitized from plan sets provided by the City of Waterloo, City of Cedar Falls, Union Pacific Railroad, CN Railroad, Iowa DOT, and USACE Rock Island District. Bathymetry, topography, and structures were incorporated into a DEM that was used to develop a numerical mesh. AECOM provided high flow calibration data, and low flow calibration data was derived from bathymetric data. Bulk flow data were collected from the USGS WaterWatch website.

5.3 Numerical simulation

A one-dimensional hydraulic model of the river channel was constructed by extracting cross-sections from a 1-meter resolution DEM. Low head dams and bridges were digitized from as-built plan sets and inserted in the 1D model. The 1-meter DEM was resampled to a 10-meter DEM to develop a two-dimensional model of the flood plain. The 1D model was calibrated using a low flow calibration set extracted from data

collected during the bathymetric survey. An initial set of floodplain roughness values was determined using established literature. Several alternate roughness parameter sets were created by multiplying the initial values by a factor. High flow calibration was accomplished by simulating the peak 2008 discharge with each set of roughness values and comparing it to 2008 flood high water marks. An investigation of the impact of levee closures on flooding in downtown Waterloo was conducted, and a sandbag plan was developed.

5.3.1 Numerical methods

The 1-meter resolution DEM was resampled to a coarser 10-meter DEM using bilinear interpolation in order to create a rectangular computational mesh. Manual editing of the DEM was necessary where the coarser DEM was unable to properly describe features such as levee walls. The coarse DEM was converted from ESRI (Environmental Systems Research Institute) grid format to ASCII format and imported into MIKE 21. The resulting rectangular computational mesh consisted of approximately 2 million nodes.

Inclusion of structural elements such as bridges and low head dams was accomplished by constructing a one-dimensional hydraulic model of the river channel using MIKE 11. Structure representations were developed using as-built plan sets and were incorporated in the MIKE 11 model. The one-dimensional MIKE 11 model was then coupled with a two-dimensional MIKE 21 model of the flood plain using MIKE Flood. MIKE 21 mesh cells of the river channel were blocked out using land values to ensure that the conveyance was not double counted. MIKE 11 cross-section geometries were extracted from a 1-meter resolution DEM at an average spacing of 80 meters. Cross-sections were placed such that endpoints were located at levee crests when possible, particularly through downtown Waterloo.

MIKE Flood 1D/2D coupling allows two models to exchange information about water levels and discharge. Due to the large quantity of structures with the reach, lateral coupling of the river channel was selected over other link types due to its ease of development. Lateral links are intended to model over-topping of a river bank or levee. A simple weir equation was selected as the governing equation for calculating flow through the lateral link. The discharge exchange depends on water levels in linked MIKE 21 cells and MIKE 11 h-points, and an internal weir structure, as shown in Figure 5.10. Lateral structure elevations are based on a bed level determined by cross-section endpoints and a width determined from the resolution of points defined along the structure (DHI 2009). The distribution of flow to and from the linked model nodes are determined based on the range of influence each structure has upon each linked node (DHI 2009).

5.3.2 Boundary conditions

Coupling the models with lateral links required specifying the perimeter of the MIKE 21 domain as land values. Boundary conditions were only specified in the MIKE 11 model in the form of an upstream inflow discharge and a downstream rating curve. The upstream inflow discharge was a steady discharge used to replicate low flow or high flow calibration conditions. The steady flows used for low flow calibration were 3,600 cfs for 7/07/09 to 07/10/09, and 3,000 cfs for 07/27/09 to 07/28/09. The steady flow for high flow calibration was 110,000 cfs. A lack of bathymetric data for Black Hawk Creek prevented the simulation of back water effects in the reach, but flow contributions were considered in simulations. A normal depth assumption was made to develop a downstream rating curve that was used as a MIKE 11 boundary condition. The downstream boundary was placed a sufficient distance downstream from the study area to avoid affecting simulation results. The endpoints of downstream cross-sections were

extended into overland areas to prevent creation of backwater effects from flow exiting the coupled model domain.

5.3.3 Modeling of bridges

The Federal Highway Administration (FHWA) WSPRO bridge method was utilized to model most of the bridges within the study reach. Calculation of losses is based on solution of the energy equation (DHI 2009). Contraction losses are calculated by using an effective flow length. Expansion losses are determined from experimentally based tables. The effects of eccentricity, skewness, wingwalls, and embankment slope were incorporated when necessary. The submergence of bridges required calculation of pressure flow, which was executed using FHWA Orifice equation for upstream and downstream submergence. Road overflow was modeled using the FHWA method, which employs a weir equation, and accounts for tail water submergence.

Bridge spans significantly wider than the river channel, such as Highway 58 over the Cedar River, required an alternate modeling method. Placing cross-sections from abutment to abutment would have introduced sudden expansions and contractions in the MIKE 11 model and caused instabilities. Therefore, the bridge was only modeled within the river channel. Overbank roughness values spanned by the bridge were increased to account for contraction losses. The submergence of the bridge is unlikely; therefore, this alternative method should be sufficient for flood simulations.

5.3.4 Modeling of low head dams

Low head dams were initially modeled using the broad crested weir option within MIKE 11. MIKE 11 calculated Q/h relationships using cross-sections immediately upstream and downstream and a defined weir geometry. Calculations assume a hydrostatic pressure distribution on the weir crest (DHI 2009). Separate calculations were made for drowned flow and free overflow, with an automatic switching between the

two methods. Head loss and calibration coefficients were altered during model calibration.

Initial calibration runs revealed that an alternative weir modeling method needed to be implemented to investigate submerged flow situations. Thus, the Extended Honma formula, shown in Equation 5.1, was used in several calibration runs.

$$Q = \begin{Bmatrix} C_o W h_u^{3/2} & for\ h_d / h_u \le (h_d / h_u)_i \\ C_o(\alpha \cdot (h_d / h_u)^q + \beta) W h_u^{3/2} & for\ other cases \\ C_o(\gamma \cdot (h_d / h_u)^r + \delta) W h_d (h_u - h_d)^{1/2} & for\ h_d / h_u \ge (h_d / h_u)_s \\ C_o = a \cdot (h_u / H)^p + b & for\ all \end{Bmatrix} \quad 5.1$$

Where W is weir width, H is weir height above the invert, h_d is the upstream water level above the crest, h_u is the downstream water level above the crest, $(h_d/h_u)_i$ is a user specified depth ratio between perfect and imperfect flow, $(h_d/h_u)_s$ is a user specified depth ratio between imperfect and submerged flow regime, and a, b, p, q, α, β, γ, and δ are user specified parameters. This formula calculates three flow regimes: perfect, imperfect and submerged overflow. The appropriate regime is determined from the ratio between downstream and upstream water depth above the weir crest.

5.3.5 Simulation run-time

The simulation times required to reach steady state conditions for a low flow (3,000 cfs) and a high flow (110,000 cfs) were 2 hours and 96 hours, respectively. A simulation was assumed to reach steady state when outflow discharge was the same as inflow discharge, as reported by the MIKE 11 component of the couple model. The simulation time required for a low flow is small because the flow stays within the MIKE 11 channel model. The high flow simulation time was calculated beginning at a bankfull condition. To improve simulation time, a separate steady state condition for 100,000 cfs was used as initial conditions for steady state 110,000 cfs simulations. When utilizing

these initial conditions, simulation times were shortened to 24 hours for a steady flow of 110,000 cfs.

Typically, improvement in simulation time is expected for coupled models versus full two-dimensional models. MIKE 21 uses parallel processing to take advantage of the capabilities of multiprocessor and multi-core CPUs. However, coupled MIKE Flood models are unable to parallel process at the present time. There was improvement in computational speed at lower discharges, but simulated discharges near the 2008 peak were much slower than if the whole reach were modeled using MIKE 21.

5.3.6 Model calibration

Model development required designating distributed roughness coefficients throughout the study reach. Table 5.1 presents initial coefficients that were selected based on the 2006 NLCD classifications shown in Figure 5.3 and values presented in the established literature. MIKE 21 utilizes Manning's 'M' values, or inverse 'n' values, to determine a Chezy number based on cell water depth in order to perform numerical simulation of the Saint Venant equations Roughness values and weir coefficients were used as calibration parameters for a low flow and high flow calibration.

5.3.6.1 Low flow calibration

Bathymetric survey data were used to create two sets of low flow calibration data sets, for two steady flows: 3,600 cfs and 3,000 cfs. The relative difference between the simulations and the calibration sets are shown in Figure 5.11. Gaps are present within the calibration results due to hysteresis during a bathymetric collection period and an inability to gather bathymetry near dams. The model was calibrated using channel roughness and low head dam loss coefficients to within approximately 0.25 meters of the calibration data. Calibration also included altering of low head dam parameters. The final calibrated channel Manning's n value was 0.029 throughout the study reach. This is well within acceptable values for a river channel as defined by Chow (1959).

5.3.6.2 High flow calibration

High water marks surveyed by AECOM following the 2008 flood were used to calibrate the coupled model to a high flow condition. Initial roughness coefficients determined from NLCD land classifications were used as a base set for calibration, as shown in Table 5.1. Due to the number of different roughness types, individual modification of parameters was not feasible. Therefore, the base roughness values were multiplied by a factor to determine a set of overbank roughness values that would reproduce similar high water marks. Initial simulations modeled weirs using the broad crested weir option in MIKE 11. Simulations were initiated using steady conditions from a 100,000 cfs simulation, inflow was increased to 110,000 cfs and simulated period of 24 hours. Results from these simulation runs are shown in Table 5.2. Positive mean over-prediction values indicate the models generally over-predict inundation. Simulation "I" most closely reproduced observed high water marks, with a mean over-prediction value of -0.03 meters and a standard deviation of 0.45 meters. Plotting the water surface profile from Simulation I with observed high water marks, as shown Figure 5.12, shows the model over-predicts inundation in the downstream portion and under-predicts in the upstream portion.

Wetland roughness coefficients were further investigated to improve high flow calibration. An important observation made from initial calibration results is model predictions change from over-predicting to under-predicting in the middle portion of the study reach, an area dominated by wetlands. Overbank roughness values of upstream and downstream reaches were multiplied by two separate factors to consider conveyance efficiency of the urbanized downstream reach and vegetation in the upstream reach. Simulations VIII and IX were created to investigate the impact of using two multiplications factors for upstream and downstream reaches, while continuing to model weirs with a broad crested method. Simulation results, shown in Table 5.3, indicate multiplying upstream and downstream roughness values by two separate values can

improve model predictions. Multiplication of the downstream and upstream roughness values by 0.7 and 1.0, respectively, reduced the relative error standard deviation. However, upon analysis of results the broad crested weir method was unable to properly model submergence of weirs.

The Extended Honma weir modeling method was implemented to investigate an alternative submerged weir model. Simulations X, XI, XII, and XIII utilized the Extended Honma weir method with default coefficients and submergence criteria. Upstream and downstream roughness multiplication factors ranged from 0.7 to 1.2, as shown in Table 5.3. Analysis of simulation results shows Simulation XIII had the lowest standard deviation at 0.38 meters, and lowest mean over-prediction error at 0.01 meters. The downstream and upstream roughness multiplication factors were 1.0 and 1.2, respectively. The simulated water surface profile from Simulation XIII is plotted with observed high water marks in Figure 5.13. An important calibration consideration is Simulation XIII was able to reproduce the overall trend of the water surface profile throughout the reach more accurately than other scenarios; therefore, this scenario was selected as the calibrated model.

5.3.6.3 Calibration uncertainty

Uncertainties in model calibration should be considered when analyzing simulation results of a complex environmental phenomenon (Hall, et al. 2005). Model calibration assumed a single parameter set could accurately reproduce observations. An exhaustive exploration of calibration parameters would likely identify several sets of optimum parameters. Also, calibration was based on coarse datasets for low and high flow conditions. Observed high water marks could have been reproduced if spatially distributed roughness parameters were used; however, lack of sufficient spatially distributed data would have required over-parameterization of the model (Hall, et al. 2005). Varying Manning roughness coefficients to reproduce observations of a low flow

condition and a single high flow condition assumes the model behaves linearly. Hence, calibrating to several intermediate flow conditions would decrease model prediction uncertainty.

5.3.7 Model application

The objective of this study was to develop a coupled 1D/2D numerical model that could accurately predict flood inundation for the study reach. An example of a flood inundation depth map is shown in Figure 5.14, along with FEMA 100 and 500-year flood boundaries. The calibrated model will be used to create a library of static inundation maps to be hosted on the Iowa Flood Center website. The inundation map libraries will provide the citizens of Cedar Falls and Waterloo a resource for evaluating their flood risk. The model will also be used to develop a levee closure plan.

5.3.8 Investigation of levee closures

The calibrated model was utilized to construct two smaller coupled 1D/2D MIKE Flood models of downtown Waterloo to investigate levee closures. Smaller model domains were necessary to improve computational speed. One model contained identical geometry, roughness, and flow parameters as the larger calibrated model, while the other model incorporated levee gaps normally closed with sandbags or gates. Flow through this smaller reach was assumed to be subcritical; therefore, the “with levee closures” model of downtown Waterloo should behave identically to the larger calibrated model described in previous sections. The “without levee closures” model was not calibrated for high flow conditions due to the lack of calibration data for a “without levee closure” scenario. Alterations present in the “without levee closure” model included the lowering of MIKE 11 cross section endpoint elevations and MIKE 21 grid cells near levee gaps. The model domain and levee closure locations are shown in Figure 5.15.

Simulating the 2008 flood using the “without levee closures” model shows significant flooding in downtown Waterloo as a result of levee gaps. The benefit of the

levee system is evident when comparing 2008 flooding extents for both scenarios in Figure 5.16. Slight differences in water surface profiles are a result of lateral discharge leaving the main channel, as shown in Figure 5.17. While this lateral discharge was small compared to the flow within the channel, the duration of the 2008 flood event produced a large volume of flood water in the downtown area.

The development of a levee closure plan cannot be completed by running the "without levee closures" model and determining the order in which closure elevations are reached. Any lateral outflow from the main channel affects upstream water surface elevations and downstream discharges. In addition to this limitation, simply determining the order in which to install closures does not give organizers any criteria on which to base their decisions. A proper plan should designate which closures to sandbag for a given discharge or river stage. Therefore, the levee closure plan was developed as follows: (1) a design hydrograph, shown in Figure 5.18, was simulated using the "with levee closures" model, and (2) for a given 5,000 cfs increment, required levee closure locations were determined using simulation results. The order of required levee closures and corresponding discharges and river stages are shown in Figure 5.19. Phase VII levee closures indicate that they should be closed at a discharge of 115,000 cfs. However, levee walls are overtopped at approximately 115,000 cfs in the upstream portion of downtown Waterloo, so this phase is unnecessary.

Uncertainties must be considered when developing a levee closure plan in the manner discussed above. Local modeling inaccuracies may affect the order in which closures are affected. Also, the procedure assumes the model reaches a steady state condition after each discharge increment. An actual flood hydrograph would likely rise more steeply on the rising limb. Direction of closure effects should not be executed based solely on observed discharges, but should instead be based on forecasted discharges. An appropriate procedure would be to execute one closure phase above the forecasted discharge to prevent a flash flood event from overwhelming closure efforts.

5.4 Summary

This study presents the development of a high resolution hydraulic model of a 17-mile reach of the Cedar River corridor through the communities of Cedar Falls and Waterloo. A coupled modeling approach was selected in order to incorporate the hydraulic effects of structures. The numerical model will be used to create a library of static inundation maps to be hosted on a web-based Google maps interface. These maps will allow citizens and community officials to assess their flood risk and respond accordingly.

A one-dimensional MIKE 11 model of the river channel and structures was developed and coupled to a two-dimensional MIKE 21 model of the flood plain using MIKE FLOOD. Data requirements included bathymetry, topographic, bulk flow, land use, and as-built structural data. IIHR-Hydroscience and Engineering collected bathymetry data. Topographic data were provided by the Iowa DNR, the City of Waterloo and the USGS. Bulk Flow data were provided by the USGS Water Watch. The USDA provided land use data. As-built structural plans were provided by the City of Waterloo, City of Cedar Falls, Union Pacific Railroad, CN railroad, and USACE. The coupled model was calibrated to a low flow condition using a water surface profile derived from data collected during the bathymetry survey. The model was calibrated to a high flow condition using 2008 flood high water marks provided by AECOM.

The calibrated model was utilized to investigate the role of levee closures in downtown Waterloo. Simulation results with and without levee closures demonstrated that levee closures are a vital component of Waterloo's levee system. A levee closure plan was developed using levee closure base elevations to prioritize sandbagging. The model will also be used to develop a library of inundation maps.

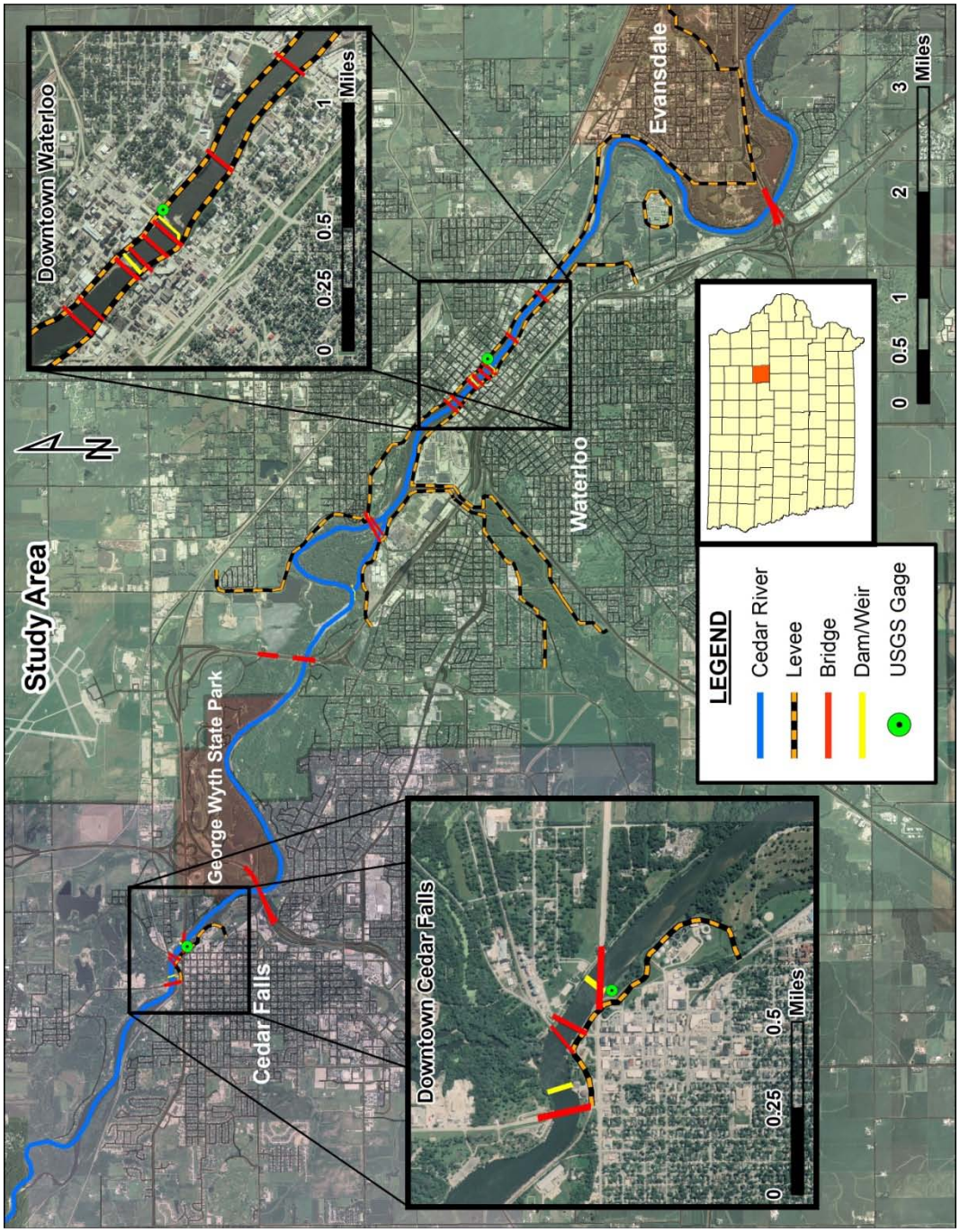

Figure 5.1. Study area along the Cedar River.

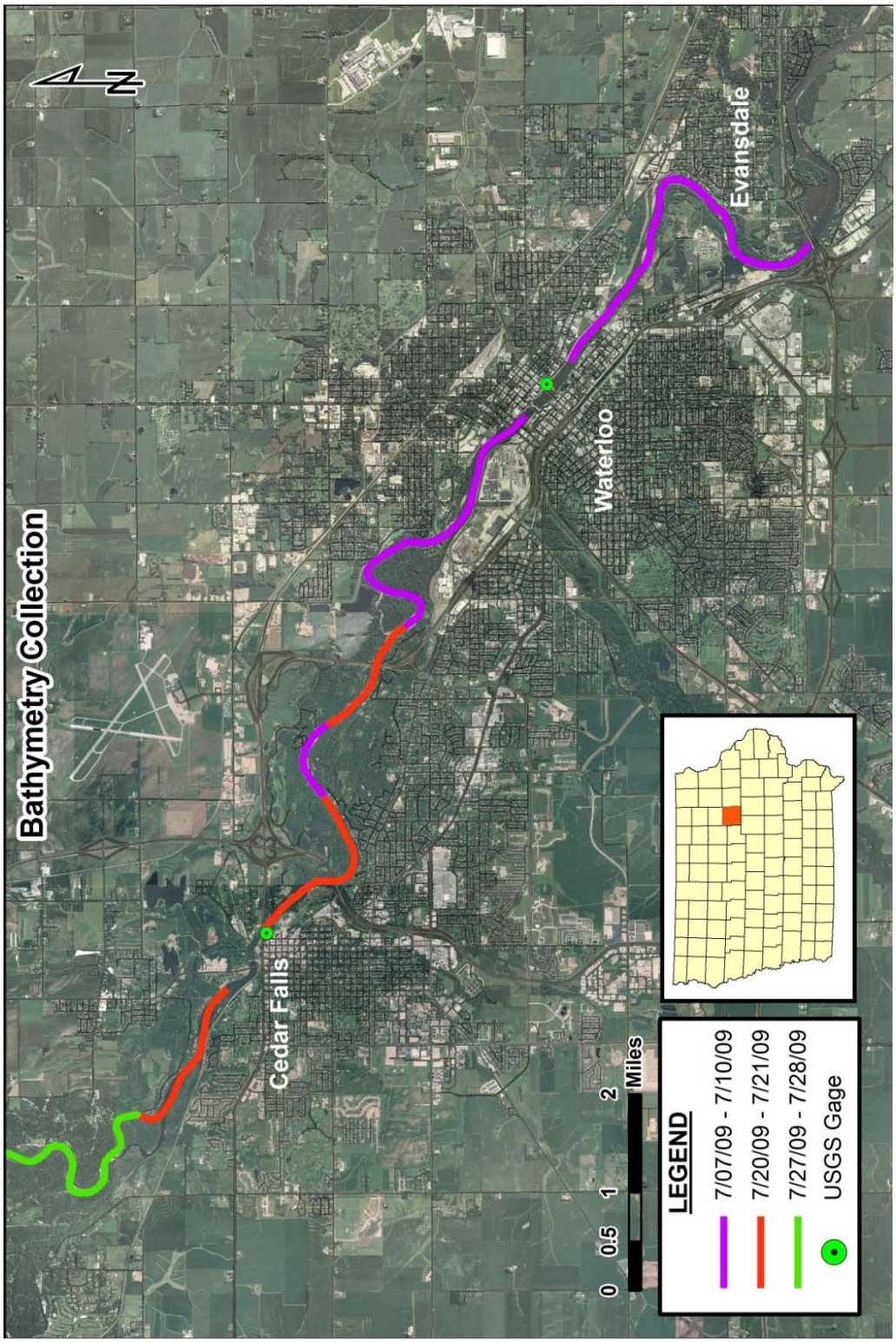

Figure 5.2. Bathymetric survey locations and times.

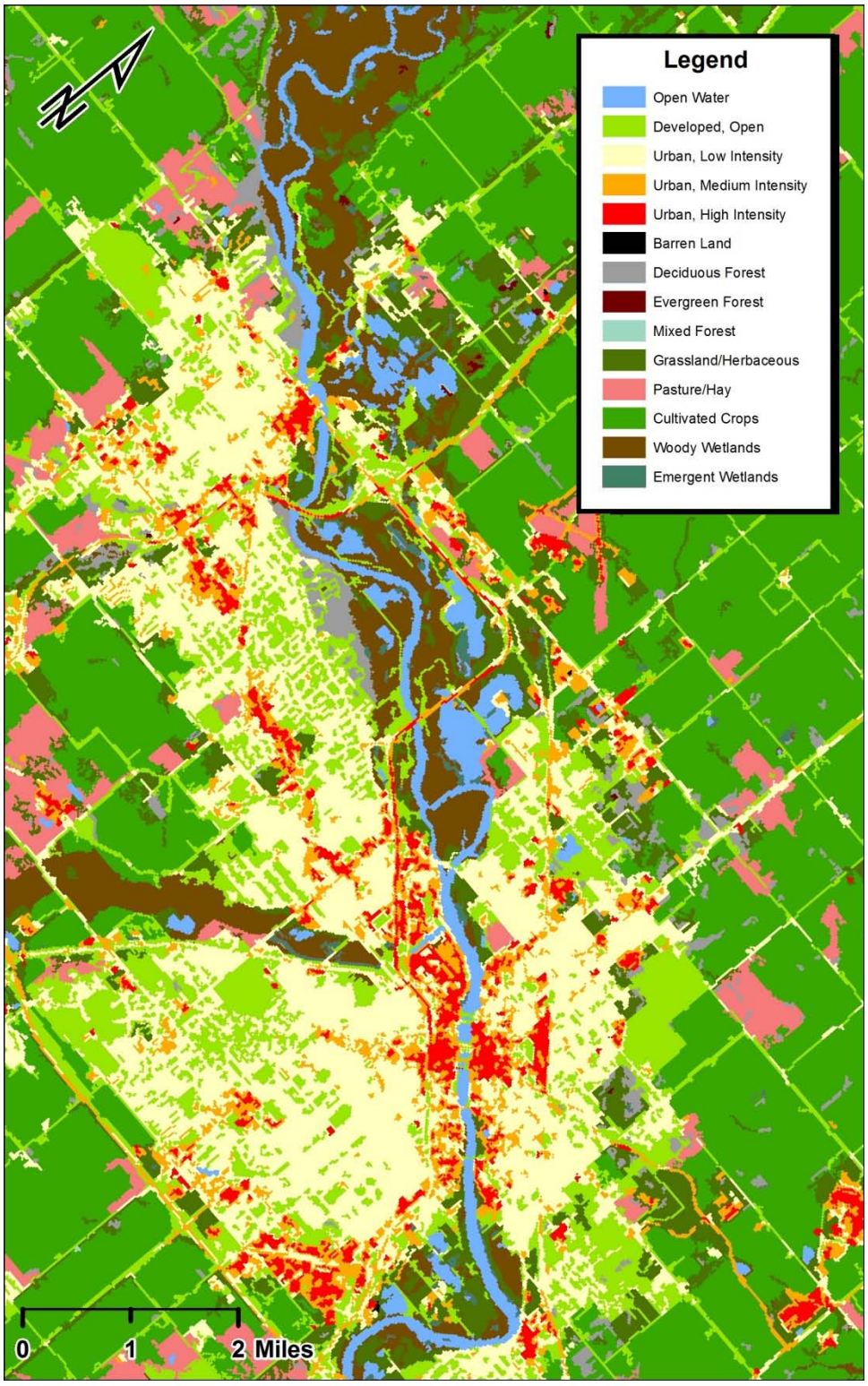

Figure 5.3. 2006 National Land Cover Dataset of study area.

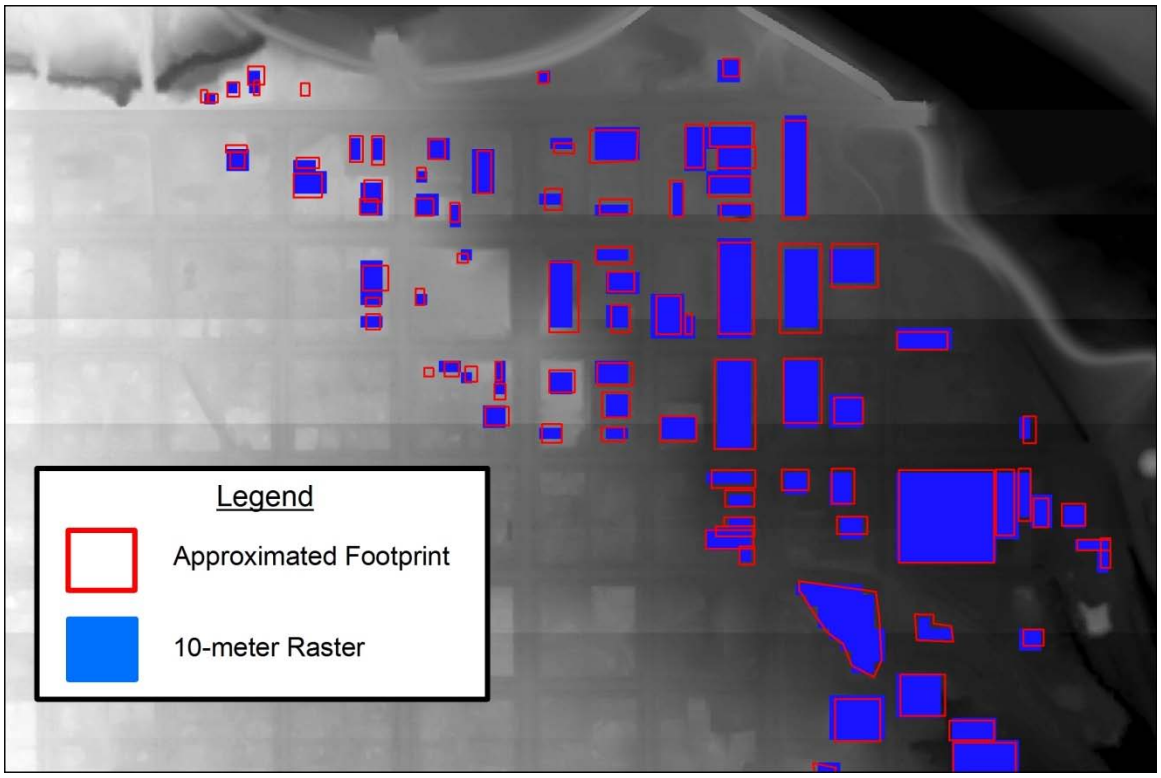

Figure 5.4. Comparison of approximated building footprints with 10-meter raster representation.

Figure 5.5. July 2009 hydrograph at Waterloo USGS gage station 05464000 during collection of bathymetry data.

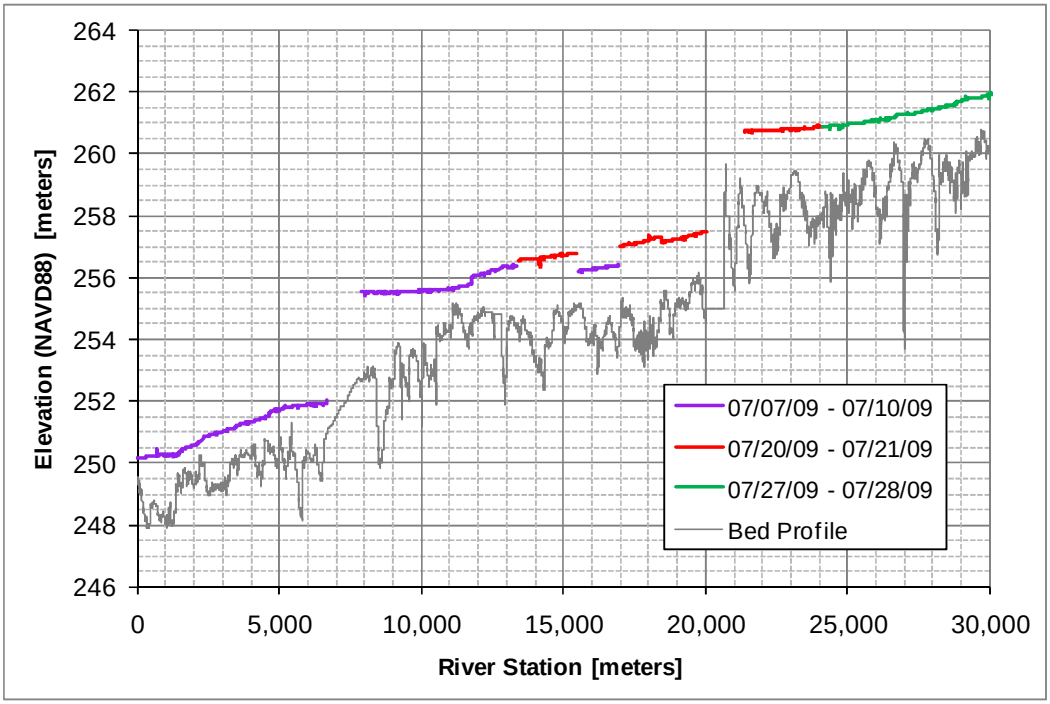

Figure 5.6. Low flow calibration profile derived from bathymetric data.

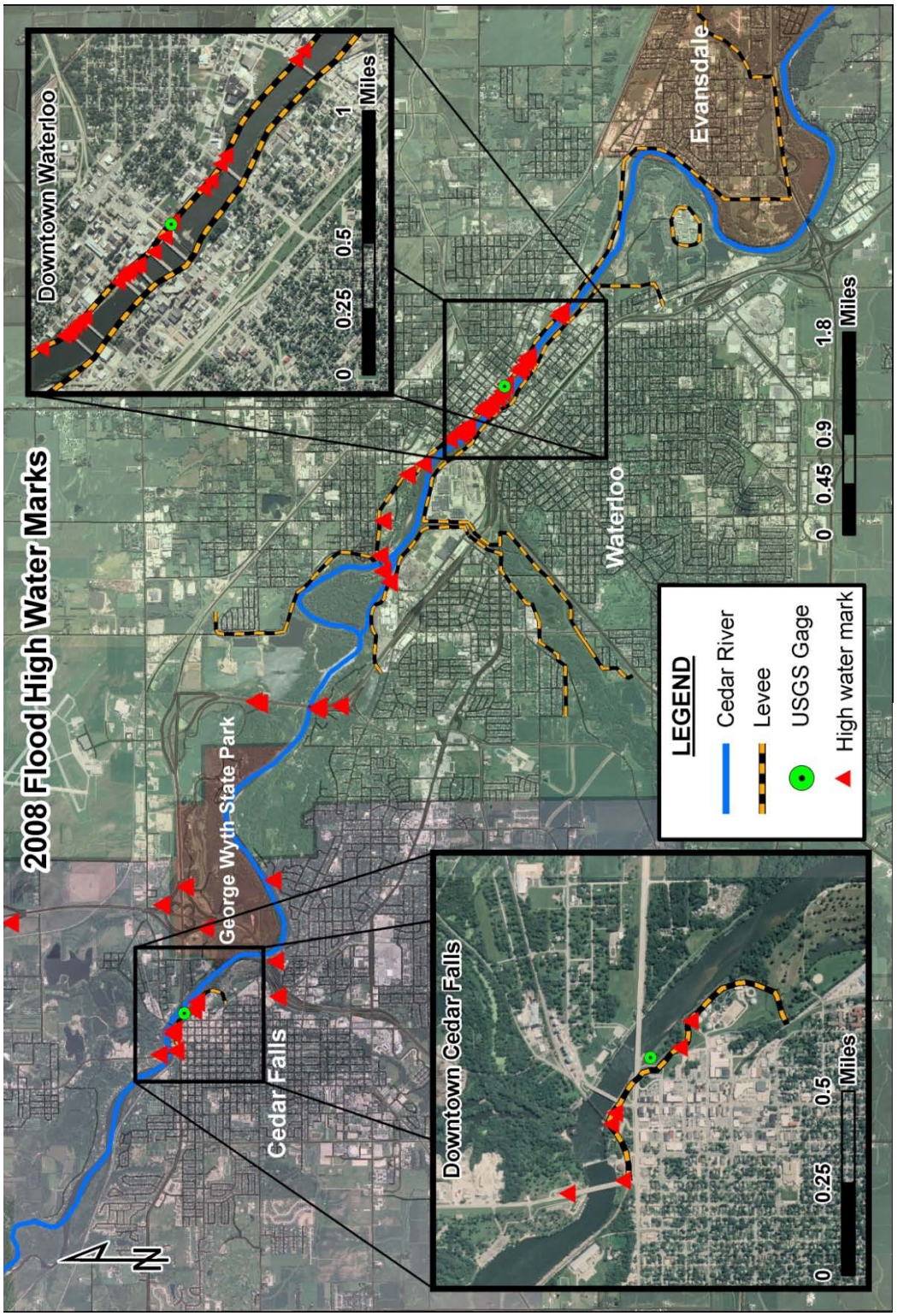

Figure 5.7. High water marks from the 2008 flood.

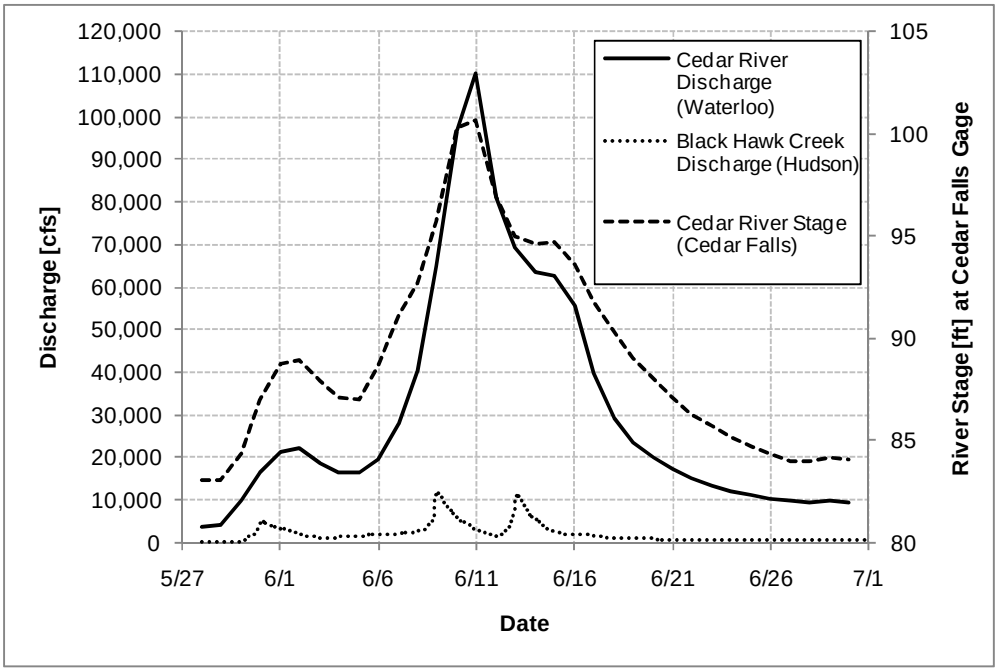

Figure 5.8. 2008 flood hydrographs observed at several USGS gage stations.

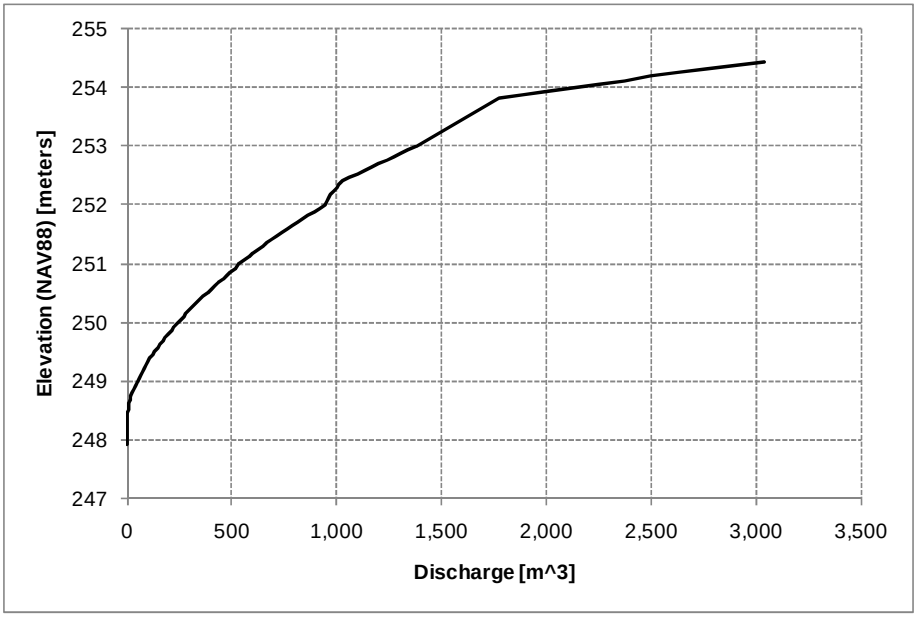

Figure 5.9. Rating curve used for downstream boundary of study reach.

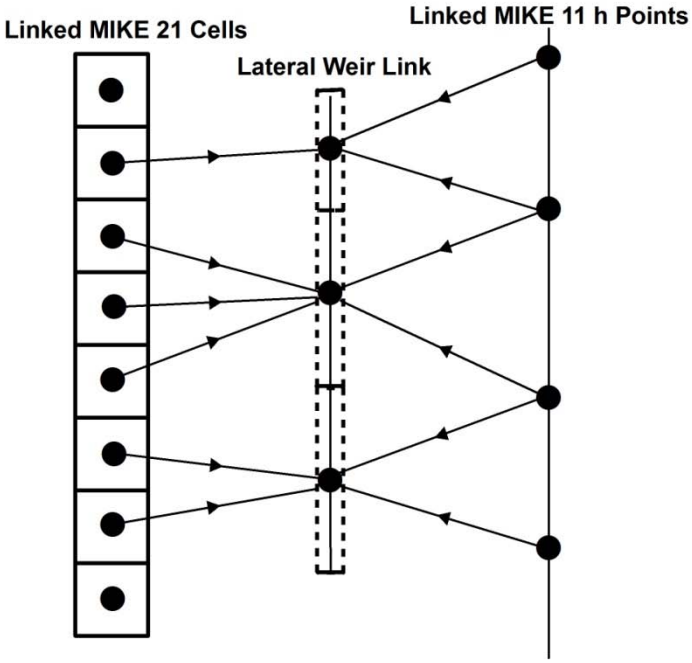

Figure 5.10. Lateral weir structure determined interpolated water levels and bed levels between MIKE 11 h points.

Source: DHI. MIKE FLOOD: 1D-2D Modelling User Manual. MIKE by DHI, 2009

Table 5.1. Distributed Manning's 'n' roughness coefficients based on NCLD classifications.

		Manning's n				
NLCD Class	Definition	Minimum	Normal	Maximum	Source	Base Values
11	Open Water	0.025	0.030	0.033	Chow 1959	0.032
21	Developed, Open Space	0.025	0.030	0.035	Chow 1959	0.030
22	Developed, Low Intensity	0.035	0.050	0.065	Calenda, et al. 2005	0.050
23	Developed, Medium Intensity	0.050	0.075	0.100	Calenda, et al. 2005	0.075
24	Developed, High Intensity	0.070	0.100	0.130	Calenda, et al. 2005	0.100
31	Barren Land	0.011	0.013	0.015	Chow 1959	0.013
41	Deciduous Forest	0.070	0.100	0.160	Chow 1959	0.100
42	Evergreen Forest	0.080	0.100	0.120	Chow 1959	0.100
43	Mixed Forest	0.070	0.100	0.160	Chow 1959	0.100
71	Grassland/Herbaceous	0.030	0.035	0.050	Chow 1959	0.035
81	Pasture/Hay	0.030	0.035	0.050	Chow 1959	0.035
82	Cultivated Crops	0.025	0.035	0.045	Chow 1959	0.035
90	Woody Wetlands	0.035	0.050	0.070	Chow 1959	0.050
95	Emergent Herbaceous Wetlands	0.035	0.050	0.070	Chow 1959	0.050

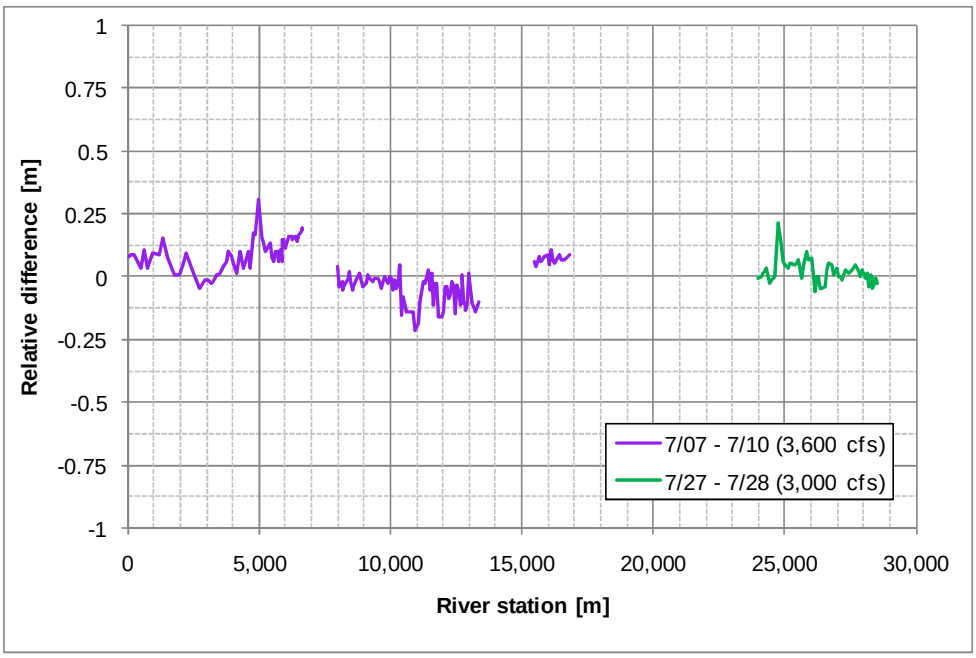

Figure 5.11. Relative differences between low flow calibration dataset and simulation results (simulation minus observed).

Table 5.2. High flow calibration roughness parameters and simulation results.

Simulation	I	II	III	IV	V	VI	VII
Multiplication factor	0.7	0.8	0.9	1	1.1	1.2	1.3
Land use	Manning's n						
Open Water	0.029	0.029	0.029	0.029	0.029	0.029	0.029
Developed, Open Space	0.021	0.024	0.027	0.030	0.033	0.036	0.039
Developed, Low Intensity	0.035	0.040	0.045	0.050	0.055	0.060	0.065
Developed, Medium Intensity	0.053	0.060	0.068	0.075	0.083	0.090	0.098
Developed, High Intensity	0.070	0.080	0.090	0.100	0.110	0.120	0.130
Barren Land	0.009	0.010	0.012	0.013	0.014	0.016	0.017
Deciduous Forest	0.070	0.080	0.090	0.100	0.110	0.120	0.130
Evergreen Forest	0.070	0.080	0.090	0.100	0.110	0.120	0.130
Mixed Forest	0.070	0.080	0.090	0.100	0.110	0.120	0.130
Grassland/Herbaceous	0.025	0.028	0.032	0.035	0.039	0.042	0.046
Pasture/Hay	0.025	0.028	0.032	0.035	0.039	0.042	0.046
Cultivated Crops	0.025	0.028	0.032	0.035	0.039	0.042	0.046
Woody Wetlands	0.035	0.040	0.045	0.050	0.055	0.060	0.065
Emergent Herbaceous Wetlands	0.035	0.040	0.045	0.050	0.055	0.060	0.065
Mean over prediction [m]	-0.03	0.20	0.25	0.31	0.36	0.46	0.50
Standard Deviation [m]	0.45	0.42	0.41	0.40	0.40	0.44	0.45

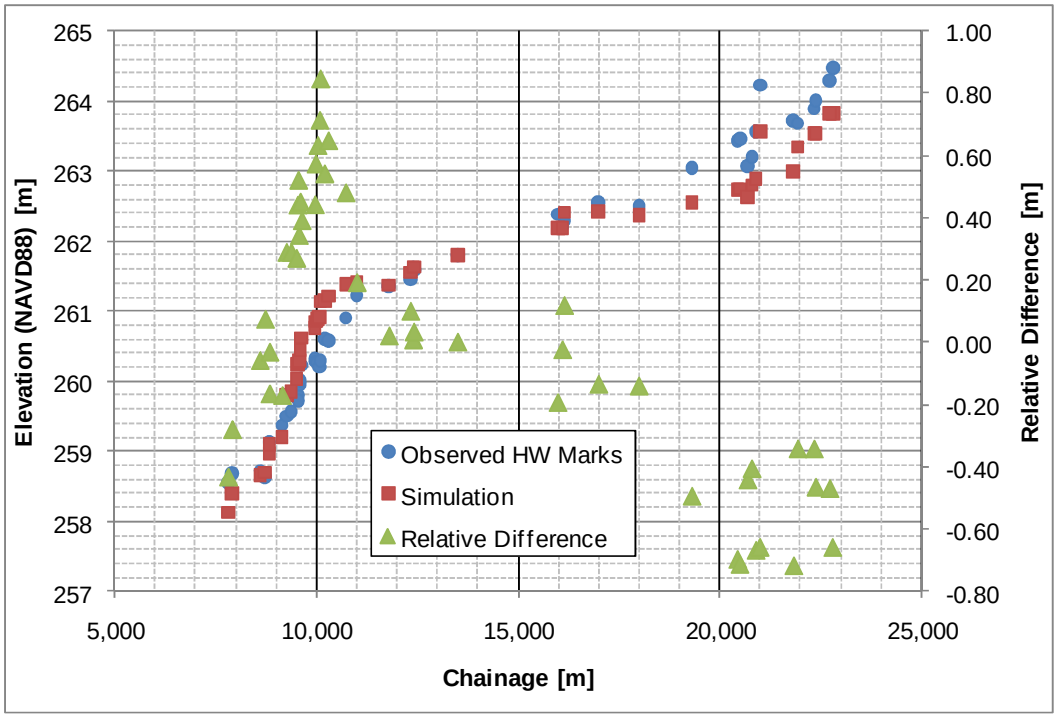

Figure 5.12. Comparison of initial calibration results of Simulation I to observed high water marks.

Table 5.3. Additional high flow calibration scenarios and simulation results.

Simulation #	D/S Factor	U/S Factor	Wetland Manning's n	Weir Method	Mean Over Prediction [m]	Standard Deviation [m]
VIII	0.7	1.0	0.05	Broad Crested	-0.08	0.39
IX	1.0	0.7	0.035	Broad Crested	0.05	0.45
X	0.7	1.0	0.05	Default Honma	-0.1	0.38
XI	1.0	0.7	0.035	Default Honma	-0.05	0.55
XII	1.0	1.0	0.05	Default Honma	0.03	0.42
XIII	1.0	1.2	0.06	Default Honma	0.01	0.38

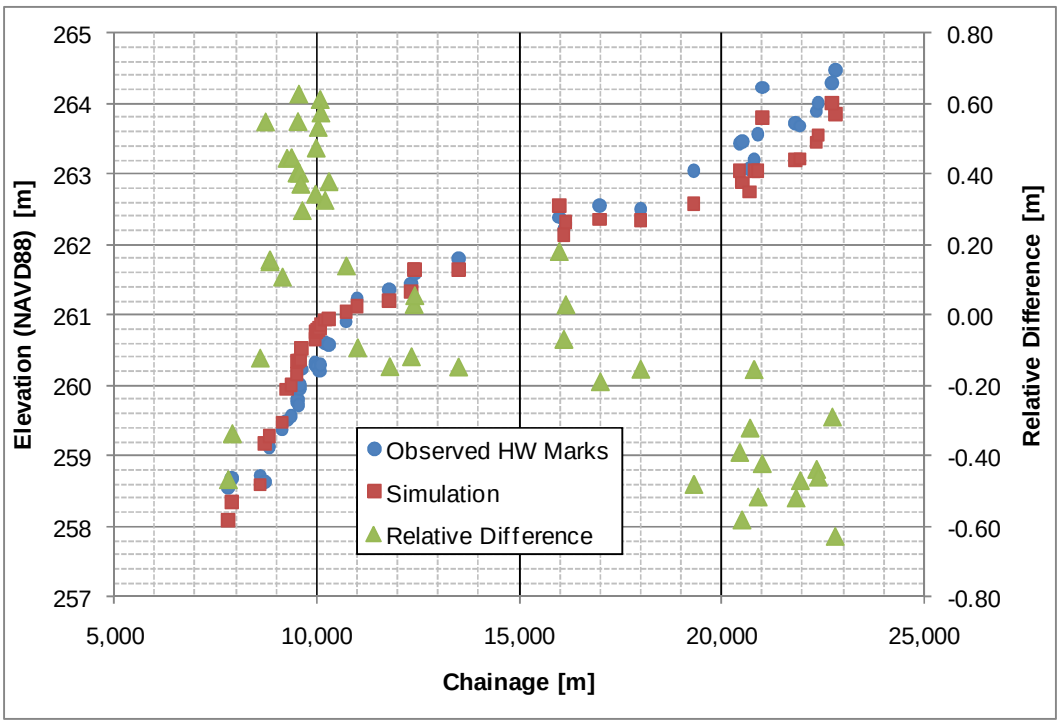

Figure 5.13. Comparison of initial calibration results of Simulation XIII to observed high water marks.

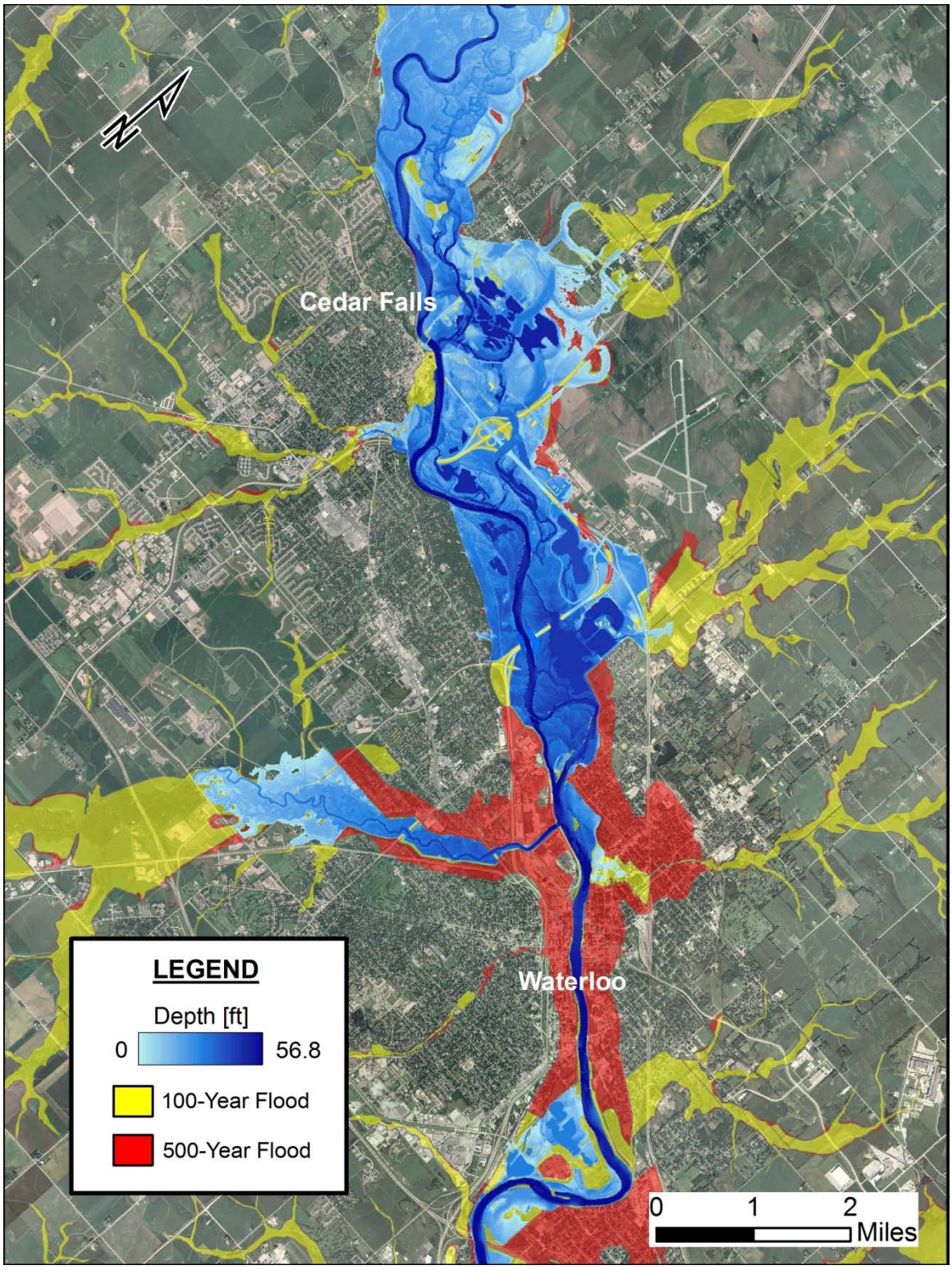

Figure 5.14. 2008 Flood inundation depths, FEMA 100 and 500-year flood boundaries.

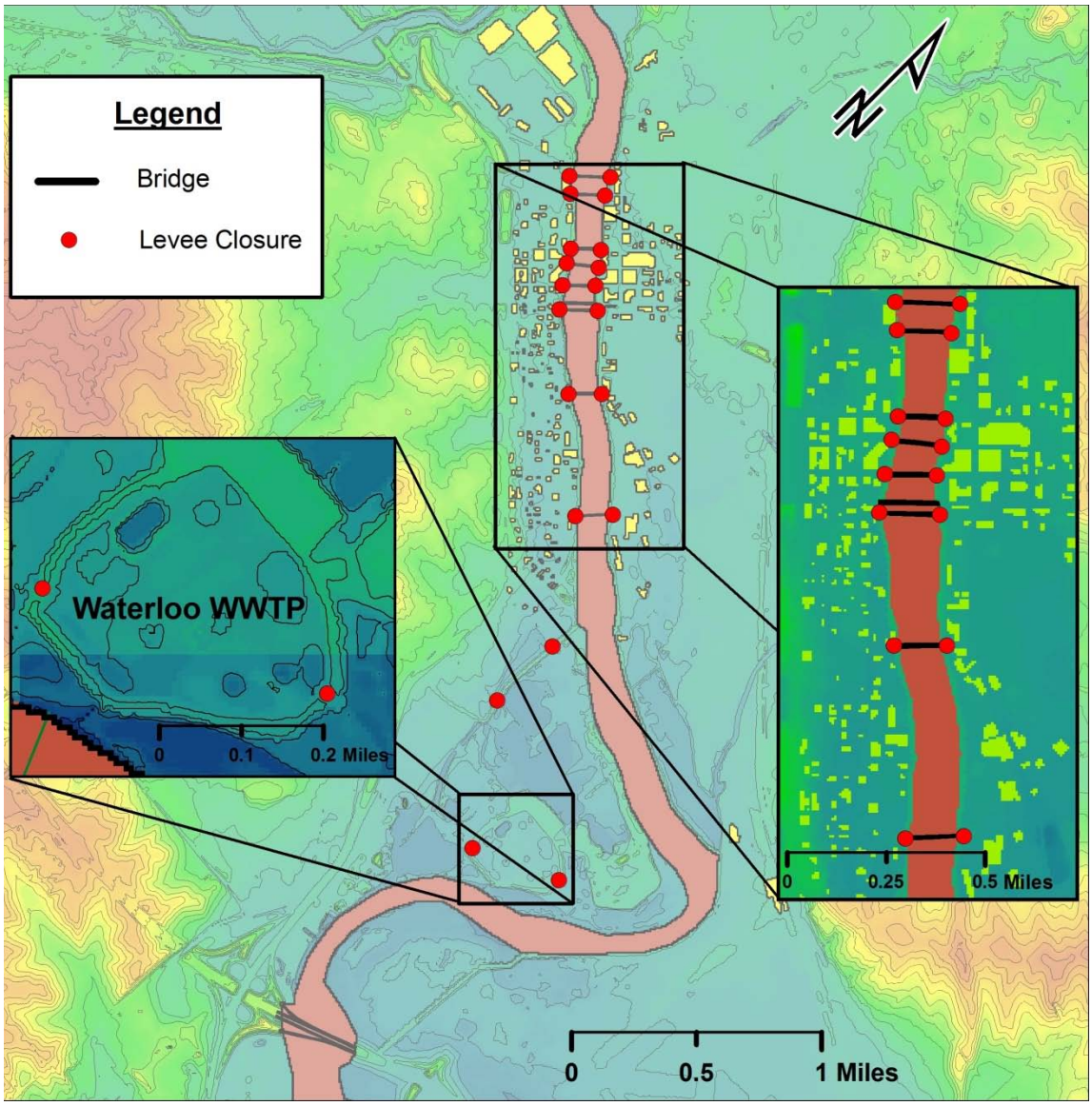

Figure 5.15. Levee closure locations in downtown Waterloo, IA.

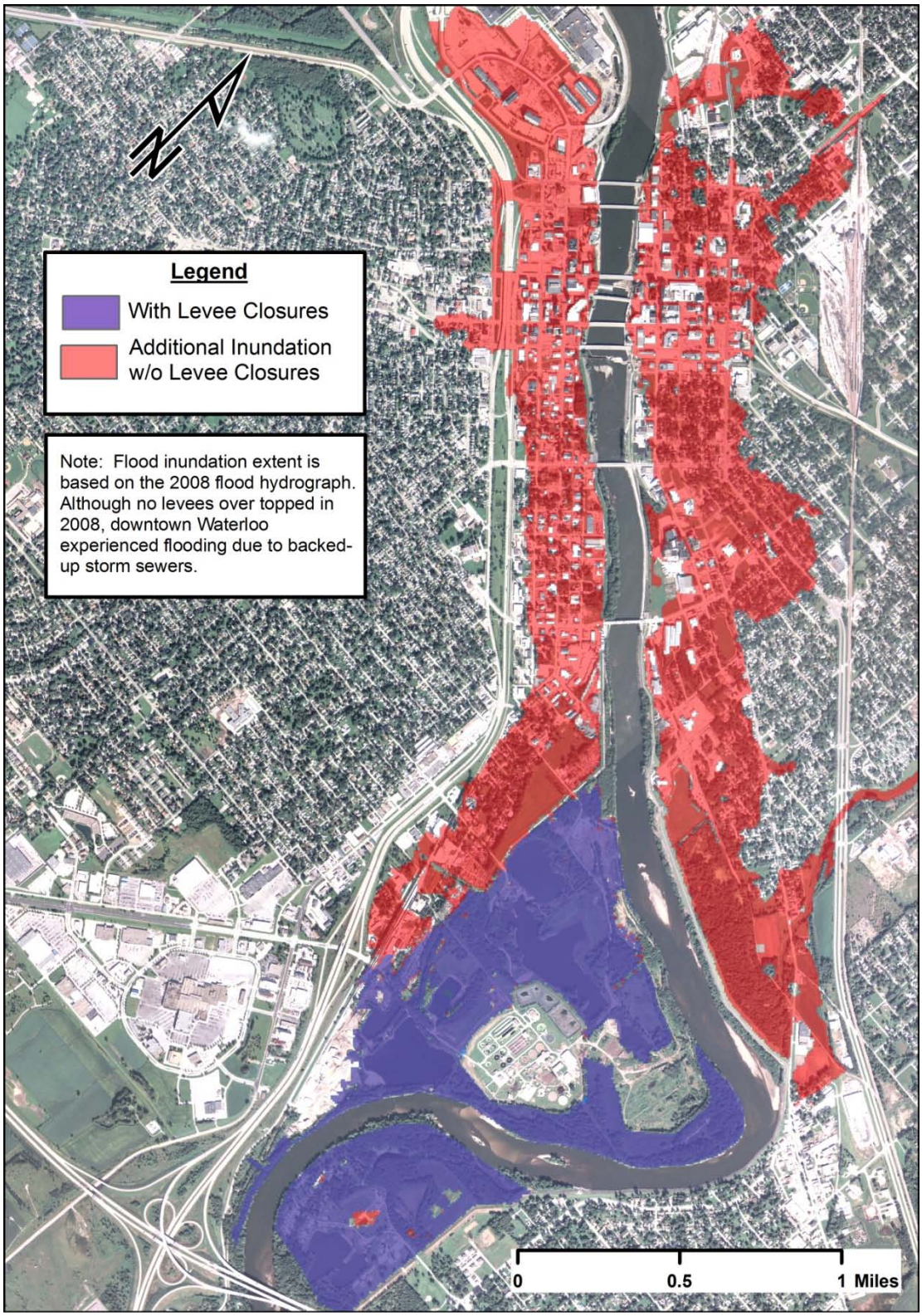

Figure 5.16. 2008 flood extent comparison of with and without levee closure scenarios.

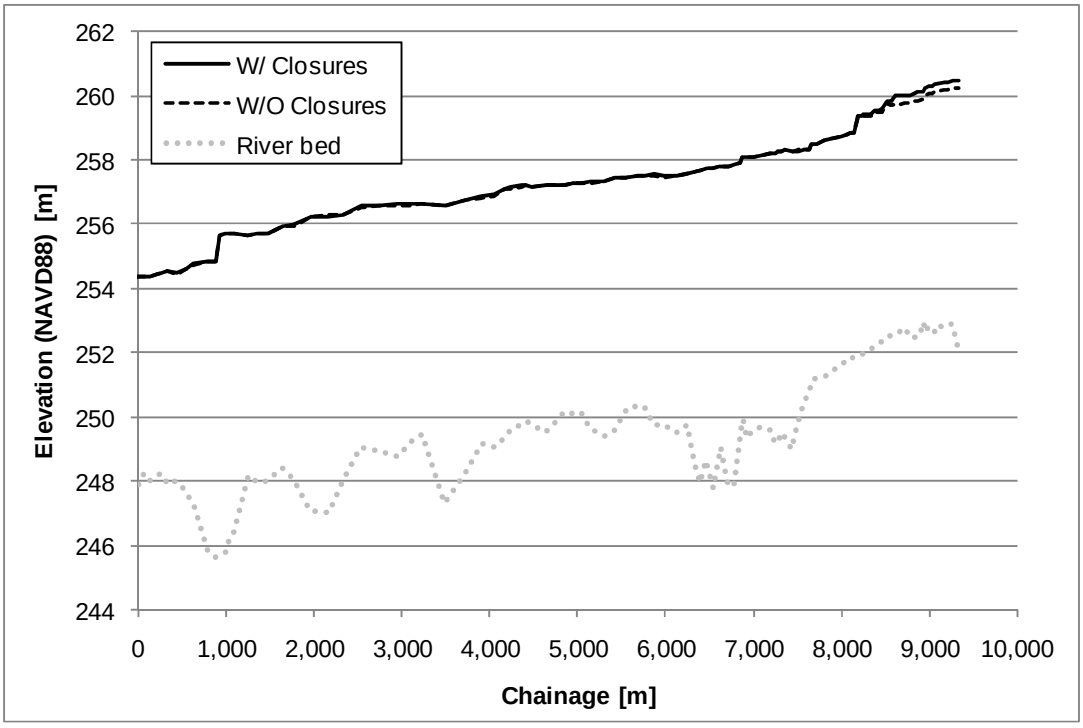

Figure 5.17. Maximum water surface profiles for with and without levee closures when simulating the 2008 flood.

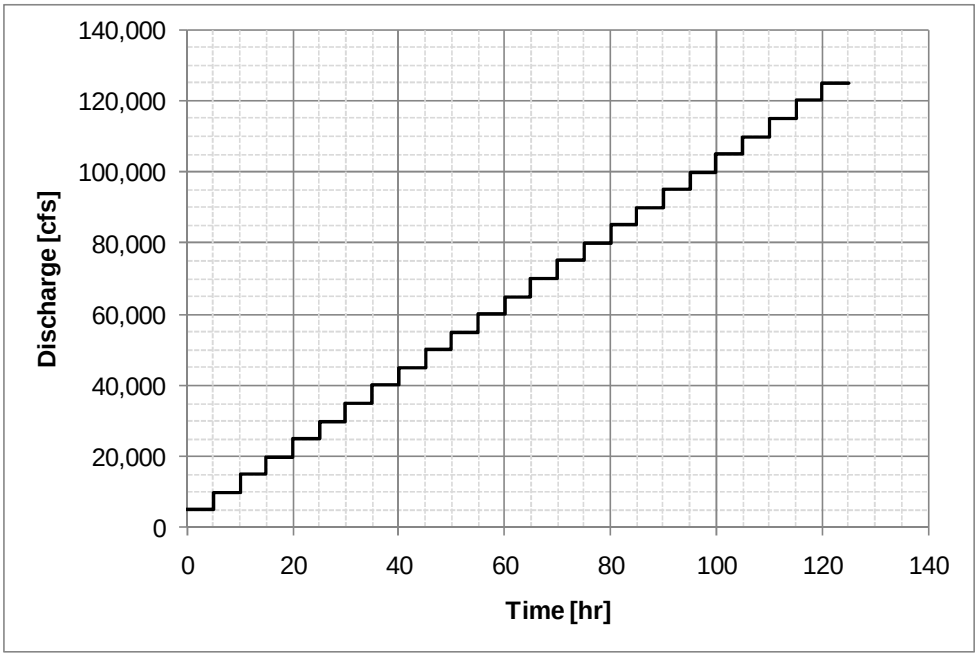

Figure 5.18. Design hydrograph used in development of levee closure plan.

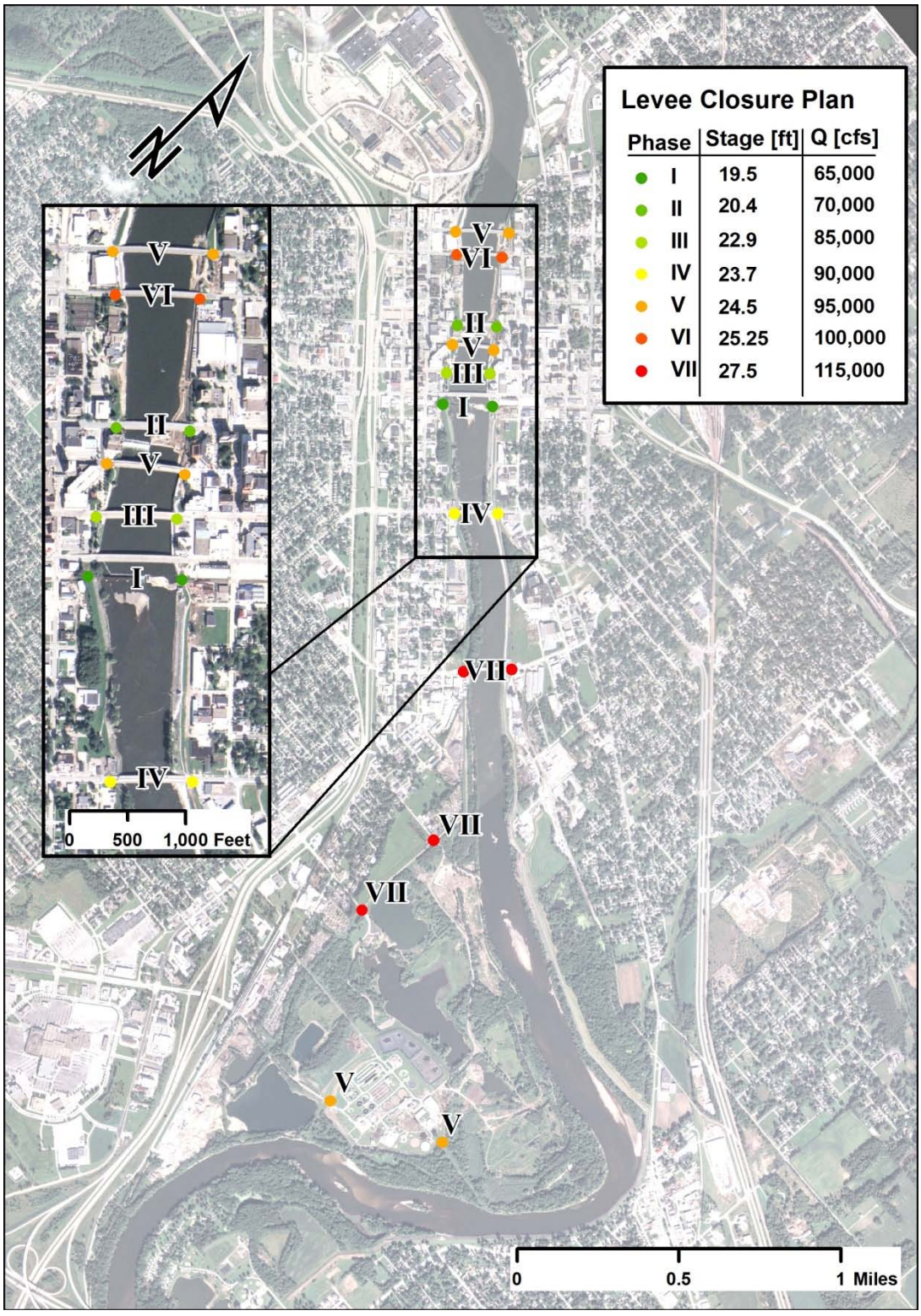

Figure 5.19. The levee closure plan is organized by phases, which are based on discharge and stage at the Waterloo USGS gage.

CHAPTER VI: SUMMARY AND RECOMMENDATIONS

6.1 Discussion

The movement of flood waters can be approximated using many different governing equations with varying degrees of detail. Forms of the Navier-Stokes equations consider physical and geometric parameters, while routing methods do not utilize any physically based parameters. Regardless of the level of detail achieved, numerical flood models are powerful tools that can be used to improve flood preparedness. As with any representation of reality, uncertainties must be considered when analyzing numerical simulation results.

A numerical HEC-ResSim model of Coralville Reservoir was utilized to evaluate operational changes and sedimentation effects for historic flood events. The volume of storage lost to sedimentation was determined to have a limited impact on major floods like those in 1993 and 2008. Simulations using predicted reservoir storage curves also showed a limited impact on major events. Utilization of a more aggressive operations plan, such as relaxation of downstream constraints and major flood pool procedures, demonstrated slight decreases in peak discharges.

A static inundation map library was developed for Coralville and Iowa City, Iowa by utilizing an existing one-dimensional hydraulic HEC-RAS model of the Iowa River. The development required bathymetry, topography, structural, and land use data. The maps will supplement discrete National Weather Service (NWS) river gage forecasts to allow for a spatial visualization of inundation extent. The maps will be hosted on the NWS Advanced Hydrologic Prediction Service website as a resource for citizens and community officials in evaluating flood risk.

A numerical flood model was developed for Cedar Falls and Waterloo, Iowa, by incorporating the benefits of both 1D and 2D hydraulic models. This was accomplished by developing a 1D hydraulic model of the river channel and a 2D hydraulic model of the

floodplain and coupling both using MIKE Flood. The development required bathymetry, topography, structural, and land use data. The model was calibrated to low and high flow observations. This model was utilized to investigate the role of levee closures in downtown Waterloo, and develop a plan to prioritize sand bagging efforts. The model will also be used to develop a library of web-based static inundation maps.

The applicability of 1D, 2D and coupled 1D/2D hydraulic models varies depending on study reach and degree of detail required. Creation of flood inundation maps for communities featuring well-defined river channels and flood plains may be executed using 1D hydraulic models. For example, the Iowa City/Coralville reach of the Iowa River is characterized by channelized sections in downtown areas and gently sloping floodplains in recreational areas. Accurate modeling of the reach was accomplished using a 1D HEC-RAS model by satisfying several assumptions inherent to 1D hydraulic modeling. These assumptions include the following: flow is one-dimensional, water level across the section is horizontal, streamline curvature is small and vertical accelerations are negligible, effects of boundary friction and turbulence can be accounted for using resistance laws analogous to those for steady flow conditions, and the average channel bed slope is small so the cosine of the angle can be replaced by unity (Cunge, Holly and Verwey 1980). Modeling of internal discontinuities, such as bridges and weirs, is handled with a high level of numerical stability. Calibration of a 1D hydraulic model is simplified due to the computational efficiency and spatial discretization of the model domain. However, prior knowledge of flowpaths is required before constructing river cross-sections. Manual editing of flood inundation maps developed from 1D hydraulic model simulation results may be necessary.

Areas featuring wide floodplains may require a 2D hydraulic modeling approach to properly resolve out of bank flow. Overbank areas along the Cedar River between Waterloo and Cedar Falls feature many secondary channels and alternate flow paths, requiring the higher degree of simulation detail provided by 2D hydraulic models. A

drawback of utilizing a 2D hydraulic model over a 1D hydraulic model is decreased computational efficiency. This decrease in computational efficiency and increased spatial resolution of 2D hydraulic models requires more resources to complete calibration compared to 1D hydraulic models. 2D hydraulic models are unable to incorporate structures, and may require coupled 1D links to include these features.

Numerical models can be used to improve flood preparedness; however, model development requires overcoming many logistical obstacles and acknowledging modeling limitations. Development of 1D and 2D hydraulic models requires a significant quantity of information describing topography, bathymetry, structures, land use, and observed hydrologic measurements. Complete high quality datasets describing these features are essential to development of an accurate model, but may be difficult to obtain. Cooperation with many government entities is required to collect necessary data. Continuous model updates are necessary to incorporate any river reach alterations affecting hydraulic behavior.

6.2 Future work

Future reservoir model investigations should include simulations of probabilistic inflows to evaluate smaller more frequent events. This will help determine any benefit gained from a more aggressive operations plan. The present investigation revealed that additional storage can be gained by utilizing an aggressive plan, at the cost of minor frequent flooding. A more detailed analysis of reservoir sedimentation should be completed to determine present sediment volume and future sedimentation.

The creation of future inundation map libraries should include disclosure of uncertainty in flood extent delineation. This can be accomplished using a framework similar to Smemoe, et al. (2007), in which a stochastic probability function was implemented to determine model inflows. The final mapping products would include zones of various uncertainty percentages.

The MIKE Flood model developed for Cedar Falls/Waterloo adequately incorporated structural elements and predicted flood inundation. However, runtimes exceeded the maximum allowable for real time forecasting. Utilizing raster-based inundation models that neglect inertial terms could allow for accurate predictions and faster runtimes. None of the levees in Waterloo and Cedar Falls failed during the 2008 flood, but flooding did occur as a result of backed up storm sewers, inadequate lift stations, and localized rainfall runoff. Including hydrologic considerations would provide additional insight into flooding issues in this area.

BIBLIOGRAPHY

Andersen, D. "Downtown businesses cope with flood damage." *Waterloo-Cedar Falls Courier*. Waterloo, IA, June 13, 2008.

Aronica, G., B. Hankin, and K. Beven. "Uncertainty and equifinality in calibrating distributed roughness coefficients in a flood propagation model with limited data." *Advances in Water Resources*, 1998: 349-365.

Ayres Associates. "University of Iowa - Hydraulic Memorandum." Iowa City, 2009.

Bales, J.D., and C.R. Wagner. "Source of uncertainty in flood inundation maps." *Journal of Flood Risk Management*, 2009: 139-147.

Bates, P.D. "A Simple Raster-Based Model for Flood Inundation Simulation." *Journal of Hydrology*, 2000: 54-77.

Bates, P.D., M.G. Anderson, and J.M. Hervouet. "Initial comparison of two two-dimensional finite element codes for river flood simulation." *Proceedings of the Institution of Civil Engineers Water, Maritime & Energy.* 1995. 238-248.

Calenda, G., C.P. Mancini, and E. Volpi. "Distribution of the Extreme Peak Floods of the Tiber River from the XV Century." *Advances in Water Resources*, 2005: 615-625.

Choudhury, P., R.K. Shrivastava, and S.M. Narulkar. "Flood Routing in River Networks Using Equivalent Muskingum Inflow." *Journal of Hydrologic Engineering*, 2002: 413-419.

Chow, Ven Te. *Open-Channel Hydraulics.* McGraw-Hill, 1959.

Cunge, J.A., F.M. Holly, and A. Verwey. *Practical Aspects of Computational River Hydraulics.* London: Pitman Publishing Limited, 1980.

De Saint Venant, B. "Théorie du mouvement non-permanent des eaux, avec application aux crues des rivières et à l'introduction des marées dans leur lit." *Acad. Sci Comptes rendus, 73*, 1871: 148-154, 237-240.

DHI. *MIKE 11 Reference Manual.* MIKE by DHI, 2009.

—. *MIKE 21 Flow Model: Hydrodynamic Module Scientific Documentation.* MIKE by DHI, 2009.

—. *MIKE FLOOD: 1D-2D Modelling User Manual.* MIKE by DHI, 2009.

Ericson, J. "Help or high water: The effort to save the Cedar Falls levee was never a sure thing." *Waterloo-Cedar Falls Courier.* Waterloo, IA, June 22, 2008.

Espinosa-Villegas, C.O., and J.L. Schnoor. "Comparison of Long-Term Observed Sediment Trap Efficiency with Empirical Equations for Coralville Reservoir, Iowa." *Journal of Environmental Engineering*, 2009: 518-525.

Federal Emergency Management Agency. *Flood Insurance Study for Johnson County, Iowa and Incorporated Areas.* Washington D.C.: U.S. Department of Homeland Security, 2007.

—. *The National Flood Insurance Program.* June 04, 2009. http://www.fema.gov/plan/prevent/floodplain/index.shtm (accessed June 2010).

Fenton, John D. "Reservoir routing." *Hydrological Sciences Journal*, 1992: 233-245.

Frank, E., A. Ostan, M. Coccato, and G.S. Stelling. "Use of an integrated one-dimensional/two-dimensional hydraulic modelling approach for flood hazard and risk mapping." In *River Basin Management*, by R.A. Falconer and W.R Blain, 99-108. Southhampton, UK: WIT Press, 2001.

Fread, D.L., and K.S. Hsu. "Applicability of Two Simplified Flood Rouing Methods: Level-Pool and Muskingum-Cunge." *1993 ASCE National Hydraulic Engineering Conference.* San Francisco, 1993.

Hall, J.W., S. Tarantola, P.D. Bates, and M.S. Horritt. "Distributed Sensitivity Analysis of Flood Inundation Model Calibration." *Journal of Hydraulic Engineering*, 2005: 117-126.

HEC. "HEC-RAS 4.0 Hydraulic Reference Manual." *Hydrologic Engineering Center Website.* 2010. http://www.hec.usace.army.mil/software/hec-ras/ (accessed 2010).

Horritt, M.S., and P.D. Bates. "Evaluation of 1D and 2D numerical models for predicting river flood inundation." *Journal of Hydrology*, 2002: 87-99.

Huang, M., G. Zhai, Y. Ouyang, and Y Liu. "Data Fusion Technique for Multibeam Echosoundings." *Geo-spatial Information Science*, 2002: 11-18.

Hydro International. "Product Survey: Multi-beam Shallow Water." *Hydro International.* December 2006. http://www.hydro-international.com/files/productsurvey_v_pdfdocument_12.pdf (accessed June 2010).

Jain, Subhash C. *Open-channel flow.* John Wiley & Sons Inc., 2001.

Koomans, R. "HydroSurveys: Single-Beam Echosounders." *Hydro International.* June 2009. http://www.hydro-international.com/files/productsurvey_v_pdfdocument_30.pdf (accessed June 2010).

Lin, B., J.M. Wicks, R.A. Falconer, and K. Adams. "Integrating 1D and 2D hydrodynamic models for flood simulation." *Preceedings of the Institution of Civil Engineers.* Water Management Incorporated, 2006. 19-25.

Maidment, D. R., ed. *Handbook of Hydrology*. McGraw-Hill, 1992.

Mason, D.C., D.M. Cobby, M.S. Horritt, and P.D. Bates. "Floodplain friction parameterization in two-dimensional river flood models using vegetation heights derived from airborne scanning laser altimetry." *Hydrological Processes*, 2003: 1711-1732.

Mays, Larry W. *Water Resources Engineering.* John Wiley & Sons, Inc., 2005.

McCarthy, G.T. "The Unit Hydrograph and Flood Routing." *Conference of North Atlantic Division.* U.S. Army Corps of Engineers, 1938.

McCowan, A.D., E.B. Rasmussen, and P. Berg. "Improving the Performance of a Two-dimensional Hydraulic Model for Floodplain Applications." *Conference on Hydraulics in Civil Engineering.* The Institution of Engineers, Australia, 2001.

Mutel, Cornelia F., ed. *A Watershed Year: Anatomy of The Iowa Floods of 2008.* Iowa City: University of Iowa Press, 2010.

Pappenberger, F., K. Beven, M. Horritt, and S. Blazkova. "Uncertainty in the calibration of effective roughness parameters in HEC-RAS using inundation and downstream level observations." *Journal of Hydrology*, 2004: 46-69.

Pappenberger, F., P. Matgen, K.J. Beven, H. Jean-Baptiste, L. Pfister, and P. Fraipont de. "Influence of uncertain boundary conditions and model structure on flood inundation predictions." *Advances in Water Resources*, 2006: 1430-1449.

Patro, S., C. Chatterjee, S. Mohanty, R. Singh, and N.S. Raghuwanshi. "Flood Inundation Modeling using MIKE FLOOD and Remote Sensing Data." *Journal of the Indian Society of Remote Sensing*, 2009: 107-118.

Perumal, Muthiah. "The cause of negative inital outflow with the Muskingum method." *Hydrological Sciences Journal*, 1993: 391-401.

Piotrowski, Jesse A. *Development of a High-Resolution Two-Dimensional Urban/Rural Flood Simulation.* MS Thesis, The University of Iowa, 2010.

Smemoe, C.M., E.J. Nelson, A.K. Zundel, and A.W. Miller. "Demonstrating Floodplain Uncertainty Using Flood Probability Maps." *Journal of the American Water Resources Association*, 2007: 359-371.

Stoer, J., and R. Bulirsch. *Introduction to Numerical Analysis 3rd ed.* New York: Springer Publishing, 2002.

U.S. Army Corps of Engineers. *HEC-1, Flood Hydrograph Package, User's Manual.* Hydrologic Engineering Center, 1990.

United States Department of Agriculture. *USDA NRCS Geospatial Data Gate.* 2010. http://datagateway.nrcs.usda.gov/ (accessed May 2010).

United States Geological Survey. *USGS WaterWatch.* June 2010. http://waterwatch.usgs.gov/ (accessed May 2010).

USGS. *The National Map Seamless Server.* August 19, 2008. http://seamless.usgs.gov/products/3arc.php (accessed June 2010).

Werner, M.G.F. "Impact of Grid Size in GIS Based FLood Extent Mapping Using a 1D Flow Model." *Phys. Chem. Earth Part B-Hydrol. Oceans Atmos.*, 2001: 517-522.

Work, P.A., M. Hansen, and W.E. Rogers. "Bathymetric Surveying with GPS and Heave, Pitch, and Roll Compensation." *Journal of Surveying Engineering*, 1998: 73-90.

Zoppou, Christopher. "Reverse Routing of Flood Hydrographs Using Level Pool Routing." *Journal of Hydrologic Engineering*, 1999: 184-188.

APPENDIX A:

CURRENT CORALVILLE RESERVOIR OPERATIONS PLAN

Table A.1. Current Coralville Reservoir operations plan

Schedule A **Normal Flood Control Operation** **Pool elevation at or forecast between 683 and 707**	Conservation pool Schedule Date — Operation 15 Feb – 20 Mar — 683 to 679^ 20 Mar – 20 May — Hold 679^ 20 May – 15 Sep — Hold 683 15 Sep – 15 Dec — Hold 683-686* 15 Dec – 15 Feb — Hold 683 *Notes: ^ Variable draw down based on snow cover, ice, and 30 day climatic conditions coordinated with IDNR* ** Dates and elevation of fall pool raise coordinated with the IDNR*

Condition	Operation
A-1 All Dates	Regulated pool level as nearly as possible without adversely affecting downstream conditions. Do not release less than minimum outflow of 150 cfs
A – 2 15 December through 1 May	Maintain conservation pool according to schedule without exceeding release of 10,000 cfs except as limited by conditions A 3, A 6 or A7
A-3 15 December through 1 May Stage at above or forecast to exceed…. Lone Tree 16.0 feet Wapello 22.0 feet	Reduce release to not less than 1,000 cfs to control flow to those discharges as near as possible during three days of crest at the respected station with due allowance to travel times.
A-4 1 May through 15 December	Maintain conservation pool according to schedule without exceeding release of 6,000 cfs except as limited by conditions A-5, A-6 or A7
A-5 1 May through 15 December Stage at above or forecast to exceed…. Lone Tree 14.0 feet Wapello 21.0 feet	Reduce release to not less than 1,000 cfs to control flow to those discharges as near as possible during three days of crest at the respected station with due allowance to travel times
A-6 All Dates Stage at above or forecast to exceed… Mississippi River at Burlington - 18.0	Reduce release to not less than 1,000 cfs during seven days corresponding to the crest flow on the Mississippi River with due allowance for travel time.
A-7 Flash Flood: Any date flow at above or forecast to exceed 16,000 cfs at Iowa City	Reduce release to not less than 1,000 cfs to keep flow at or below 16,000 cfs at Iowa City

Table A.1 – continued

Schedule B **Major Flood** **Pool Elevation at above or forecast to exceed 707 feet NGVD**	

Condition	Operation
B-1 Inflow has not Peaked	Determine the pool elevation that would occur at the peak of the inflow hydrograph. Release not more than allowed on table below: **15 Dec – 1 May** / **1 May – 15 Dec** **Elev.** **Outflow** / **Elev.** **Outflow** 707 10000 / 707 7000 708 10000 / 708 8000 709 10000 / 709 9000 710 10000 / 710 10000 711 11000 / 711 11000 711.1 12000 / 711.1 12000 711.2 13000 / 711.2 13000 711.3 14000 / 711.3 14000 711.4 15000 / 711.4 15000 711.5 16000 / 711.5 16000 711.6 17000 / 711.6 17000 711.7 18000 / 711.7 18000 711.8 19000 / 711.8 19000 711.9 20000 / 711.9 20000 712.0 and above - Gates Fully open
B-2 Inflow has Peaked	Determine the minimum outflow required to utilize the remaining storage below 712.0. Release that flow or the present outflow – whichever is higher.
B-3 Reservoir Pool Falling	Release outflow established by B-2 until elevation 707 is reached then gradually reduce flows to Schedule A
B-4 Emergency: flow forecast to exceed the control flow established by the U.S. Army Corps of Engineers for public exigency downstream	Reduce release to keep flow at or below the control flow established by the "Corps".

Table A.1 – continued

Schedule C **Drought -- All Dates** **Any time pool below conservation according to Schedule A and inflow not sufficient to get to conservation pool.**	
C-1 Pool between Conservation and 678.0	Release 150 cfs
C-2 Pool between 677.0 and 678.0	Reduce release to 100 cfs
C-3 Pool below 677.0	Reduce release to 75 cfs

APPENDIX B:

HISTORIC CORALVILLE RESERVOIR ELEVATION-STORAGE CURVES

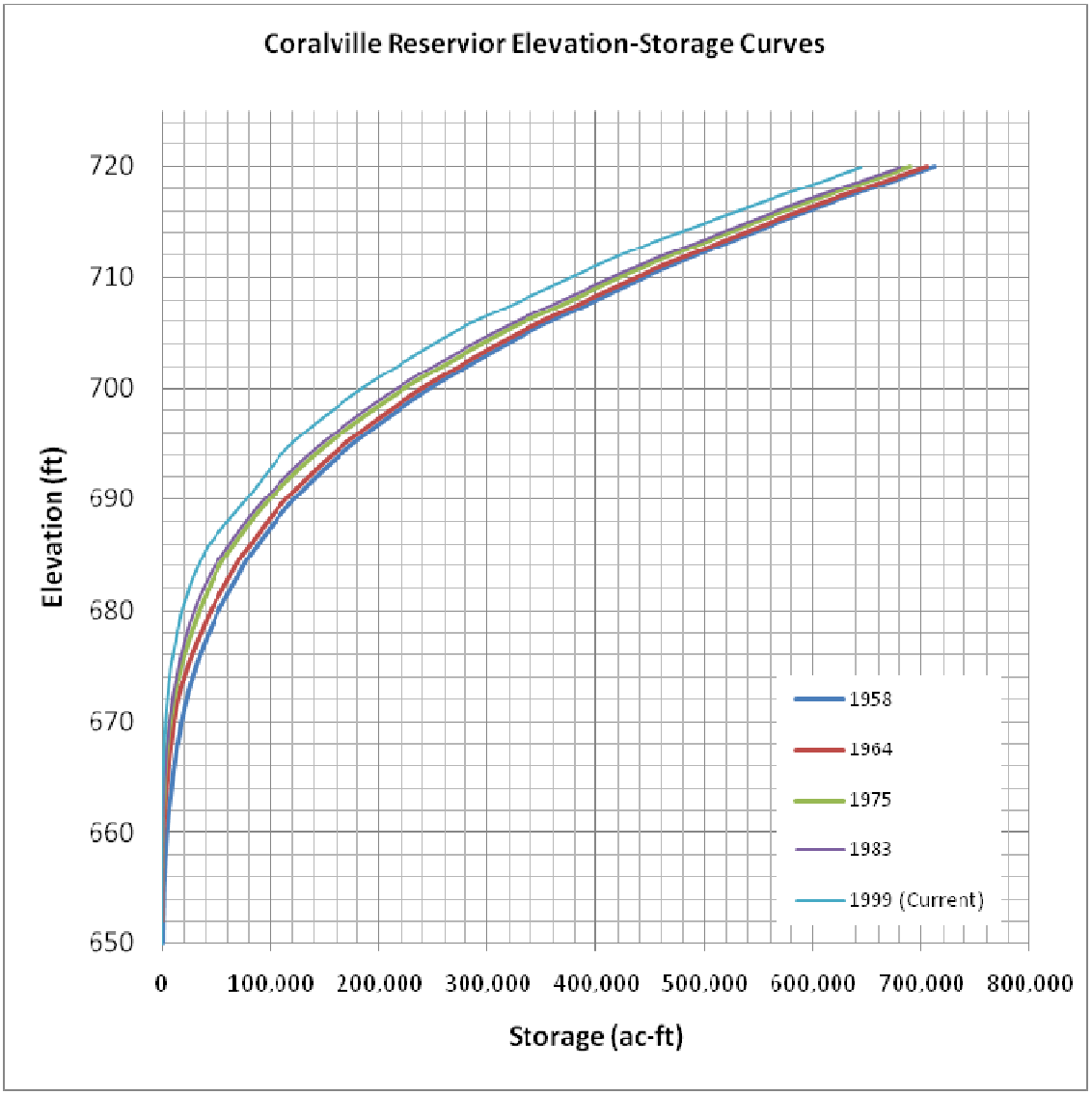

Figure B.1. Elevation storage curves for Coralville Reservoir.

APPENDIX C:

CORALVILLE RESERVOIR REGULATION HISTORY

Coralville Regulation History

December 1939: Project Submitted to Chief of Engineers
Top of Flood Pool 708 feet (400,000 acre-feet storage)

January 1940: State of Iowa objected to plan based on conservation practices

September 1948: Revised Corps' Plan
Top of Flood Pool 712 feet (492,000 acre-feet storage)
Conservation pool 670 feet

September 1958: Plan at implementation
Conservation pool - normal 680 feet
Spring 670 feet
Winter release 10,000 cfs
Summer release 8,500 cfs

Farmers complain about high summer time releases

1961 Interim Plan
Summer releases varied between 5,000 cfs and 6,500 cfs

1963 new plan
Summer releases varied between 4,000 cfs and 6,000 cfs
Major flood release at pool elevation 710.4 feet
Conservation pools: Spring 670 feet, Normal 680 feet,
Fall 683 feet

1983 Spring Conservation pool raised to 675 feet
From complaints about mudflats and fish habitat

New Regulation plan 1991
Conservation pool: Spring 679 feet, Normal 683 feet,
Fall 686 feet
Summer release 6,000 cfs, Winter release 10,000 cfs
Major Flood Pool at 707 feet

January 2001: New Regulation Manual
Proposed summer release rate to 8,000 cfs -
Coralville, Iowa City, and UofI objected
Down-stream farmers objected
Only regulation change - spring draw down variable

APPENDIX D:

1983 CORALVILLE RESERVOIR OPERATIONS

PLAN B

CORALVILLE RESERVOIR REGULATION SCHEDULE

Approved by Office, Chief of Engineers 21 January 1964 1982

Regulation Schedule	Condition	Operation
A. Conservation Storage	I. Normal	Regulate pool level in accordance with: Fig (c) of Plate 2 as nearly as possible without adversely affecting downstream conditions as follows: DATE — OPERATION 1 Feb-15 Feb — Lower from 680 to 675 15 Feb-15 Jun — Hold elev 675 15 Jun-25 Sep — Hold 680 25 Sep-15 Dec — Hold 683 15 Dec- 1 Feb — Hold 680 Do not release less than a minimum outflow of 150 cfs, nor exceed releases specified in Schedules B and C.
B. Flood Control	I. 15 December to 21 April	Maintain pool levels specified under Schedule A as nearly as possible without exceeding release of 10,000 cfs except as limited by Conditions B.IV, B.VII, and Schedule C.
	II. 21 April to 1 May Reservoir at or Above Conservation Elevation	Release 6,000 cfs to 10,000 cfs as indicated by Fig (a) of Plate 2 depending on amount of flood control storage occupied on 21 April except as limited by Conditions A.I, B.V, B.VII, and Schedule C.
	III. 1 May to 15 December Reservoir Above Conservation Elevation	Release 4,000 cfs to 6,000 cfs as indicated by Fig (b) of Plate 2 depending on amount of flood storage occupied on 1 May until reservoir recedes to conservation level, after which it shall be held at that level insofar as possible without exceeding release determined on basis of 1 May reservoir elevation or 5,000 cfs whichever is smaller, except as limited by Conditions B.VI, B.VII, and Schedule C.
	IV. 15 December thru 21 April Discharge at Lone Tree or Wapello are above, or forecast to exceed 15,000 cfs or 35,000, respectively	Reduce release to not less than 1,000 cfs to control flow to those discharges at respective stations insofar as possible during 3 days of crest at respective station, except as limited by Schedule C.
	V. 21 April to 1 May discharge at Lone Tree or Wapello above or forecast to exceed 5,000 cfs or 26,000 cfs respectively plus release in Condition B.II.	Same as Operation for Condition B.IV.
	VI. 1 May to 15 December discharge at Lone Tree or Wapello above or forecast to exceed 5,000 cfs or 26,000 cfs respectively plus release in Condition B.III	Same as Operation for Condition B.IV.
	VII. Any date, stage at, above or forecast to exceed 17.5 feet on Mississippi River gage at Muscatine, Iowa	Reduce release to 1,000 cfs during several days corresponding to crest flow in the Mississippi River with due allowance for time of travel, except as limited by Schedule C.
C. Major Flood Emergency	I. Any date reservoir elevation is rising and above or forecast to exceed elevation 710.4 feet	When predictions indicate that anticipated runoff from a storm will appreciably exceed the storage capacity remaining in the reservoir when operated under Schedule B, increase in outflow rates will be made as necessary to prevent reservoir from exceeding elevation 712.0 on basis of those predictions, but not less than given in the following schedule:

Pool Elev	Outflow cfs	Pool Elev	Outflow cfs
710.4	4,000	711.3	13,000
710.5	5,000	711.4	14,000
710.6	6,000	711.5	15,000
710.7	7,000	711.6	16,000
710.8	8,000	711.7	17,000
710.9	9,000	711.8	18,000
711.0	10,000	711.9	19,000
711.1	11,000	712.0	20,000
711.2	12,000		

Plate 1

APPENDIX E:

1964 CORALVILLE RESERVOIR OPERATIONS

BASE PLAN 1
CORALVILLE RESERVOIR REGULATION SCHEDULE

PLAN 8 : Approved by OCE 21

Regulation Schedule	Condition	Operation
A. Conservation Storage	I. Normal	Regulate pool level in accordance with Fig (c) of Plate 2 as nearly as possible without adversely affecting downstream conditions as follows: DATE — OPERATION 1 Feb-15 Feb — Lower from 680 to 670 15 Feb-15 Jun — Hold elev 670 15 Jun-25 Sep — Hold 680 25 Sep-15 Dec — Hold 683 15 Dec-1 Feb — Hold 680 Do not release less than a minimum outflow of 150 cfs nor exceed releases specified in Schedules B and C.
B. Flood Control	I. 15 December to 21 April	Maintain pool levels specified under Schedule A as nearly as possible without exceeding release of 10,000 cfs except as limited by Conditions B.IV, B.VII, and Schedule C.
	II. 21 April to 1 May Reservoir at or Above Conservation Elevation	Release 6,000 cfs to 10,000 cfs as indicated by Fig (a) of Plate 2 depending on amount of flood control storage occupied on 21 April except as limited by Conditions A.I, B.V, B.VII, and Schedule C.
	III. 1 May to 15 December Reservoir Above Conservation Elevation	Release 4,000 cfs to 6,000 cfs as indicated by Fig (b) of Plate 2 depending on amount of flood storage occupied on 1 May until reservoir recedes to conservation level, after which it shall be held at that level insofar as possible without exceeding release determined on basis of 1 May reservoir elevation or 5,000 cfs whichever is smaller, except as limited by Conditions B.VI, B.VII, and Schedule C.
	IV. 15 December thru 21 April Discharge at Lone Tree or Wapello are above, or forecast to exceed 15,000 cfs or 35,000, respectively	Reduce release to not less than 1,000 cfs to control flow to those discharges at respective stations insofar as possible during 3 days of crest at respective station, except as limited by Schedule C.
	V. 21 April to 1 May discharge at Lone Tree or Wapello above or forecast to exceed 5,000 cfs or 26,000 cfs respectively plus release in Condition B.II	Same as Operation for Condition B.IV.
	VI. 1 May to 15 December discharge at Lone Tree or Wapello above or forecast to exceed 5,000 cfs or 26,000 cfs respectively plus release in Condition B.III	Same as Operation for Condition B.IV.

	VII. Any date, stage at above or forecast to exceed 17.5 feet on Mississippi River gage at Muscatine, Iowa	Reduce release to 1,000 cfs during several days corresponding to crest flow in the Mississippi River with due allowance for time of travel, except as limited by Schedule C.
Major Flood Emergency	I. Any date reservoir elevation is rising and above or forecast to exceed elevation 710.4 feet	When predictions indicate that anticipated runoff from a storm will appreciably exceed the storage capacity remaining in the reservoir when operated under Schedule B, increase in outflow rates will be made as necessary to prevent reservoir from exceeding elevation 712.0 on basis of those predictions, but not less than given in the following schedule.

Pool Elev	Outflow cfs	Pool Elev	Outflow cfs
710.4	4,000	711.3	13,000
710.5	5,000	711.4	14,000
710.6	6,000	711.5	15,000
710.7	7,000	711.6	16,000
710.8	8,000	711.7	17,000
710.9	9,000	711.8	18,000
711.0	10,000	711.9	19,000
711.1	11,000	712.0	20,000
711.2	12,000		

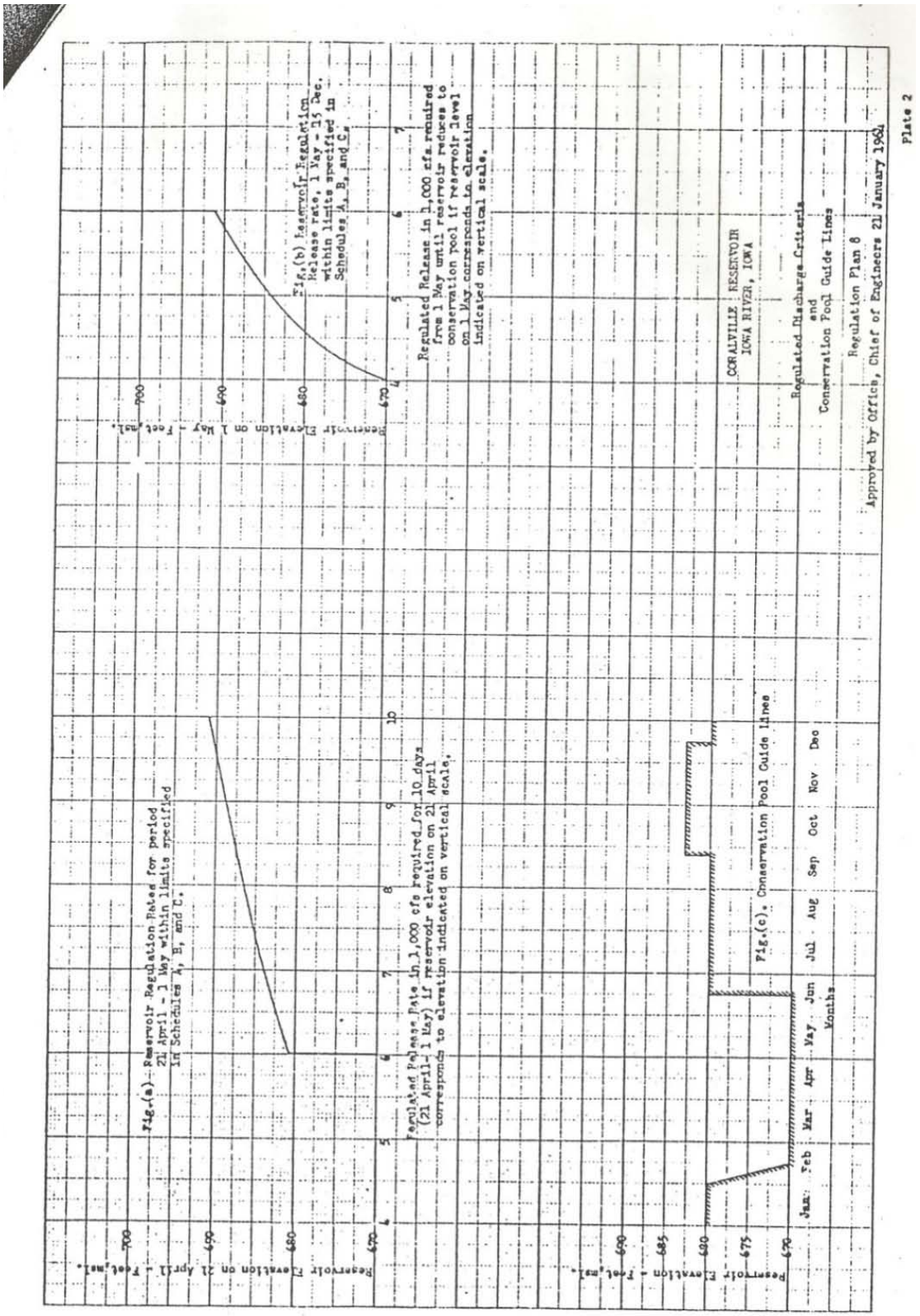
Fig.(a) Reservoir Regulation Rates for period
21 April - 1 May within limits specified
in Schedules A, B, and C.
Reservoir Elevation on 21 April - Feet msl.
Reservoir Elevation on 1 May - Feet msl.
Fig.(b) Reservoir Regulation
Release rate, 1 May - 15 Dec.
within limits specified in
Schedules A, B, and C.
Regulated Release in 1,000 cfs required
from 1 May until reservoir reduces to
conservation pool if reservoir level
on 1 May corresponds to elevation
indicated on vertical scale.
Regulated Release Rate in 1,000 cfs required for 10 days
(21 April - 1 May) if reservoir elevation on 21 April
corresponds to elevation indicated on vertical scale.
Fig.(c), Conservation Pool Guide Lines
Reservoir Elevation - Feet msl.
Jan Feb Mar Apr May Jun Jul Aug Sep Oct Nov Dec
Months
CORALVILLE RESERVOIR
IOWA RIVER, IOWA
Regulated Discharge Criteria
and
Conservation Pool Guide Lines
Regulation Plan B
Approved by Office, Chief of Engineers 21 January 1954
Plate 2

APPENDIX F:

2008 FLOOD WATERLOO/CEDAR FALLS HIGH WATER MARKS

Table F.1. High water marks following 2008 flood for Waterloo and Cedar Falls.

HIGH WATER LOCATIONS AND ELEVATIONS FOR THE 2008 FLOOD EVENT
CEDAR RIVER

Waterloo and Cedar Falls, Iowa

SHOT NUMBER	NORTH	EAST	ELEVATION	DESCRIPTION
HW1	3643116.70	5239170.10	848.29	NORTHEAST SIDE OF THE CEDAR RIVER - 240' SOUTHEAST OF THE 18TH STREET BRIDGE- WATERLOO
HW2	3643266.08	5238985.74	848.70	NORTHEAST END OF THE 18TH STREET BRIDGE OVER THE CEDAR RIVER - WATERLOO
HW4	3644662.78	5237064.04	848.82	NORTHEAST SIDE OF THE CEDAR RIVER - 170' SOUTHEAST OF THE 11TH STREET BRIDGE- WATERLOO
HW5	3644770.71	5236886.54	848.51	END OF THE 11TH STREET BRIDGE OVER THE CEDAR RIVER - WATERLOO
HW6	3644960.09	5236556.17	850.19	NORTHEAST SIDE OF THE CEDAR RIVER - 410' NORTHWEST OF THE 11TH STREET BRIDGE- WATERLOO
HW7	3645097.93	5236398.08	850.17	NORTHEAST SIDE OF THE CEDAR RIVER - 625' NORTHWEST OF THE 11TH STREET BRIDGE- WATERLOO
HW8	3645718.19	5235729.08	850.96	NORTHEAST SIDE OF THE CEDAR RIVER - 370' SOUTHEAST OF THE 6TH STREET BRIDGE- WATERLOO
HW9	3645869.69	5235417.95	851.39	OF THE E. 6TH STREET BRIDGE OVER THE CEDAR RIVER - WATERLOO
HW10	3646099.82	5235120.84	851.59	OF THE E. 5TH STREET BRIDGE OVER THE CEDAR RIVER - WATERLOO
HW11	3646392.56	5234859.88	852.22	OF THE E. 4TH STREET BRIDGE OVER THE CEDAR RIVER - WATERLOO
HW12	3646459.92	5234830.60	852.37	OF THE E. 4TH STREET BRIDGE OVER THE CEDAR RIVER - WATERLOO
HW13	3646578.62	5234770.17	852.13	NORTHEAST SIDE OF THE CEDAR RIVER BETWEEN PARK AVENUE AND E. 4TH STREET - WATERLOO
HW14	3646699.52	5234641.57	852.88	OF THE PARK AVENUE BRIDGE OVER THE CEDAR RIVER - WATERLOO
HW15	3646626.97	5234718.72	853.04	NORTHEAST SIDE OF THE CEDAR RIVER BETWEEN PARK AVENUE AND E. 4TH STREET - WATERLOO
HW16	3646807.57	5234511.90	853.77	OF THE PARK AVENUE BRIDGE OVER THE CEDAR RIVER - WATERLOO
HW17	3647473.75	5233799.17	854.07	THE 1ST STREET BRIDGE OVER THE CEDAR RIVER - WATERLOO
HW18	3647569.87	5233713.50	853.95	OF THE 1ST STREET BRIDGE OVER THE CEDAR RIVER - WATERLOO
HW19	3647666.58	5233612.95	853.88	NORTHEAST SIDE OF THE CEDAR RIVER BETWEEN MULLAN AVENUE AND 1ST STREET- WATERLOO
HW20	3647760.90	5233526.72	853.68	OF THE MULLAN AVENUE BRIDGE OVER THE CEDAR RIVER - WATERLOO
HW21	3647794.08	5233485.80	853.97	OF THE MULLAN AVENUE BRIDGE OVER THE CEDAR RIVER - WATERLOO
HW22	3647884.61	5233425.12	855.02	NORTHEAST SIDE OF THE CEDAR RIVER - 140' NORTHWEST OF MULLAN AVENUE - WATERLOO
HW23	3648331.96	5233168.56	854.90	NORTHEAST SIDE OF THE CEDAR RIVER AT NORTHWEST END OF SYCAMORE STREET - WATERLOO
HW24	3649559.77	5231980.96	855.99	NORTHEAST SIDE OF THE CEDAR RIVER AT FAIRVIEW AVENUE - 190' SOUTHEAST OF BOAT RAMPS - WATERLOO
HW25	3650311.77	5231480.66	857.04	195' SOUTH OF THE INTERSECTION OF PARK ROAD AND ENTRANCE TO BOAT RAMPS - WATERLOO
HW26	3651435.74	5229299.06	857.44	330' SOUTH OF CONGER STREET 0N BURTON AVENUE - WATERLOO
HW28	3651561.26	5227654.80	857.78	NORTHEAST END RAILROAD BRIDGE OVER THE CEDAR RIVER SOUTHEAST OF CONGER STREET - WATERLOO
HW29	3651441.07	5226932.01	858.34	NORTHWEST SIDE OF CONGER STREET AT ENTRANCE TO SANS SOUCI ISLAND - WATERLOO
HW30	3651426.98	5226950.82	858.26	NORTHWEST SIDE OF CONGER STREET AT ENTRANCE TO SANS SOUCI ISLAND - WATERLOO

Table F.1 – continued

HW31	3651109.46	5226416.99	858.92	OF THE CONGER STREET BRIDGE OVER BY PASS CHANNEL - WATERLOO
HW32	3653404.15	5220601.98	860.83	390' NORTHWEST OF GREENHILL ROAD BRIDGE OVER HWY 218 - WATERLOO
HW33	3654402.22	5220574.11	860.27	CEDAR RIVER NEAR GREENHILL ROAD INTERCHANGE - WATERLOO
HW34	3654473.59	5220442.26	860.54	CEDAR RIVER NEAR GREENHILL ROAD INTERCHANGE - WATERLOO
HW35	3657450.28	5220770.73	861.39	380' NORTH OF NORTH END BRIDGE OVER EAST LAKE ON THE WEST SIDE OF HWY 218- WATERLOO
HW36	3657192.80	5220683.68	861.24	145' NORTH OF NORTH END BRIDGE OVER EAST LAKE ON THE WEST SIDE OF HWY 218- WATERLOO
HW37A	3656511.13	5212385.38	863.04	SOUTH SIDE OF THE CEDAR RIVER 1010' EAST OF LOOK OUT PARK ON PARK DRIVE - CEDAR FALLS
HW38A	3656372.94	5208571.42	864.30	SOUTH SIDE OF THE CEDAR RIVER NEAR THE BIKE TRAIL BRIDGE IN PFEIFFER PARK - CEDAR FALLS
HW39	3656244.88	5206925.71	864.38	NORTHWEST CORNER HWY 58 AND WATERLOO ROAD - CEDAR FALLS
HW40	3660635.69	5212052.06	863.10	140' SOUTH OF HWY 218 NEAR HWY 58 ENTRANCE RAMP TO EAST BOUND HWY 218 - CEDAR FALLS
HW41	3661738.52	5211194.90	863.54	660' SOUTH OF LINCOLN STREET NEAR NORTH BOUND ENTRANCE RAMP HWY 218 & HWY 58 - CEDAR FALLS
HW42	3659682.41	5210135.50	864.70	1030' SOUTH OF 1ST STREET NEAR SOUTH BOUND RAMP HWY 58 - CEDAR FALLS
HW43	3668845.81	5210315.43	866.88	550' SOUTH OF LONE TREE ROAD NEAR SOUTH BOUND ENTRANCE RAMP TO HWY 218 - CEDAR FALLS
HW44	3660065.30	5206642.48	865.22	SOUTHWEST SIDE OF THE CEDAR RIVER - 740' SOUTH OF 1ST STREET - CEDAR FALLS
HW45	3660218.55	5206258.68	865.10	SOUTHWEST SIDE OF THE CEDAR RIVER - 580' SOUTH OF 1ST STREET - CEDAR FALLS
HW46	3661138.06	5205315.16	865.78	SOUTH SIDE OF THE CEDAR RIVER BETWEEN MAIN STREET AND RAILROAD BRIDGE - CEDAR FALLS
HW47	3661198.50	5205157.55	866.18	SOUTHWEST END RAILROAD BRIDGE OVER THE CEDAR RIVER - CEDAR FALLS
HW48	3661020.99	5204348.05	867.72	EAST SIDE CENTER STREET - 380' SOUTH 0F THE CENTER OF THE CEDAR RIVER - CEDAR FALLS
HW49	3661817.26	5204155.54	867.10	EAST SIDE CENTER STREET - 500' NORTH 0F THE CENTER OF THE CEDAR RIVER - CEDAR FALLS